

Air Force Institute of Technology

AFIT Scholar

Theses and Dissertations

Student Graduate Works

9-2020

Chronos Spacecraft with Chiron Probe: Exploration of the Hydrosphere, Principle Satellites, Atmosphere, and Rings of Uranus

Payton E. Pearson

Follow this and additional works at: <https://scholar.afit.edu/etd>



Part of the [Space Vehicles Commons](#), and the [The Sun and the Solar System Commons](#)

Recommended Citation

Pearson, Payton E., "Chronos Spacecraft with Chiron Probe: Exploration of the Hydrosphere, Principle Satellites, Atmosphere, and Rings of Uranus" (2020). *Theses and Dissertations*. 4333.
<https://scholar.afit.edu/etd/4333>

This Thesis is brought to you for free and open access by the Student Graduate Works at AFIT Scholar. It has been accepted for inclusion in Theses and Dissertations by an authorized administrator of AFIT Scholar. For more information, please contact AFIT.ENWL.Repository@us.af.mil.



**CHRONOS SPACECRAFT WITH CHIRON PROBE: EXPLORATION OF THE
HYDROSPHERE, PRINCIPLE SATELLITES, ATMOSPHERE, AND RINGS OF
URANUS**

THESIS

Payton E. Pearson, Captain, USAF

AFIT-ENG-MS-20-S-015

**DEPARTMENT OF THE AIR FORCE
AIR UNIVERSITY**

AIR FORCE INSTITUTE OF TECHNOLOGY

Wright-Patterson Air Force Base, Ohio

APPROVED FOR PUBLIC RELEASE; DISTRIBUTION UNLIMITED The views expressed in this thesis are those of the author and do not reflect the official policy or position of the U.S. Air Force, the Department of Defense, or the U.S. Government.

The views expressed in this thesis are those of the author and do not reflect the official policy or position of the U.S. Air Force, Department of Defense, or the U.S. Government. This material is declared a work of the U.S. Government and is not subject to copyright protection in the U.S..

AFIT-ENG-MS-20-S-015

CHRONOS SPACECRAFT WITH CHIRON PROBE: EXPLORATION OF THE
HYDROSPHERE, PRINCIPLE SATELLITES, ATMOSPHERE, AND RINGS OF
URANUS

THESIS

Presented to the Faculty

Department of Aeronautics and Astronautics

Graduate School of Engineering and Management

Air Force Institute of Technology

Air University

Air Education and Training Command

In Partial Fulfillment of the Requirements for the
Degree of Master of Science in Electrical Engineering

Payton E. Pearson, BS

Captain, USAF

September 2020

APPROVED FOR PUBLIC RELEASE; DISTRIBUTION UNLIMITED.

AFIT-ENG-MS-20-S-015

CHRONOS SPACECRAFT WITH CHIRON PROBE: EXPLORATION OF THE
HYDROSPHERE, PRINCIPLE SATELLITES, ATMOSPHERE, AND RINGS OF
URANUS

Payton E. Pearson, BS

Captain, USAF

Approved:

Dr. Carl Hartsfield

Dr. Carl Hartsfield
Chair

Dr. Robert Mills
Member

Maj Robert Bettinger, PhD
Member

Maj Joshua Hess, PhD
Member

Abstract

A design reference mission using improved technologies has been developed for exploration of the outer reaches of our Solar System, specifically Uranus and its system of satellites. This mission will utilize theoretical technologies mostly without regard to their current technological readiness level (TRL), though most systems have a TRL of at least 5. The primary innovations explored in this thesis are the new launch systems that provide far greater payload capacity potentially sent to anywhere in the Solar System, new Stirling-engine radioisotope thermoelectric generators (SRTGs), vastly improved data storage technologies, optimized satellite antenna relay of data using much higher transfer frequencies and wider arrays, and much more precise gyroscopes that allow for more powerful communications, only to name a few improvements. The final result is a payload capacity of greater than 3,000 kg that can be sent to Uranus, data transfer rates of upwards of 10 Mbps that the Earth will receive from the probe and its satellite system, 6 kW (4.5 kW at time of reaching Uranus) of power generated by all SRTGs onboard the spacecraft, all accomplished in a single launch that will take approximately 15 years to reach the water world.

Acknowledgments

I would like to express my sincere appreciation to my faculty advisor, Dr. Carl Hartsfield, for his guidance and support throughout the course of this thesis effort. The insight and experience he provided was certainly appreciated.

Captain Payton E. Pearson

Table of Contents

	Page
Abstract	1
Table of Contents	3
List of Figures	6
List of Tables	9
CHRONOS SPACECRAFT WITH CHIRON PROBE: EXPLORATION OF THE HYDROSPHERE, PRINCIPLE SATELLITES, ATMOSPHERE, AND RINGS OF URANUS	10
I. Introduction	10
1.1 Uranus and the Purpose of Space Exploration	10
1.2 Thesis Objectives.....	13
1.3 Problem Statement.....	18
II. Literature Review	20
2.1 Chapter Overview.....	20
2.2.1 Mariner II through IX.....	21
2.2.2 Viking I and II	27
2.2.3 Voyager I, II	31
2.2.4 Galileo	33
2.2.6 Mars Pathfinder	40
2.2.7 Cassini-Huygens.....	41
2.2.8 Uranus Pathfinder	49
2.3 Patched Conics and Hohmann Transfers.....	50
2.4 Uranus.....	51
III. Methodology	60

3.1 Chapter Overview.....	60
3.2 Stirling RTGs.....	62
3.3 Communications and Data Handling.....	65
3.4 Traveling-Wave Guide Amplifier (TWTA) Calculations:	82
3.5 Constellation Design	83
3.6 Inclination Changes	88
3.7 Launch Window Design	90
3.8 Tidal Force Effects	101
3.9 Probe Design	106
3.10.1 Doppler and Collision Broadening Science	110
3.10.2 Collision Broadening Calculations Methodology	111
3.10.3 Doppler and Overall Broadening Calculations.....	116
3.10.4 Doppler and Collision Broadening Modelling Through Filters	117
3.11 Falcon 9 Heavy Launch Vehicle	119
3.12 Orbital Dynamics.....	121
3.13 Launch ΔV Estimations.....	129
3.14 Atmospheric Insertion Dynamics	132
IV. Analysis and Results.....	137
4.1 Chapter Overview.....	137
4.2 Results of Doppler and Collision Broadening Models.....	137
4.3 Settled Upon Frequency Range.....	138
4.4 Settled Upon General Probe Design.....	141
4.5 Settled Upon Launch Specifications	145

4.6 Settled Upon SRTG Dynamics.....	147
4.7 Summary.....	154
V. Conclusions and Recommendations	155
5.1 Conclusions of Research	155
5.2 General Algorithmic Development and Doppler and Collision Broadening	155
5.3 Design Reference Mission Algorithmic Development.....	157
5.4 Significance of Research	158
5.5 Recommendations for Action.....	159
5.5.1 Chiron Probe Sub-scale Models	159
5.5.2 Doppler and Collision Broadening Extrapolation Models	161
5.6 Recommendations for Future Research.....	162
5.6.1 Pareto Front Optimizations.....	162
5.6.2 New/Different Launch Vehicles.....	164
5.7 Final Remarks.....	164
Bibliography	167
Appendix 1: MATLAB Code	175

List of Figures

Figure 1: Drone Array/Satellite Array Rough Analogy [3].	12
Figure 2: Earth Atmosphere Discontinuities.	15
Figure 3: Trajectory of Mariner 10 Spacecraft [17].	26
Figure 4: Five Mission Phases Functional Parts [18].	28
Figure 5: Voyager Flight Paths [21].	32
Figure 6: Sunpower Systems SRTG Schematic.	62
Figure 7: Engineering Scale Model of Stirling RTG.	63
Figure 8: Schematic of a Stirling Engine.	64
Figure 9: Normal Distribution for Beamwidth Error Probability.	66
Figure 10: Probability of Error as a Function of Frequency.	67
Figure 11: Number of Corrections Needed Per Day.	68
Figure 12: Binomial Distribution Expected Errors in 2,500 Trials.	69
Figure 13: Cumulative Distribution Function for Errors.	70
Figure 14: Frequency Attenuation Through Earth's Atmosphere.	71
Figure 15: Beamwidth Versus Frequency for Different Antenna Diameters.	72
Figure 16: Mothership Signal Beamwidth to Earth.	72
Figure 17: Mothership Signal Beamwidth with Earth Conjunction.	73
Figure 18: Mothership Signal Beamwidth with Earth Opposition (100 GHz Carrier).	73
Figure 19: 100 GHz Beamwidth with Earth-Mothership Conjunction.	74
Figure 20: Inscribed Radii Between Earth and Uranus.	74
Figure 21: Maximum Apparent Angle Change Earth-Mothership (1).	75
Figure 22: Maximum Apparent Angle Change Earth-Mothership (2).	75

Figure 23: Probe with SRTG Embedded Inside.	78
Figure 24: Uplink/Downlink Ratio.	81
Figure 25: Diagram of a TWTA.	83
Figure 26: Ideal Location of Probe with Respect to Earth.....	84
Figure 27: Illustration of Importance of Constellation Satellite System.	85
Figure 28: Worst-Case Scenario Probe Location with Respect to Earth and Mothership.	85
Figure 29: Elevation Angle and Range Between the Probe and Mothership.	88
Figure 30: Uranus' Orbital Inclination Versus Mothership's Orbit.....	89
Figure 31: Orbital Periods of Uranus and Earth.	92
Figure 32: Schema Used for Launch Window Optimization.....	93
Figure 33: Jupiter's Orbital Period around the Sun.	94
Figure 34: Orbits of Uranus and Earth Superimposed.....	95
Figure 35: Jupiter and Earth Orbits Superimposed.....	96
Figure 36: Jupiter and Uranus Orbits Superimposed.....	97
Figure 37: Earth, Uranus, and Jupiter's Orbits Superimposed.	97
Figure 38: Orbital Locations at Time of Ideal Launch.	99
Figure 39: Means of Calculating Distance.....	99
Figure 40: Flight Path Angles.	100
Figure 41: Mass Proportions of Uranus' Various Moons.....	103
Figure 42: Change in Pointing Direction Due to Tidal Forces.	105
Figure 43: Uplink/Downlink Ratio with Flat-Panel, Square Antenna.	109
Figure 44: Attenuation Spectra of CH ₄ , He, and H ₂ in the X-ray Band.	113
Figure 45: Attenuation of the Uranian Atmosphere.	114

Figure 46: Selected Filters Before Broadening Effects.	117
Figure 47: Filter for Methane’s Higher Frequency Bands.....	118
Figure 48: Attenuation Bands After Broadening Coefficients Implemented.	118
Figure 49: Final Uranian Atmospheric Attenuation for X-rays, After Broadening.....	119
Figure 50: Possible Payload Fairings of the Delta IV Rocket.	120
Figure 51: Hypothetical Jupiter Gravity Assist Maneuver.	126
Figure 52: Pareto-Optimal Front of Payload Mass Versus ΔV	131
Figure 53: Temperature Behind Normal Shock for Uranus.....	135
Figure 54: Solar Sail Design Concept [70].	139
Figure 55: Single Transmission-Reception Timeline.	140
Figure 56: Daily Transmission-Reception Timeline.....	140
Figure 57: Side View of Probe Design.	141
Figure 58: Top-View of Probe Design.....	142
Figure 59: Probe Design with Deployable SRTG Booms.	143
Figure 60: Final Probe Design.	145
Figure 61: Final Launch Vehicle Fairing Setup.....	146
Figure 62: Ideal Stirling Cycle [72].	148
Figure 63: Temperature Circuit Analog.....	149
Figure 64: Convection Coefficient with Trendline.....	151
Figure 65: Convection Coefficient Versus Temperature Change.....	152
Figure 66: 3D Printer with Sample Lattice.	160
Figure 67: 3D-Printed Aluminum Lattice.....	160
Figure 68: Example Skip Entry Maneuver Diagram.	163

List of Tables

Table 1: Objectives Summary [9].	18
Table 2: Uranus Versus Hypothetical Planet.	57
Table 3: Mission Subsystem Improvements Summary.	58
Table 4: Mission Cost Percentage Change.	59
Table 5: Planetary True Anomalies.	91
Table 6: Falcon 9 Heavy Payload Capacity Versus Mission Distance Desired.	121
Table 7: Top-Level General Figures.	129
Table 8: Interim Calculations.	130
Table 9: ΔV Figures.	130
Table 10: Ballistic Coefficients of Probe Shapes [67].	136
Table 11: Change in Convection Coefficient Versus Pressure/Temperature [74].	150
Table 12: Sample Variable Ranges for Doppler and Collision Broadening.	161

CHRONOS SPACECRAFT WITH CHIRON PROBE: EXPLORATION OF THE HYDROSPHERE, PRINCIPLE SATELLITES, ATMOSPHERE, AND RINGS OF URANUS

I. Introduction

1.1 Uranus and the Purpose of Space Exploration

At the edge of our Solar System lie two, as of yet mostly unexplored, massive planets. These planets have been dubbed the “ice giants,” in the astronomical and scientific community due to their massive size and extremely cold temperatures. Very little is known about these celestial bodies, other than a few general characteristics about their orbital dynamics and composition. Uranus, one of these two ice giants in our Solar System, has features of such stunning nature that it deserves greater observation and inquiry. The fact that Uranus has not been explored further despite the promise of discerning more about its nature and the potential habitability of celestial bodies like it only highlights the difficult and expensive reality of space exploration. A close analog to this is the Cassini-Huygens mission to the planet Saturn. Operating on as lean and efficient a development budget as possible, this mission still ended up costing \$3.3 billion in 1997. With a constant 2% inflation rate, this would be approximately \$5.5 billion today [1]. This mission to what was a much closer planetary system,¹ one that took the Cassini-Huygens mission seven years to reach, used three general purpose heat sources in the form of radioisotope thermoelectric generators (RTGs), providing a total of 900 W of

¹ 10.12 AU as opposed to 20.11 for Uranus.

electrical power. The overall system had a mass of 5,800 kg at launch, which included 2,700 kg dry mass, and 3,100 kg of propellant. Such challenges of optimizing mass, volume, power generation, cost, data rates and more would only be compounded on a mission to Uranus. But this difficulty is surmountable, by human ingenuity and knowhow.

As discerned from radio-resonance imaging of the planet through early flybys of the Voyager 2 mission, water is abundant in liquid form under the shroud of Uranus' thick atmosphere, in a mixture with various other chemicals, including ammonia [2]. This thesis presents a spacecraft and probe designed to intercept Uranus' orbit, pierce its atmosphere, and conduct an extensive battery of measurements for at least seven years.

New and innovative technologies, including but not limited to:

1. Stirling Radioisotope Thermoelectric Generators (SRTG's) that improve power production efficiency by a factor of nearly four, from roughly 7% up to 25%. Mass and volume of power generation remains insignificantly different, thus also improving effectiveness by the same measure.
2. Improved data storage, millions of times denser and many times more reliable than previous missions.
3. Improved data transfer, with data rates thousands of times greater than previous missions, at frequencies thousands of times greater.
4. Multiple satellite arrays, allowing for implementation of relay technology which grant much the same capabilities as modern drone arrays [3].

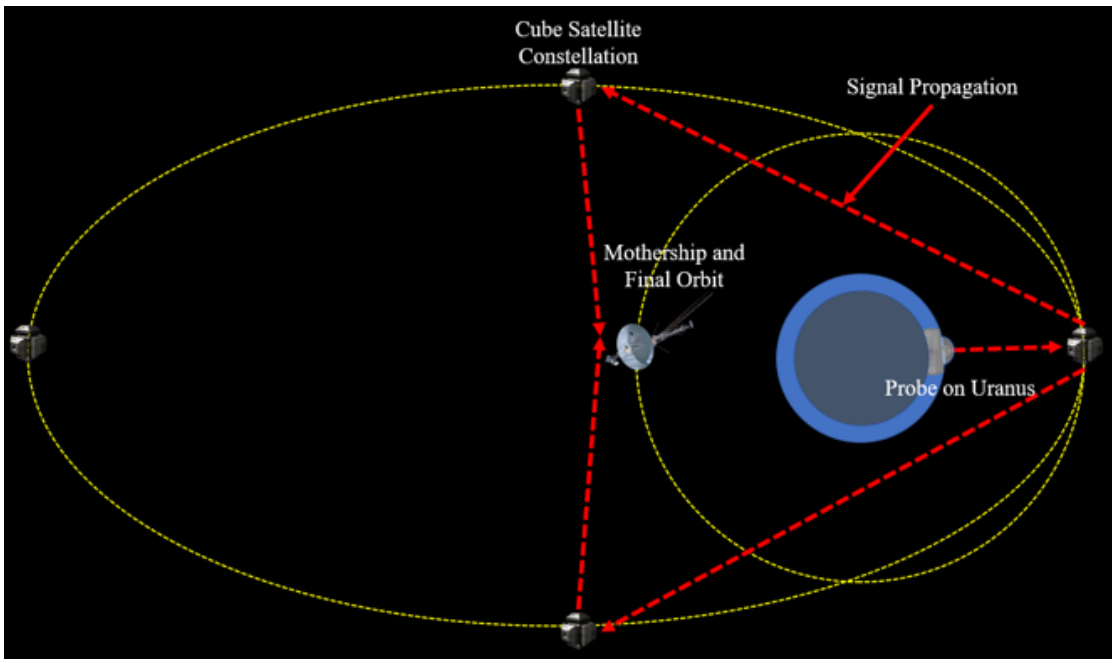
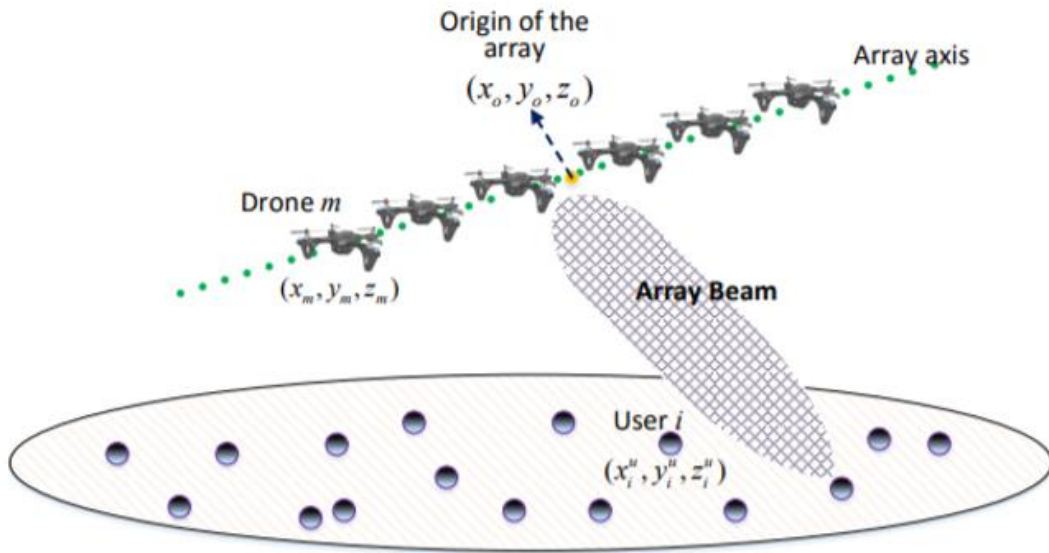


Figure 1: Drone Array/Satellite Array Rough Analogy [3].

5. Launch systems that allow for anywhere from ten to 100 times the payload capacity to be sent to Uranus than was previously possible.

These new technologies will be combined on one mission set, will come together in one design reference mission that provides orders of magnitude greater capabilities than anything previously accomplished, and can be replicated on future missions to other celestial bodies, including but not limited to Mars, Neptune, Jupiter, and Saturn.

1.2 Thesis Objectives

The objectives of this thesis are manifold, but they can be mostly whittled down to the following points:

1. Attain greater fidelity with respect to atmospheric models developed in the scientific community, not simply for Uranus, but also for those of the Earth and other celestial bodies. These models will include temperature lapse rate models, electromagnetic transmission models, molecular composition models, pressure gradient models, and more. Much needed edge-case data will be gleaned from the execution of the proposed mission, but also from the theoretical models derived in this thesis. These data would be utilized especially in GPS tracking, building more robust aircraft and spacecraft, and discerning human potential acclimatization and survival in potentially more extreme environments, among other things. To that point, a detailed model will be developed, covering the atmospheric attenuation of various signal frequencies in the Uranian atmosphere, and how to relate it to the Earth's. This model will incorporate Doppler and collision broadening modelling aspects, which will yield a method by which such models may be estimated for future work.

2. Developing a system that can sustain exceptionally high pressures while being both versatile and relatively lightweight is perhaps of important utility to not only the scientific community, but also to the Department of Defense [4].

That is, it is far less of an issue to make a machine that can survive in extreme pressure and temperature environments, but how to do so in a lightweight manner is another question entirely. The Uranian atmosphere is roughly equivalent to a very warm, deep-sea diving environment, with tropospheric surface pressures approximating 100 meters below the surface of Earth's oceans [4] [5].

3. Greater fidelity provided for the construction of particular equations, which harkens back to more accurate atmospheric models. These Equations will be outlined later, but in particular:
 - a. The hypsometric Equation showing the standard pressure lapse rate as elevation above the surface increases, has discontinuities where various atmospheric layers appear (refer to Figure 2 below to see an example). It is not known precisely what causes these atmospheric layers to develop, how thick they should be, where they should be, or really anything on the matter; their general likelihood of development is known only through empirical data and not through rigorous scientific pattern. All that is known are ways to estimate the atmospheric layer's characteristics. A working hypothesis is that it has something to do with the interaction of the various atmospheric constituents and the structure of the molecules themselves.

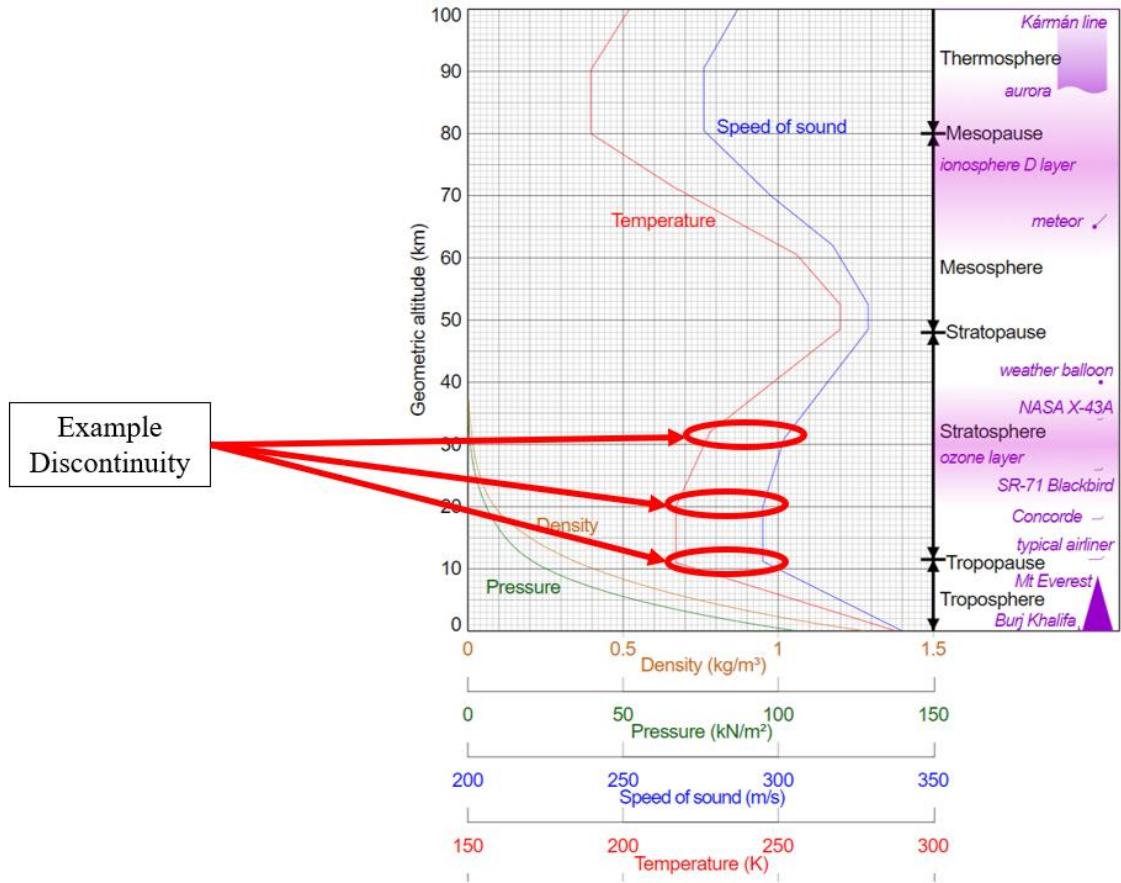


Figure 2: Earth Atmosphere Discontinuities.

- b. The Atmospheric Density Equation and why scale heights vary the way they do, despite mountains of empirical data, is not fully understood. This is because that data is mostly exclusive to the atmosphere of Earth, which has very specific, mostly unwavering parameters of temperature, pressure, mass, density, and volume among other bulk characteristics. With more data on aspects of another dense and thick atmosphere that extends far out beyond the tropospheric

base,² how these components affect atmospheric evolution can be explored. One way or another, Uranus has a completely divergent atmosphere from that of Earth; it is far more massive, less dense, distended, and varying in temperature. This is highly valuable edge-case data.

- c. The atmospheric surface temperature equation, used for determining the greenhouse capacity of celestial bodies—in particular, Mars—would have more valuable edge-case data to improve its fidelity.

Many of these Equations have not been significantly re-examined in decades. Being empirically derived with very few data points beyond Earth to utilize as the reference, the Equations could very well be refined.

4. Discern potential habitability in extreme conditions, providing more resolution to the extremophile extraterrestrial life hypothesis, that life can evolve and exist in environments well beyond normal human survivability. Data on this concept, especially if life is discovered in the Uranian ocean, would provide a bridge. Observing the differences these creatures may have from humans, and adapting human beings with both physiological and technological improvements would be a possibility [6]. This could provide greater purpose for military experimentation with respect to high-pressure diving, and other circumstances that require extreme pressures.

² Meaning a large amount of gravitational variation throughout the bulk of the atmosphere.

5. Greater fidelity on what is considered the Goldilocks Zone in astronomical sciences [7]. This has been partially discussed in some of the author's own most recent works where conditions for a habitable planet, just inside the orbit of Uranus, were described [8].
6. Provide a reasonable design reference for new technologies. This thesis will show theoretically how improved power generation, data collection, data storage, communications relays, and an extraterrestrial satellite array can work together seamlessly, and provide orders of magnitude greater mission effectiveness than any other mission to the outer Solar System humanity has ever conducted.

Table 1: Objectives Summary [9].

Thesis Objectives	Objective Breakout	Result
Atmospheric Modeling	-Radio communications -Temperature lapse rate -Pressure lapse rate	-Data transmission through Uranian atmosphere at 100+ Mbps. -5,000-km-thick atmosphere to observe and test. -Uniform atmosphere/minimal constituents minimizes variables.
Application of New Technological Concepts	-New comm antennas. -New SRTGs -New launch vehicle -New data storage devices -Extraterrestrial comm array concept -Higher frequency data transmission	-10+ Mbps data transfer rates seen at Earth. -16x more power than ever generated from an interplanetary space mission. - 1×10^6 times more data storage capacity than ever before. -First-ever true satellite array in the outer Solar System. -Data transmission at 100 GHz.
High-Pressure Environment Analysis	-Submersible probe -Various scientific instruments	-Largest probe ever sent to another planet. -Largest ever interplanetary submersible probe. -Most capable probe ever sent to another planet, a full SRTG onboard.
Performance Analysis	-Efficient travel to Uranus. -Improved equations and calculations.	-13 years to reach Uranus using Jupiter gravity assist. -Temperature Equation for Uranus.

1.3 Problem Statement

Determining the potential of sustaining human life in extreme environments, and the economic viability of ferrying human beings to said environments, is an integral part of the military's strategic interests, especially considering that future frontiers in space

and a developing space economy will both require and possibly compromise the U.S.' dominance of space [10]. More specifically, two of the Lines of Effort of the National Space Strategy are to:

1. Promote responsible, peaceful, and safe use of space.
2. Provide improved U.S. space capabilities.

Determining the varying pressures, temperatures, and atmospheric compositions of those environments, as well as ΔV 's to get to said environments, cost of new launch vehicles, and thorough data collection upon arrival, provide a "global" approach to maintain state of the art innovation and situational awareness for today's military force, as well as the burgeoning U.S. Space Force (USSF) [11].

II. Literature Review

2.1 Chapter Overview

In this chapter, background research will be surveyed on the many seminal space missions to various bodies in the Solar System, that shared at least some characteristics represented in this proposed Uranus mission design. Concepts such as probe and lander design, subsystem trades and capacities, launch vehicles accessible and utilized, travel time, and general memorable mission history will be explored. Specific topics discussed will be:

1. The scientific objectives of each mission. For brevity, only the highlights will be considered.
2. Flight path and time of flight, as well as propellant requirements. This will also include overall feasible payload capacity upon arrival at the destination in question.
3. Probes and/or landers involved in the mission, as well as major subsystems and their capabilities.
4. The radio frequency bands used to transmit data to and from the mission location. This will also lead to elaboration on the antenna system.
5. Overall telecommunications capabilities of the various missions.
6. The command and data subsystems, which include data storage, telemetry, and more.
7. Elaboration on the power subsystems of each mission, their capabilities, and how they compare to other missions and their budgets.

Some of this was briefly alluded to in the previous chapter, but it bears further clarification. Missions will be discussed/explored in a chronological order for those missions that have already taken place or are currently taking place, and proposed missions and reference missions will be discussed after. Beyond this, a discussion on the orbital dynamics methods used, and the background of their development will be accomplished. How the utilization of patched conics in order to at first estimate required thrust and travel times to reach Uranus led to a starting point for in-depth orbital dynamics models articulated by advanced computational methods all required a great deal of seminal work to elucidate upon said methods' accuracy and viability. This will also include discussion on gravity assist maneuvers and how they were established. The background of those methods will be explored. Additionally, a survey of background information on Uranus itself will be conducted. Basic statistics, such as orbital velocity, inclination, planetary size, location in the Solar System, and more will be explained. The implications of these immutable characteristics of the planet on mission requirements will be discussed, transitioning to actual numbers in the following chapter.

2.2.1 Mariner II through IX

Back in November 1964, at the dawn of the golden age of space exploration for humanity, the U.S. launched the first ever successful mission to another planet that could now potentially be seen for many reasons as a rough analog—or at the very least, a mission that tested many applicable design concepts—to a mission to Uranus: the Mariner series of missions. This primitive, first-ever attempt at such a Herculean feat had

four primary system objectives that needed to be met in order for the mission to be successful, or at the very least even possible:

1. Structural weight needed to be minimized.
2. Subsystems needed to be able to perform their functions during flight and interact properly with other subsystems.
3. Spacecraft ground tests and operations needed to be accomplished in a safe and timely fashion.
4. Subsystem compromises needed to be minimized.

These bare-bones requirements continued through the entirety of the Mariner missions. Now, those same requirements have developed so far as to go without saying, but at the time explicit clarification was necessary. The way Mariner 3 accomplished these requirements however, was particularly creative considering the limitations of the time.

The Mariner 3 spacecraft had a payload capacity of 260 kg. This was while being launched on an Atlas-Agena D rocket, to reach a distance approximately a tenth that of Uranus—a Mars flyby. The spacecraft itself was stored within a 1.65m (65-inch³) diameter shroud at the top of the rocket. With a travel period of 29 days the overall travel time stood at roughly 1/6 the time it would take the shortest proposed manned space flights to Mars, and a whopping 156 times shorter than the 13-year minimum expected flight time to reach Uranus [12] [13]. Since all the Mariner missions were merely flyby's, no onboard propellant was required for the trip specifically for orbital insertion, though a

³ Imperial units are provided for launch vehicle fairing dimensions due to the continued prevalence of this system of measurement in the launch vehicle industry.

hydrazine monopropellant for midcourse corrections was present in the form of a 222-N, 4-jet vane vector motor installed on one of the sides of the octagonal structure.

Power was supplied by a four-panel solar-cell array, with each panel being 1.58 m² in size. They provided 310 W of power at Mars. A rechargeable 1,200 W-hr silver-zinc battery was also used for maneuvers and backup power. With dual, S-band 7-W triode cavity amplifier/10-W traveling-wave tube amplifiers and a single receiver which could send and receive data via the low- and high-gain antennas, these solar arrays provided ample power for communications. In fact, maximum power draw from all subsystems combined was never observed to exceed 200 W. Data transmission happened at a rate of 8.3 bps for the low-gain antenna, and 33.3 bps for the high-gain antenna (HGA). The HGA was 1.22 m (4 feet) in diameter. Data was stored on a tape recorder with a capacity of 5.24 million bits. This allowed the storage of 21 pictures at a time for later transmission back to Earth.

For this relatively near-Earth mission,⁴ a three-axis stabilization system using twelve cold nitrogen gas thrusters was implemented, keeping the four solar panel arrays oriented towards the Sun. With an antenna transmission beam width of approximately 88 degrees, this was more than sufficient [14]. To simplify manufacturing and fabrication processes and costs, Mariner 3 and 4 were built as identical spacecraft.

Mariner 5 saw a massive increase in overall power output, increasing available power from 310 W up to 555 W. This was mostly due to the closer proximity to the Sun as per its mission set that required it to do a flyby of Venus, as its solar panels were in

⁴ At least relative to a Uranus mission.

fact somewhat smaller than those of the previous missions. It had four panels totaling 4.09 m^2 , as opposed to four panels on the previous missions totaling 6.54 m^2 . Its overall size was essentially the same as the Mariner 3 and 4, with a height 1 cm greater, and a mass approximately 14 kg lighter. There were no changes to the data rates, and more or less all subsystems remained the same.

Mariner 6 and 7 saw a large increase in overall mass and power consumption, moving up from approximately 260 kg to 414 kg (an increase of 60%), with a power output capacity of 449 W (an increase of 164%). The increase in power was accomplished with 7.7 m^2 of photovoltaic cells, which provided up to 800 W of total power at Earth. Three probes were constructed for the mission, with two meant to fly and one used as a spare in the event of a mission failure. Both successful launches were accomplished aboard Atlas Centaur rockets. Communications were accomplished on three separate channels, designated A, B, and C. A channel transmitted engineering data at the same rates as Mariner 3 and 4, but channel B carried scientific data that was transmitted at much higher rates of 66.6 bps or 270 bps depending on utilization of either LGA and HGA in unison or not. Channel C transmitted data at 16.2 kbps [15]. This was an increase in data rates of nearly 50,000%, though nominally data rates increased only by a factor of four in the transmission of scientific data. This was accomplished with transmitters operating at higher output powers of 10 or 20 W [16], as opposed to the 7-W transmitters of Mariner 3 and 4. Mariner 6 and 7 still used tape recorders to store data, but at much higher density than Mariners 3-5. Data density increased from 5.24 million bits of storage up to 195 million bits of storage, an increase of approximately 3,600%.

From there, the program moved on to Mariner 8. Its intended mission was to orbit Mars rather than accomplish a flyby. This was feat that required much more propulsion for orbital insertion. However, due to oscillations in the upper stage of the launch, the spacecraft re-entered Earth's atmosphere 1,500 km from its launch location. Nevertheless, its mass again more than doubled, weighing in at 998 kg, an increase of 140% over the Mariner 7 and 8, and 285% over Mariner 3 and 4. Power available again jumped up, this time from 449 W to 500 W, an increase of 11%. These spacecraft used newer, 20 Amp-hr, nickel-cadmium batteries. En route propulsion was provided by a 1,340-N gimbale engine, capable of up to five restarts. This was a 500% increase in total propulsion capability, undoubtedly necessitated by the drastically increased spacecraft mass. Again, maximum scientific data transmission rates vastly increased up to 16.2 kbps. This was an increase of 6,000% on those specific data's relay back to Earth. Due to the storage media being changed to a single 8-track tape, data storage capacity slightly decreased to 180 million bits, a decrease of 8%. However, this was at the tradeoff of several newly available playback rates of 16, 8, 4, 2, and 1 kbps, with a maximum recording rate of 132 kbps.

Mariner 9 was identical to Mariner 8. However, its mission was successful, achieving orbit of Mars on 14 November 1971, beating out the Mars 2 Soviet probe by six months. It successfully returned 7,329 images over the course of its mission, which concluded in October 1972. The Mariner program concluded with Mariner 10, the first ever spacecraft to perform a gravity assist in order to perform flybys of multiple planets. It accomplished this feat by using Venus to bend its flight path and bring its perihelion

down to the level of Mercury's orbit. Launched on 3 November 1973, approximately two years after Mariner 9, it would conduct flybys of Mercury and Venus.

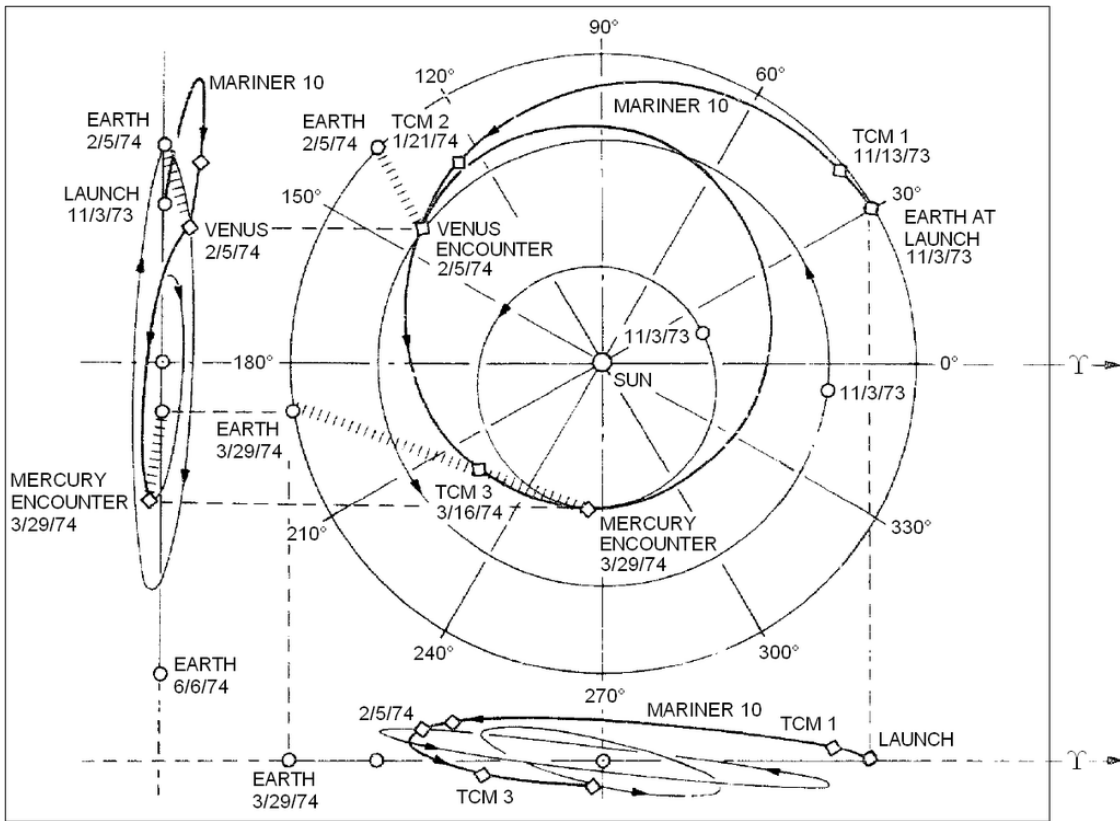


Figure 3: Trajectory of Mariner 10 Spacecraft [17].

Due to the complexity of Mariner 10's flight path, it required a dramatically increased propellant payload. This decreased its overall mission mass to 473 kg, a reduction of 53% from the previous pair of spacecraft. Most of the spacecraft subsystems were pared down in order to allow for this feat, but this did not include the data transmission. Telecommunication data rates increased from 16.2 kbps up to 117.6 kbps, an improvement of 726%. Telecommunications were conducted on S- and X-band frequencies, nearly matching data recording rates of 132 kbps [17]. Data storage remained the same at 180 million bits, on the same 8-track tape. The power subsystem

required between 340 to 490 W, and used the same nickel-cadmium batteries for power storage as its predecessor. Mariner 10 was the culmination of a nine-year program. The Mariner series of missions saw the first ever flyby of another celestial body, and concluded with the use of complex orbital dynamics and highly refined subsystems, ultimately paving the way to the next program, Viking.

2.2.2 Viking I and II

Launched on 9 September 1975—two years after the launch of the final Mariner mission, Viking I sought to accomplish something that had never been done before by the U.S.: land on the surface of another planet and conduct highly complex and precise scientific experiments [18]. The Viking I mission accomplished this by having both an orbiting spacecraft and lander working in tandem, in order to collect data, and relay it back to Earth at reasonable rates.

Launched on a Titan/Centaur rocket in 20 August 1975, and after an 11-month cruise to the red planet consisting of five major phases (launch, cruise, orbital, entry, and land—shown in the figure below), the orbiter began returning images of Mars about five days before orbit insertion, finally inserting into orbit on 19 June 1976.

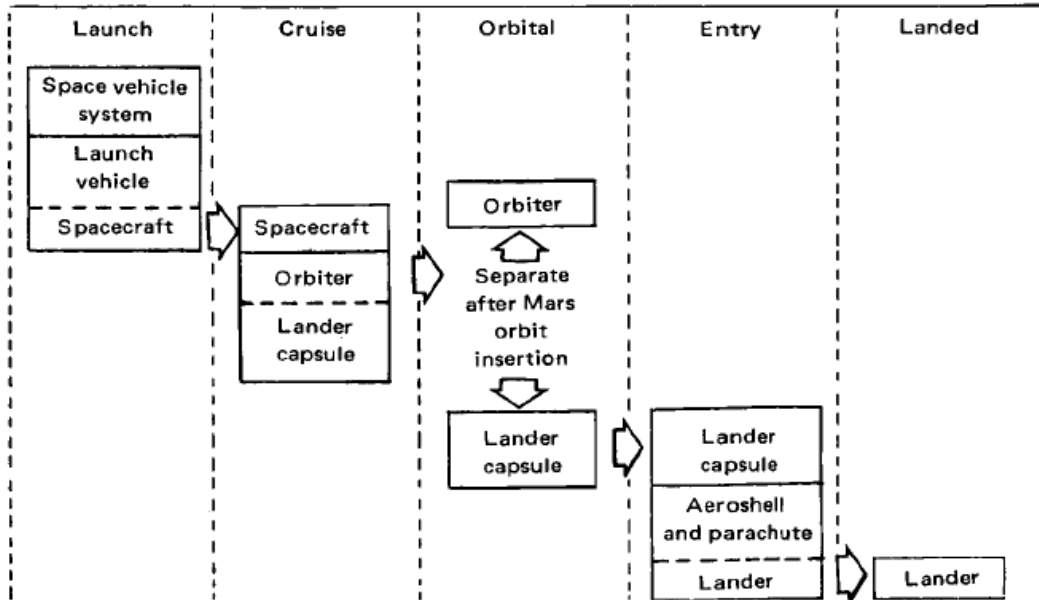


Figure 4: Five Mission Phases Functional Parts [18].

Sitting at 885 kg for the orbiter and 573 kg for the lander, the Viking I was a titanic spacecraft system, especially when compared to its predecessor, the Mariner 10. Mariner 10, which at just over 454 kg was dwarfed by the Viking I system. Viking I's mass was an impressive 200% greater. The power subsystem to feed the colossal orbiter measured 16 m² in surface area, boasting an impressive 620 W of electrical power in orbit around Mars. This was an increase of peak power generation of approximately 40% from the Mariner program. Power storage was provided by two, 30-Amp-hr nickel-cadmium batteries, a 50% increase in capacity from those of the latest Mariner spacecraft. Telecommunications required two separate relays, one from the lander to the orbiter, the next from the orbiter back to Earth. Data rates achieved were between 4 and 16 kbps, essentially remaining unchanged from the Mariner 10 mission. This accomplishment itself was impressive, with the necessity of two relays as opposed to one

(Lander → Orbiter → Earth). Data storage aboard the orbiter had increased from 180 million bits up to over 640 million bits, an increase of 255%. This was also a much-needed improvement, as data could be sent between the lander and the orbiter for a much greater period, or up-time, than the orbiter relaying information back to Earth. Despite data relay rates from the lander to the orbiter only being capable of reaching a maximum of 16.2 kbps for engineering data, and 1 kbps for scientific data,⁵ those data would inevitably need to be stored with much greater frequency than in previous missions.

These engineering obstacles have direct, and strong, analogs to the mission proposed in this thesis. To that point, the power subsystem on the Viking probes utilized two, 13.6 kg RTGs, each providing 30 W of continuous power at 4.4 volts. Four wet-celled sealed nickel-cadmium 8 Amp-hr, 28-volt rechargeable batteries were also onboard to handle peak power loads [19]. No solar panels were implemented in the power subsystem of the lander, which would have required deployment mechanisms on a lander that had never previously been tested, adding yet more potential for mission failure.

With the amount of power provided by the RTGs, the lander could power two separate 20 W traveling-wave tube amplifiers (TWTAs). These amplifiers fed a two-axis steerable, parabolic HGA, and an omnidirectional LGA operating in the S-band. A UHF frequency (381 MHz) antenna provided a one-way relay to the orbiter using a 30 W signal. Data storage was on a 40 Mbit tape recorder, an increase of 525% more capacity than any mission up to that point.

⁵ A limitation created by the limited power capacity of the lander perhaps more than any other factor.

The total mass of the lander was 572 kg, including a 91-kg scientific payload. With 85 kg of propellant needed to descend and land upon the surface, the overall mass of the lander was initially 657 kg, with the mass of the orbiter upon insertion being 900 kg. Overall wet mass launched atop a Titan IIIE-Centaur rocket was 3,530 kg. The 304-day cruise to Mars was roughly 1/16th the length of travel proposed in this thesis in order to reach Uranus. Finally, the orbiter began its mission, on a highly elliptical orbit between 300 km and 56,000 km altitude [20].

The orbiter's telecommunications array utilized a 2.1 GHz S-band uplink, and two separate downlink transmitters operating with 20 W output power. Their frequencies were 2.3 GHz (S-Band), and 8.4 GHz (X-band) respectively. The orbiter's HGA was approximately 1.5 m (59 in) in diameter, capable of sending signals back to Earth that would be acquired at the 16 kbps rate stated earlier. Any data acquired by the orbiter's 71 kg of scientific instruments, or data sent to it by the lander, could be stored in its two tape recorders touting a whopping 1,280 Mbits of storage space. This was an increase of 20,000% over any previous data storage mechanisms. The only comparable storage device up to this point was that of the lander itself, at 40 Mbits of data storage. Power for the orbiter was provided by eight 1.57x1.23 m solar panels, two on each wing. The solar panels produced a total of 620 W of power at Mars, an improvement of 38% over Mariner 9, the previous U.S. orbiter to be sent to Mars. Power was stored on two nickel-cadmium, 30-Amp-hr batteries.

Viking II and its lander were essentially identical to those of Viking I. It also accomplished the same mission set as that of Viking I. Both the Viking I and Viking II landers boasted impressive service records, with the Viking I lander lasting 2,306 days

and the Viking II lander lasting 1,316 days before final contact. These two space missions touted the record for longest lasting craft to land on another world until May 2010, when they were finally surpassed by the Opportunity Rover.

2.2.3 Voyager I, II

Voyager I and II were ambitious missions, set to conduct a grand tour of the Solar System. They were launched back in 1977 within a three-year period that occurs once every 176 years when a unique alignment of Earth, Jupiter, Saturn, Uranus, and Neptune allows for the opportunity to visit all planets with one mission. These missions posed a number of challenges, namely:

1. The most complicated orbital maneuver sequences attempted up to that point would be attempted.
2. Using gravity assists from multiple planets.
3. Pushing the capability of precision timing and pointing accuracy to previously unmatched levels.

The mission presented in this thesis will require similar maneuvers, utilizing a gravitational assist from Jupiter, in travelling to the far reaches of the Solar System. Indeed, Voyager I and II are still travelling to this day. Having achieved interstellar space, they have spanned the greatest distance from Earth any man-made object has ever travelled.

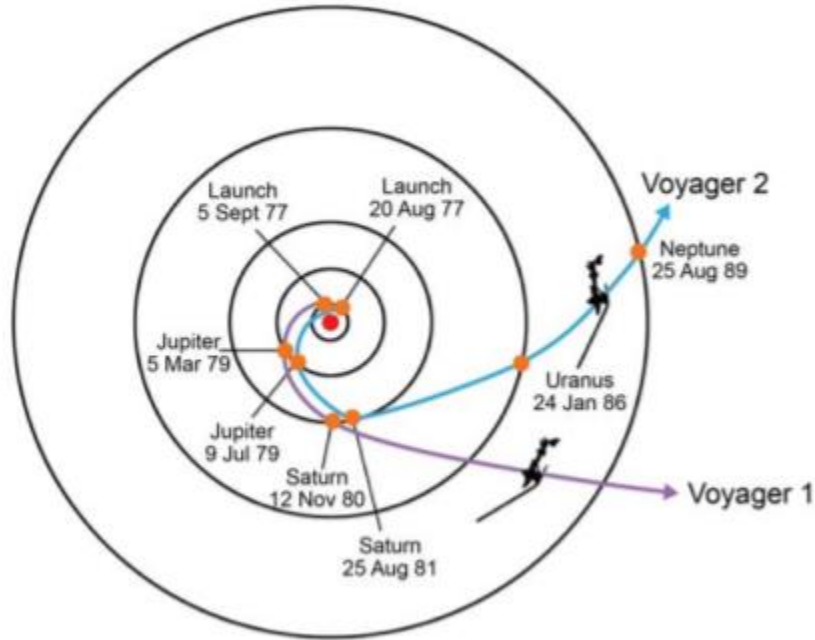


Figure 5: Voyager Flight Paths [21].

The data rates from the pair of Voyager spacecraft are constantly degrading due to space attenuation from their ever-increasing distance from the Deep Space Network's (DSN) antenna network. As of 2007 and 2011 respectively, their link capabilities were 7.2 kbps. The spacecraft each utilized a 3.7 m (12 ft) diameter, Cassegrain HGA, providing 48 dB of gain on a 22 W output signal (an increase of 10% from the Viking Orbiters), and transmitted on frequencies of 2.3 GHz and 8.4 GHz. The spacecraft's LGA provided 7 dB of gain. Any data that was stored was loaded into Voyager's 67 MB of space, provided by their digital tape recorders. This was an increase of 235% when compared to the Viking Orbiters.

Three separate RTGs provided power to the Voyager spacecraft, producing a total of 470 W of electric power at launch. As of 6 March 2020, Voyager I had about 71.5% of the plutonium-238 remaining that it had at launch, the power source within its RTGs [22].

This means it is currently producing a maximum of 336 W of electrical power. Voyager II produced roughly the same amount. This was a reduction of 24% in total power from the Viking missions due to the inability to effectively utilize solar panels. For missions travelling much beyond the orbit of Jupiter, power generation must exclusively come from RTGs, as the amount of energy from the Sun beyond Jupiter attenuates too drastically to produce useable levels of power. Though even at Jupiter, this was not the case at the time of the Galileo spacecraft's launch, which also used RTGs. For comparison, the mission proposed in this thesis will utilize between five and ten separate SRTGs, depending upon the final design selected. Both of the Voyagers' launch masses were 825.5 kg, launched atop separate Titan IIIE rockets. Due to the fact that the Voyager spacecraft ultimately would be travelling well beyond the edge of the Solar System, mission mass necessarily was reduced from the Viking missions by approximately 77%.

2.2.4 Galileo

Launched in October 1989 by the Space Shuttle *Atlantis*, Galileo arrived at Jupiter in December 1995 after gravitational assist maneuvers from Venus and Earth. A noncomprehensive list of Galileo's seminal achievements is as follows:

1. Galileo was the first ever spacecraft to orbit Jupiter.
2. Galileo launched the first ever probe toward/inside Jupiter.
3. Galileo achieved the first ever asteroid flyby, approaching 951 Gaspra.

Though perhaps the most publicly remembered element of the Galileo mission was not where it succeeded, but where it failed: it's HGA. Designed in an umbrella-like fashion, Galileo's HGA was meant to deploy upon its first flyby of Earth. The antenna

had 18 ribs, and when the driver motor started and put pressure on the ribs, they were supposed to pop out of the cup their tips were held in, deploying a massive 4.6-m (15 ft) diameter antenna that would provide approximately 50 dB of gain to any outgoing signal. Of the 18 ribs, only 15 popped out, leaving the antenna a lop-sided, half-open umbrella. It was concluded that during the 4.5 years that Galileo spent in storage after the 1986 *Challenger* disaster [23], the lubricant coatings between the tips of the ribs and the cup were eroded and worn away from vibration during three cross-country journeys by truck between California and Florida for the spacecraft. Through negligence and discontinuity of administrations, checking the lubricant coatings on the ribs was overlooked and not accomplished before launch. To fix this malfunction, engineers tried thermal-cycling the antenna, rotating the spacecraft up to its maximum spin rate of 10.5 rpm, and “hammering” the antenna deployment motor, but all attempts failed to open the HGA. This meant that all data transmission needed to be sent through the LGA, reducing any outgoing signal’s gain from around 50 dB, down to 7 dB, or a reduction of about 18,000 times.

The HGA was meant to transmit at 134 kbps, whereas the LGA was only intended to transmit at a maximum of 16 bps—or over 8,300 times slower. The LGA transmitted with a maximum gain of 10 dB, and upon reaching Earth would be attenuated by 170 dB. Through the implementation of sophisticated arraying of several DSN antennas, and sensitivity upgrades to the receivers used to listen to the Galileo signal, the data throughput was increased to a maximum of 160 bps. By further using data compression, the effective data rate could be raised to 1,000 bps. This was 16.2 times lower than that of the Viking missions, yet under the circumstances, a successful failure for Galileo. Despite

the dramatic reduction in Galileo's bandwidth available, 70% of the mission's science goals would still be met.

Onboard the Galileo spacecraft was the Galileo probe, meant to hurl through the Jovian atmosphere and conduct in-depth scientific measurements with greater fidelity and robustness than had ever been accomplished before. The Galileo probe separated from the main spacecraft and was launched toward Jupiter in July 1995, five months before reaching Jupiter. Once its 339 kg mass reached the planet, it implemented no braking beforehand, relying on the atmosphere itself to slow it down from 47 km/s to subsonic speed. This was accomplished in less than two minutes, burning away over 80 kg of its heat shield. From that point, the 4.3-m (14 ft) wide probe parachuted slowly through 156 km of the planet's many atmospheric layers. This descent lasted for 58 minutes, where it accomplished its atmospheric data collection objective, ceasing transmission once the ambient pressure reached 23 bar and temperatures reached 153° C. The data was sent via two separate L-band transmitters, operated at 1 kbps, back to the orbiter. These transmitters, along with all the probe's electronics were powered by two lithium sulfur dioxide primary batteries, which provided 580 W with an estimated capacity of 21 Amp-hrs upon arrival at Jupiter. This power source, only required for the probe's descent, provided 3 hours of power that was 8.3 times greater than the Viking Lander's' sustained 70 W RTGs. This is also a critical difference of the probe design in this thesis proposal.

This probe provided critical proof-of-concept work on the survivability of spacecraft systems when sent through extreme environments, both in temperature and pressure. While previous missions to other worlds had sent landers and orbiting satellites, gravitational slingshots and flyby's, the Galileo probe needed to survive intense winds,

scorching entry temperatures in excess of 15,500K (15,227 degrees Celsius)—only made possible by a heat shield designed to ablate as the probe descended, the intense gravitational pull of Jupiter at its nominal surface⁶ greater than 2.5 times that of Earth, powerful weather systems that included lightning and acid rain, and much more [24]. Had the probe lasted longer than an hour, it would have perhaps entered regions of diamond rain, liquid and metallic hydrogen, and pressures over 1 million bar. If pressure equalization were accommodated for, and temperatures were within a reasonable range for electronics to survive, perhaps through a super-cooling mechanism, the probe could have survived far greater pressure than what it experienced at its point of failure. Similar to the way whales survive thousands of bars of pressure when diving to the bottom of the ocean [25], this would indicate that the limiting factor was likely the temperature. The problem, then, is not the pressure itself, but equalization of pressure. This is a critical design element to be considered in this thesis. Equalization of pressure would prevent the structure from collapsing as the primary loads on them are due to pressure differentials across them. This may not be true for other components, such as semi-conductors, batteries, and more, but this can and will be addressed by other means.

In addition to the various seminal technological feats that the Galileo probe accomplished, it also further verified the feasibility and engineering capacity for near-autonomous satellite-probe/lander relays at vast distances from Earth. Also, while the Viking landers' telecommunications relays needed to penetrate through an atmosphere roughly 0.6% as dense as the Earth's,⁷ the effects of greater atmospheric densities on

⁶ Where the atmospheric pressure equals the surface pressure of Earth.

⁷ A pressure roughly equivalent to 100,000 feet above the surface of Earth [26].

such a relay could be extrapolated from the data gleaned. While they were not anticipated to be large hurdles to overcome, depending on the chemical makeup of the atmosphere, certain signal frequencies would not be usable. On Earth, those frequencies are roughly 20 and 60 GHz due to water and molecular oxygen bands [26]. Jupiter also has these water bands depending on altitude. Additionally, the atmosphere of Jupiter's primary constituents are molecular hydrogen and helium gases, at 23.4% and 15.4% abundances respectively. This is generally analogous to Uranus, having a molecular hydrogen abundance of 83% and a helium abundance of 15% as its primary constituents, though the difference in hydrogen abundance is vast. This is typical of protostars, something all the gas giants of our Solar System could be classified as, on the continuum of planetary to solar object compositions. While there are no known attenuation bands for molecular hydrogen or helium within the frequency ranges proposed in this thesis—or those of any missions discussed thus far—research on the manipulation of pressure, density, temperature, and composition of atmospheres and their effects on collision broadening and signal transmission at mission-critical frequency ranges is incomplete. The Galileo probe provided several more data points in this body of work. Some of hydrogen's spectral lines are shown in the graph below:

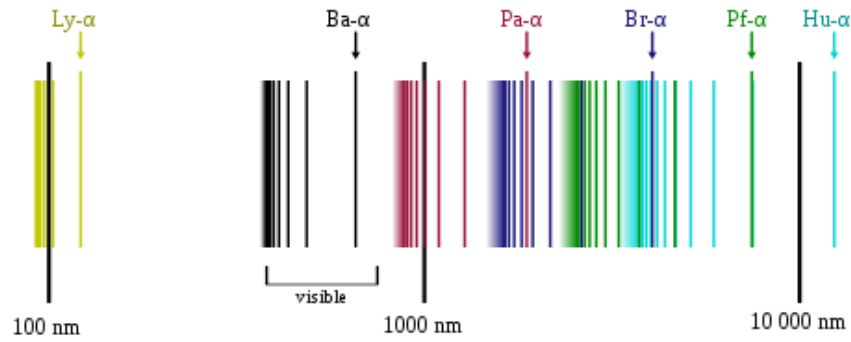


Figure 1: Hydrogen Spectral Lines, 100 nm to 10,000 nm (3 THz to 300 GHz) [27].

To continue, a true surface within Jupiter, or at least one that can be reached before a prospective probe would melt under the intense heat or crushed by the immense pressure, is not present. Had such an atmospheric base existed, the design of the Galileo probe would perhaps be yet more like the one proposed in this thesis. Additionally, yet more information on how higher pressures of Jupiter’s atmospheric constituents affected signal transmission and collision broadening would have been gleaned. Much work is yet to be done.

To compare, the surface of Uranus—measured at the base of its troposphere, the surface of its liquid ocean—experiences a pressure of 100 bar, and temperatures of roughly 40 degrees Celsius. Therefore, the final probe design will differ in several crucial ways from the probe proposed in this thesis. Principal among these differences is the mission duration. While the Galileo probe only lasted for just shy of an hour, the Chiron probe will be designed to last for many, many years. The pressures it will experience will be roughly five times that of the Galileo probe, but the temperature, measured in Celsius, will be roughly 33% less severe (423 K vs. 320 K). As stated prior, it is likely that the high temperatures of Jupiter were the limiting factor for the Galileo probe before the

pressure was, having conceivably overheated the electronics before they may have been crushed. To this point, based upon Mil Handbook 217F, failure rate of transistors doubles for every 40 degrees Celsius increase in temperature. The rates of failure have a much shallower change for increases in pressure [28].

At launch, the Galileo spacecraft touted a mass of 2,562 kg. This was 27% less mass than was launched for the Viking missions due to the far greater distance the spacecraft would need to travel in order to reach its destination. Additionally, compared to the Voyager spacecraft, Galileo was 210% more massive. Both the Space Shuttle and the Titan-class launch vehicles had much less launch mass capacity than the Falcon 9 Heavy for escape orbits.

Power generation aboard the orbiter was accomplished by two RTGs, each mounted on a 5-m boom, carrying 7.8 kg of plutonium-238. These RTGs provided the spacecraft and its 118 kg scientific payload with 570 W of electric power, a decrease of 8% from the Viking orbiters and an increase of 21% from the Voyager spacecraft, though much of this difference can be attributed to plutonium consumption en route. Had Galileo implemented solar panels, it would have taken 65 m² of them to provide the same amount of power. At about 2.1 kg/m² [29], this would add 136.5 kg to the overall mission mass, a truly miniscule “bang for the buck,” when compared to a 40-kg RTG. This is a 70% reduction in power subsystem mass. Though, it should be noted that 2.1 kg/m² is based upon modern designs. It is likely that it was slightly higher than this in 1982.

2.2.6 Mars Pathfinder

Seven years later, in December 1996, the Mars Pathfinder mission was launched toward the red planet atop a Delta II rocket. Consisting of a base station dubbed the Carl Sagan Memorial Station, and a lightweight roving probe, the first ever on another planet outside the Earth-Moon system, the mission reached its destination on 4 July 1997. There it would conduct scientific experiments and measurements of Ares Vallis, in a region called Chryse Planitia. With a launch mass of only 890 kg, this mission was far less robust, and therefore short-lived, compared to previous Viking missions to Mars, but included many new and innovative technologies. These were primarily the moving parts required to semi-autonomously operate a moving vehicle hundreds of millions of kilometers away. No standard operating procedures to do this had been created before, with both Viking landers being stationary and having scientific instruments with minimal range of movement. Criticized by many as being more of a novelty Mars mission than a scientifically extensive one, it nevertheless proved it possible to remotely operate such machines despite time lags of minutes to even hours between planets, a critical requirement for the probe proposed in this thesis [30].

Also of note, the Pathfinder mission was the first ever to use an airbag landing technique. This technique involved inflating several inflatable bags deployed from the exterior of the Pathfinder chassis just seconds before a parachute landing, and bouncing across the Martian surface for several minutes before settling in final position. The lander dropped from as much as 30.5m (100 feet) above the surface, and safely stopped without incident. This same technique was used for the follow-on rover missions, Spirit and Opportunity.

Part and parcel to the criticisms of the Pathfinder mission were the paring down of many subsystems. For instance, both the Sojourner rover and the Pathfinder lander were woefully underpowered when compared to Viking, with a mere 13 W and 35 W of electrical power respectively. These were 81% and 50% decreases from the Viking landers correspondingly. Due to the drastically decreased scientific payload mass on the lander of only 25 kg including the rover, this was all that was required. This was a reduction of 73% from the Viking missions, and 79% from that of the Galileo mission. The rover also had a battery capable of storing 300 W-hr of power.

This reduction in available power also significantly reduced the power that could be allotted to the telecommunications equipment [31]. This, combined with the spartan design of components led to a maximum output data rate of 11.06 kbps using an X-band direct link, a decrease of 92% from the designed capacity of the Galileo mission, and 32% from the Viking missions launched several decades earlier. The rover could store up to 4 MB of information in its random-access memory (RAM) and 64 MB of information in its mass memory storage. This was a reduction of 3 MB (4%) from the Voyager missions, but all of this was done on a shoestring budget of only \$265 million in 1997, for a mission that was 83% cheaper [32]. After accounting for 2% inflation per year over the two decades elapsed, the reduction in mission cost was even more drastic, with Pathfinder costs a mere 1/10 those of the Viking missions [1].

2.2.7 Cassini-Huygens

In 1997, the same year Pathfinder reached Mars, NASA launched the Cassini-Huygens mission [33]. This mission would carry aboard the first probe to ever land on

the surface of another planet's moon, Saturn's moon Titan. Titan is a giant moon, just under twice the size of the Earth's. It is the largest of Saturn's moons, and second largest moon in the Solar System. Titan has a gaseous atmosphere of greater volume and density than that of Earth's, and a pressure 1.4 times greater as well. This mission carried with it new and innovative technologies for the time, meant to peer into the very limits of human ingenuity and understanding of the universe. It explored some of the greatest depths of space science we could reach, and is perhaps the strongest analogy of all missions described to the one proposed in this thesis.

Though not the first, nor the only, space mission to ever reach Saturn and the other planets of the outer Solar System, this mission would explore in greater detail than ever before the Saturnian system. It spent over 13 years closely observing the majority of the planet's moons, its intricate rings, its many weather phenomena, and much more. With spacecraft subsystems refined by several decades of technological, engineering, and experiential improvements, the capabilities of the Cassini-Huygens' mission would extend this legacy of cutting-edge science and state-of-the-art design, while ushering in an age of collaboration between several space agencies. Indeed, the Cassini-Huygens mission was the first to be undertaken by NASA, ESA, and the Italian Space Agencies cooperatively.

Launched on 15 October 1997 using the Titan IV/Centaur launch vehicle on its 8-year trip to Saturn and Titan, the spacecraft had a mass of 5,712 kg at launch, by far the largest of any unmanned spacecraft launched into space to date [34]. Despite the much greater distance the spacecraft needed to travel to reach its destination, its mass was a whopping 123% greater than its next closest mission analog, Galileo. This was because

the Titan IV launch vehicle had a far greater dedicated planetary escape payload capacity than the Space Shuttle, since the Shuttle had to remain in low Earth orbit (LEO) and use a solid booster to push Galileo onto an escape trajectory. Cassini-Huygens would travel through space for six years, 261 days before reaching its destination on 1 July 2004. The voyage to Saturn included flybys of Venus, Earth, the asteroid 2685 Masursky, and Jupiter. The mission used gravity assists from Venus, Earth, and Jupiter, getting as close as 300 km to the surface of the respective celestial bodies. This increased the spacecraft's velocity relative to Venus up to 13 km/s.

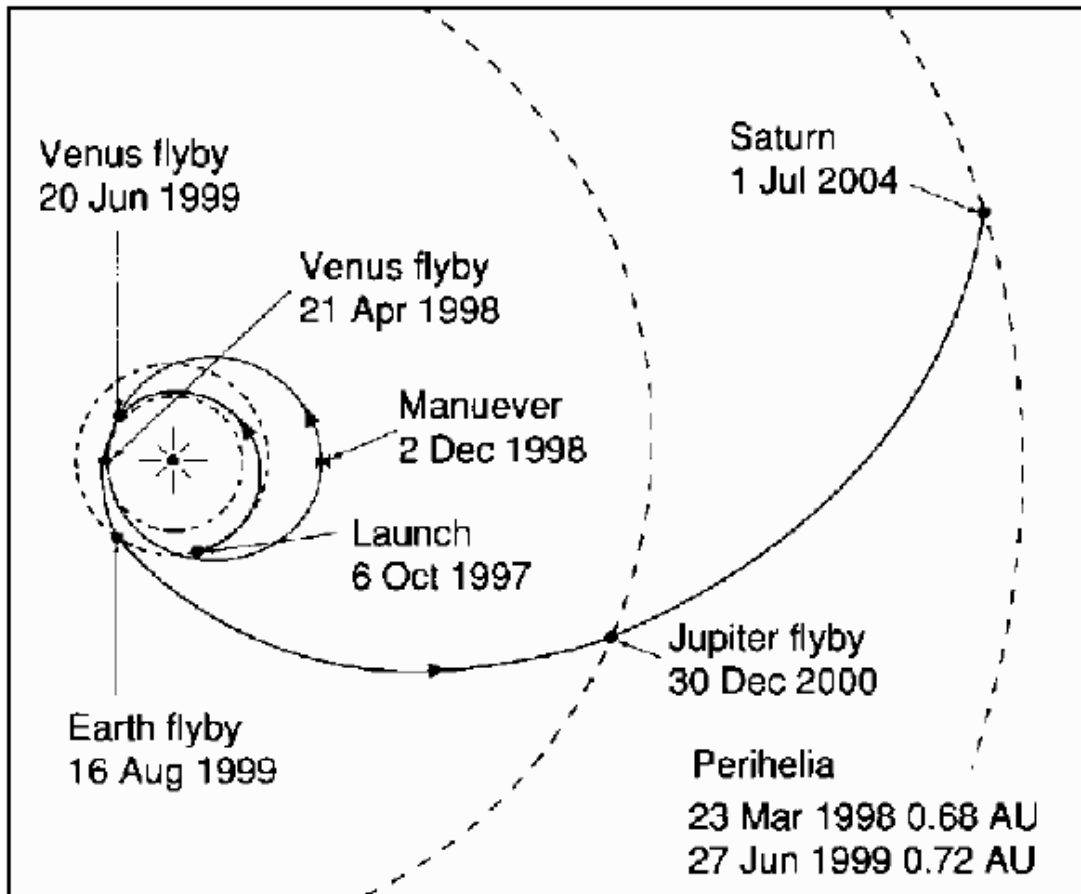


Figure 2: Cassini-Huygens Interplanetary Trajectory [33].

Cassini's mission involved many different scientific pursuits. Among them were the following:

1. Search for gravitational waves at opposition after the Jupiter flyby.
2. A flyby of the Jovian satellite, Phoebe, achieving a closest approach of approximately 50,000 km from the satellite's surface.
3. Hundreds of flybys of Saturn's giant moon, Titan, to include launch of the Huygens probe to pierce through the moon's atmosphere.
4. In-depth chemical analysis of the Titanian atmosphere starting at 160 km above the surface, over the course of a 2.5-hour descent.
5. Proof-of-concept of sending a probe through a dense atmosphere and landing on a surface.
6. Twelve scientific instruments carried by the orbiter alone. Total scientific payload mass was 365 kg. This was an increase of 210% over the Galileo mission.

Of the Cassini-Huygens' initial launch mass of 5,712 kg, about 2,700 kg of it was dry mass and 3,100 kg propellant. The large amount of propellant was a result of the many orbital maneuvers the mission required in order to accomplish all desired scientific endeavors and orbital changes; the Titan rocket only had the ΔV available to launch the spacecraft slightly farther than geostationary orbit. This was true despite the massive gravitational assists the spacecraft would receive from the interactions between Titan and Saturn, gravitational assists that would at least lower propellant requirements once the spacecraft had entered into the Saturnian system.

Cassini's propulsion system was modular, incorporating two redundant gimbaled 445-N engines with a specific impulse (I_{sp}) of 308 seconds. It used nitrogen tetroxide and monomethylhydrazine, with four clusters each containing four thrusters each providing between 0.2 and 1 N of thrust. The power and pyrotechnics subsystem (PPS) utilized three separate plutonium-based RTGs, providing 816 W of total primary power at the beginning of the mission and 641 W at the end of the mission. This was an increase over Galileo's mission of 12.5%, as the technological readiness level (TRL), refinement, and public trust in the systems' efficacy continued to improve. Additionally, three RTGs provided 50% greater power generation redundancy.

This greater electrical power capacity allowed for a yet stronger telecommunications relay between the spacecraft and Earth. Cassini could send over 7.15 and 8.425 GHz via its 4-m fixed HGA up to 249 kbps, an increase from Galileo's designed data rate of 86% [35]. Two transponders using redundant TWTAs provided 20-W radio frequency output. The HGA also had built-in Ka-, Ku-, and S-band transmit/receive capabilities.

The Huygens probe could deliver a maximum 250 W of electrical power via five LiSO_2 batteries capable of 1,600 W-h of energy storage. This was all that was necessary for the planned three hours of probe operation. The probe weighed a total of 320 kg. When compared to the Galileo probe, this was a decrease of 19 kg (6%), but on a mission 84% farther away, and with a mission to enter into the atmosphere of a moon at a much lower velocity (6 km/s as opposed to 48 km/s) with far less gravity (0.138 G's as opposed to 2.5 G's).

The telecommunications relays of the Huygens probe operated at a higher frequency than any other mission to date at 15.4 and 15.8 GHz, providing tighter beam width, and thus greater gain in signal transmission. With 10 W of transmitted power via 125x162mm (4.9 x 6.4 inch) planar antennas that provided +/- 57 degrees of beam width, the Huygens probe could achieve data rates of up to 16 kbps. This was 8,650 times the data rate achieved by the Galileo probe, allowing for not only transmission of atmospheric data, but also entire images of the descent [36]. At 640x480 resolution and 32-bit color, images usually are around 300 kB in size. Compression, reduction in color scale, and more, can lead to far smaller sizes. Over its three-hour lifespan, it sent over 175 MB of data up to Cassini, an accomplishment that could not have been attained without this marked improvement in data rate. Quick data transmission was also a necessity due to Huygens' limited data storage, only 20 kB. This alludes to the possibility of eventually sending streaming video back to Earth of the descent of a Uranian probe.



Figure 3: Huygens Probe Image of Titan Surface [37].

The attitude and articulation control system (AACS) provided at least two mrad of pointing knowledge accuracy through vibrating (nonrotating) gyros. The system used redundant MIL-STD-1750A flight computers, a technology originating in the 1980s and also used on platforms such as the Air Force F-16, the Navy's F-18, and the Army's AH-64D Apache Longbow Helicopter [38]. It has been inactive since 1997, replaced by newer designs. Generally speaking, modern commercial off-the-shelf (COTS) AACS can

provide far greater pointing accuracy, enabling far narrower beam width, and therefore higher amplification of signals transmitted back to Earth.

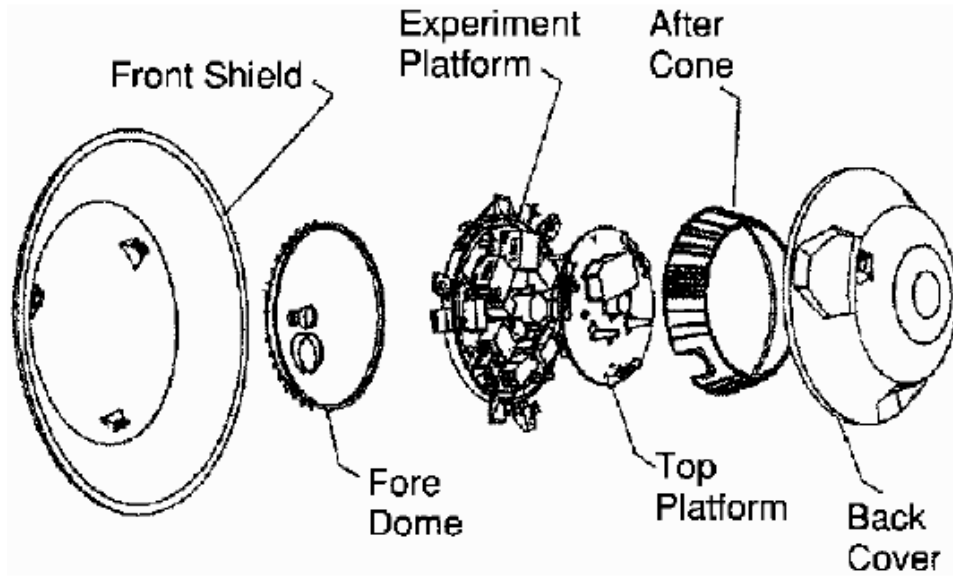


Figure 4: Huygens Probe Exploded View.

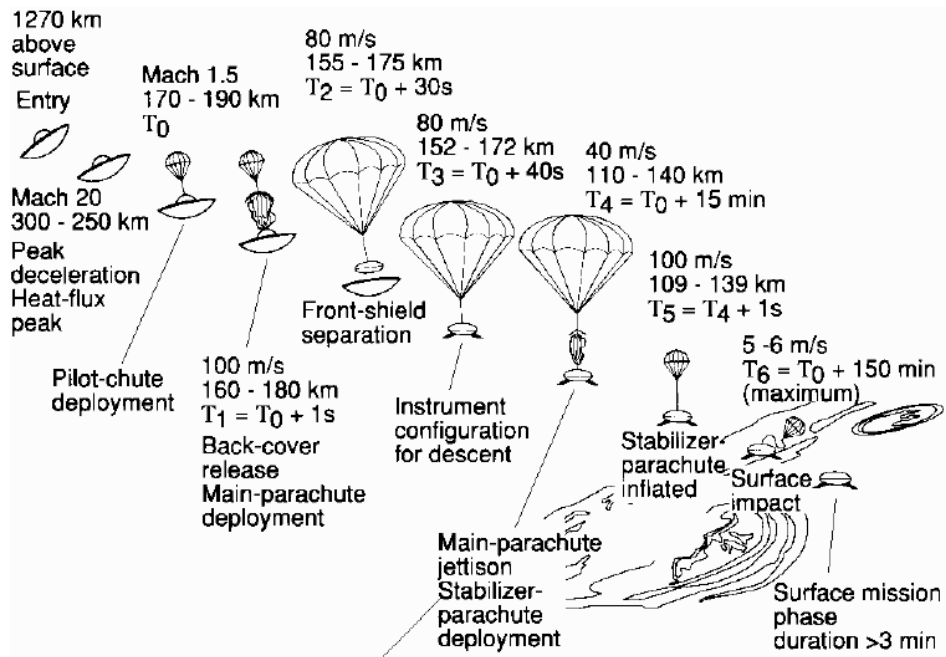


Figure 5: Huygens Probe Descent.

2.2.8 Uranus Pathfinder

The Uranus Pathfinder is the European Space Agency's (ESA) design reference mission developed to reach the ice giants of our Solar System. Developed in 2011, this document is in need of updating with dramatic improvements in all essential mission systems. The mission profile requires an orbiter to expand on the flyby science carried out by Voyager II, explained earlier in this section. Uranus Pathfinder is designed to be the first spacecraft to enter into orbit around an Ice Giant planet and undertake an orbital tour of said planetary system.

Telemetry, tracking and control is based around X- and Ka-band communications to ESA ground stations with telemetry data transfer rates of between 2 and 8.3 kbps. This assumes a 3.5-meter (11.5 ft) HGA with 30 W power input and 50% TWTA efficiency (15 W transmitted power) [31]. While TWTA technology typically yields a 20% power efficiency, this document lists a 50% efficiency as something that is feasible. All telemetry rates are subject to a 20% margin.

The overall proposed scientific payload mass would be 62.6 kg, and would draw 88.1 W of power when all systems were operating. Due to the large distance from the Sun, it would require over 700 m² of solar panels, weighing 1,470 kg,⁸ to produce this amount of power, so RTGs are therefore a requirement for power generation. Proposed power generation devices would produce 192 W of useable power, including margin.

The total dry mass of the proposed mission is 836 kg, meeting the launch capability of the Soyuz-Fregat launch vehicle with an 8% margin [39], a number very

⁸ Based on 2.1 kg/m² calculations shown earlier [29].

similar to that of the Mars Express mission. This is a design constraint that has been significantly eased with the Falcon 9 Heavy.

2.3 Patched Conics and Hohmann Transfers

Patched conics are a method by which the trajectory and amount of ΔV required to travel from one celestial body to another can be estimated with a relatively high degree of accuracy and robustness. This method involves dividing space into various parts by assigning each of the n bodies (e.g. the Sun, planets, moons, etc.) its own sphere of influence. When the spacecraft is within the sphere of influence of a smaller body, only the gravitational force between the spacecraft and that smaller body is considered, otherwise the gravitational force between the spacecraft and the larger body is used, also depending on the degree of mass difference between the bodies. This reduces the complicated n -body problem to multiple two-body problems [40]. In two-body problems, the solutions are well-known conic sections of Kepler orbits [41].

A good example of this was the Galileo mission, which required gravity assists from both Venus and Earth, and eventually settled around Jupiter. A hyperbolic escape velocity was required to escape first the gravity well of Earth, then the gravity well of Venus, and again the gravity well of Earth. The initial escape from Earth's sphere of influence required the development of an elliptic trajectory within the Sun's sphere of influence to transfer from the Earth's sphere of influence to that of Venus. Using Venus as a gravitational assist would mean that the velocity of Galileo would put it on yet another hyperbolic trajectory, but while within the sphere of influence of Venus, ΔV and trajectory calculations would be modified to suit Venus's sphere of influence. This idea

would continue until Galileo reached Jupiter, where it would slow down enough for orbital insertion. By patching all of these conics together and matching the position and velocity vectors between segments, the appropriate mission trajectory can be found.

2.4 Uranus

Uranus, the seventh planet from the Sun, orbits between 18.33 and 20.11 astronomical units (AU's), or between 2.7 and 3 billion km. This is an orbit that takes 84 years to complete. With a mass 14.5 times that of Earth, its gravity well makes it host to dozens of satellites. Notable among these moons principally for their relatively large sizes are Puck, Miranda, Ariel, Umbriel, Titania, and Oberon. These moons are also of significant scientific interest, with possible liquid oceans residing several km below their icy surfaces.

Due to the composition of Uranus' atmosphere being primarily helium, molecular hydrogen, and methane, it appears as a pale blue to the naked eye, and of all planets with atmospheres, Uranus' is the most uniform. Much like the giant moon Titan, Uranus finds itself in an interesting celestial regime. Due to its vast distance from the Sun, the planet does not experience extreme magnetic field sputtering of its massive, 5,000-km-thick atmosphere, nor does it experience extreme tides.⁹ Thus, the evolution of atmospheric gases, caused by the collection of colliding asteroids, outgassing from the planet's internal structure, and many other sources, whatever gaseous compounds that have reached the base of the troposphere remain for far longer than they would on almost any other celestial body in the Solar System.

⁹ These calculations will be expanded upon in later chapters.

Combined with a relatively stable internal structure that produces little heat (thermal flux) compared to other orbiting bodies—it radiates 2.61 times as much energy to space as it receives from the Sun—there is little in the way to disturb the growing uniformity of Uranus’ veil. Comparing this to Earth’s heat flux ratio of 1.06, and the difference becomes clearer [42].

To put this in clearer mathematical terms, if Uranus produced the same amount of internal heat as the Earth from its core, Uranus would experience a surface heat flux of roughly 1/16 that of Earth based purely upon its surface area. That is 16 times Earth’s heat flux. Combining this with an internal heat flux that varies with the cube of the radius of the planet, and with Uranus having a radius 3.91 times that of Earth, Uranus should further see a surface heat flux reduction of roughly 60 times, for a total combined reduction of 99.9%, or 1/960 the expected surface flux. Combining this with a solar flux that reduces with the square of the distance from the Sun, and Uranus should experience a solar flux 400 times less than that of Earth. This yields a ratio of 2.4, close to the 2.61 stated earlier. However, heat flux is expected to *increase* with the radius of a planet. Therefore, the heat generation should be 60 times that of Earth based purely upon Uranus’ radius. This yields an internal heat flux of 3.75 times that of Earth, and with the orbital distance,¹⁰ the difference between internal and solar heat flux should therefore be closer to 1,354. This kind of expected heat production from the internal structure of Uranus would necessarily lead to a perhaps far less stable hydrosphere and atmosphere. Through satellite observations, the stability of the Uranian atmosphere has been further

¹⁰ The mean radius of Uranus’ orbit is 19 AU.

verified. This stable aspect of Uranus is crucial for the development of the appropriate type of probe, with the appropriate instruments, to pierce Uranus' veil.

This also yields some truly astonishing possibilities with the planet that are not seen anywhere else in the Solar System. The most intriguing of these possibilities is caused by the relatively cool temperatures at the base of the troposphere. Based upon measurements conducted by the Voyager 2 spacecraft, the base of Uranus' troposphere is an astounding 320 Kelvin (47.2 °C). This is impressive for multiple reasons:

1. This temperature is within the range of being able to sustain human life on a planet that is 3×10^9 km from the Sun, albeit at very high pressures.
2. Additionally, it is paradoxical that this temperature is not lower considering the extreme distance from the Sun, looking at it purely through the lens of the planet's black-body absorption equilibrium temperature of space, which is approximately 65 Kelvin! Comparing that to Earth's black-body equilibrium temperature of 254 Kelvin at 150 million kms from the Sun, with a surface temperature of approximately 288 Kelvin, and we can see the stark juxtaposition [43].
3. From point (2), one can glean that the planet therefore appears to be host to its own internal Goldilocks Zone.

Yet another fascinating result of Uranus' Goldilocks Zone—which Neptune also appears to be host to, albeit at slightly higher G's and temperatures beginning to fall outside the range of human habitability—is that due to this high temperature at the base of Uranus' troposphere, Uranus' water "ices" are actually liquid water! That is, Uranus is a giant ocean planet occluded by a thick, distended atmosphere. This opens doors to new

possibilities with respect to human understanding of habitability zones, which seem to be contingent primarily upon the atmospheric evolution of a planet beyond a certain range from a host star. That is, closer to a host star of a Solar System, the star's radiated heat will be the primary determining factor of a planet's habitability, but farther out, it depends on the host planet's atmospheric and geologic composition.

Due to the way Solar Systems evolve, with heavier elements migrating towards the center of the Solar System—much like lighter liquids will float above heavier liquids when mixed in a vessel—Solar Systems automatically “sort” lighter molecular densities to the outer Solar System. This would indicate that planets like Uranus and Neptune are perhaps not terribly uncommon. Therefore, the science that is available to a mission sent to Uranus may provide immeasurable utility in the future. With any number of planetary characteristics even slightly modified, say changing the mass of an ice giant to 10 times that of Earth rather than 14.5 times that of Earth, could yield a planet with even more ideal habitability characteristics. Understanding that gravitational pull is what draws in and thickens an atmosphere, mass is the determining factor that leads to a powerful magnetic field when heavy metallic compounds are not present, which itself prevents atmospheric sputtering, and atmospheric thickness is what produces the insulation necessary for surface heating of sufficient levels for habitability. Thus, such a regime could lead to habitable planets completely outside the purview of what modern science understands to be possible. Uranus will provide a powerful frame of reference for future exploration and deeper understanding into this idea. The following table shows Uranus' principle characteristics, and an example of what could be possible if such a hypothesis were true. Comparing this to the profile of Uranus' atmosphere, and also considering that

proximity to a hypothetical planet's tropospheric base would lead to exponentially greater heating, one can gather deeper understanding into this concept.

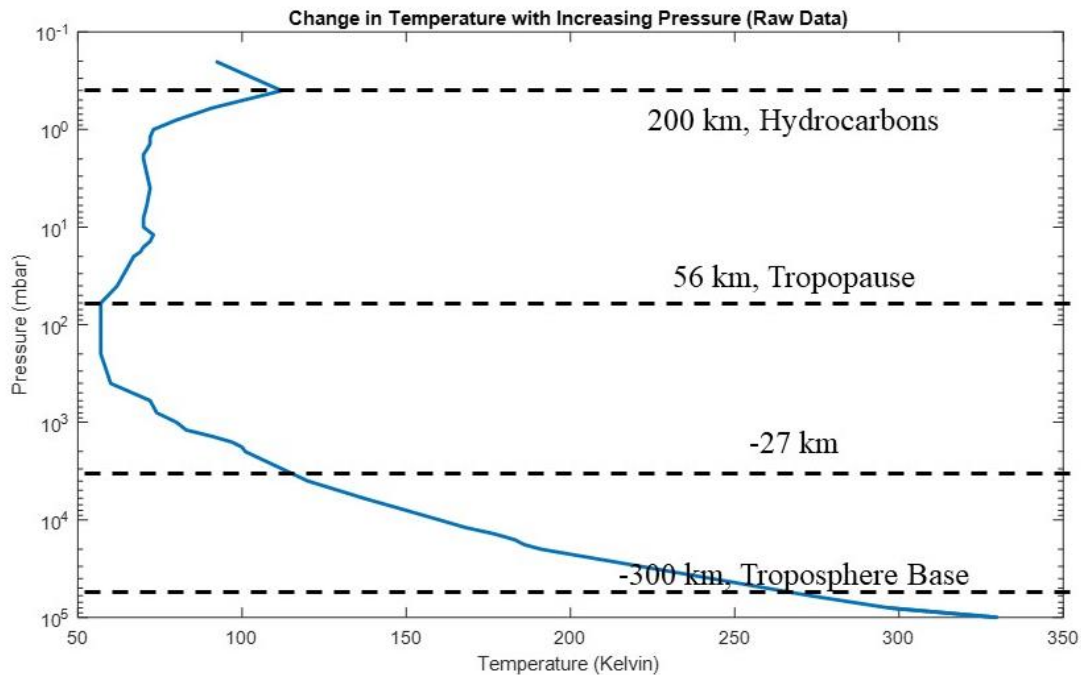


Figure 6: Uranus Atmosphere Profile.

All the scientific exploration that can be done on Uranus previously discussed notwithstanding, it continues to be a conundrum to atmospheric scientists today as to why and how certain atmospheric components interact the way that they do, and can lead to such disparate outcomes with respect to the final stable states of atmospheres despite what might superficially seem like situations where stable states should be similar. A prime example of this is the difference between Venus and Earth's final atmospheric state, or even Mars and Earth's final atmospheric state. With so many different variables that can be manipulated—from solar energy, to partial pressures, to gravitational pull, and much more—the theoretical signal transmission through various media is a field still ripe for greater exploration, and can illuminate the path for greater predictive capabilities.

This will be the primary scientific takeaway from the work done in this thesis, apart from the design reference mission update.

Table 2: Uranus Versus Hypothetical Planet.

	Uranus	Hypothetical Goldilocks Planet	Difference from Uranus
Equatorial Radius	25,559 km	20,000 km	5,559 km, 21.75% less
Mass	14.5 M _E	10 M _E	4.5 M _E , 31% less
Sidereal Rotation	17h12m36s (+/- 72s)	25 h	~7.75 h, 45% greater
Obliquity	97.77 deg	5 deg	~92 deg, 95% less
Semi-Major Axis	19.2 AU	19.2 AU	0, 0% difference
Dipole Moment	3.75x10 ²⁴ Am ²	x	X
Magnetic Field Strength	1x10 ⁵ nT	1x10 ³ nT	2 orders of magnitude less
Dipole Tilt	-59 deg	x	x
Dipole Offset	0.31 R _U (south)	x	x
Natural Satellites	27	30	3
Tropospheric Base Pressure	100 bar	30 bar	70 bar
Tropospheric Base Temperature	320K (47C)	297K (24C)	23K

Table 3: Mission Subsystem Improvements Summary.

Mission	Date	Subsystem	Capability	% Improvement
Mariner I,II	July 22, 1962; August 27, 1962	Data Storage	N/A	N/A
		Data Transmission Rate	0.00829 kbps	N/A
		Power Generation	220 W	N/A
		Launch Payload Mass	202.8 kg	N/A
Mariner III	November 5, 1964	Data Storage	--	N/A
		Data Transmission Rate	--	N/A
		Power Generation	300 W	36.3
		Launch Payload Mass	260.8 kg	28.5
Mariner IV	November 28, 1964	Data Storage	--	N/A
		Data Transmission Rate	0.033 kbps	298.1
		Power Generation	170 W	-43.3
		Launch Payload Mass	260.68 kg	No change
Mariner VI	February 25, 1969	Data Storage	195M bits	N/A
		Data Transmission Rate	16.2 kbps	48,990
		Power Generation	449 W	164.1
		Launch Payload Mass	411.8 kg	57.9
Mariner IX	May 30, 1971	Data Storage	180M bits	-7.7
		Data Transmission Rate	16.2 kbps	No change
		Power Generation	500 W	11.4
		Launch Payload Mass	558.8 kg	35.7
Viking I	August 20, 1975; September 9, 1975	Data Storage	640M bits	255.5
		Data Transmission Rate	16.2 kbps	No change
		Power Generation	690 W	38
		Launch Payload Mass	1458 kg	160.1
Galileo	October 18, 1989	Data Storage	912M bits	42.5
		Data Transmission Rate	Plan: 134 kbps Actual: 1 kbps	Plan: 727.2 Actual: -93.8
		Power Generation	1,150 W	130
		Launch Payload Mass	2,562 kg	75.7
Mars Pathfinder	December 4, 1996	Data Storage	512M bits	-43.9
		Data Transmission Rate	11.06 kbps	Plan: 91.7 Actual: 1,000.1
		Power Generation	48 W	-95.8
		Launch Payload Mass	890 kg	-65.2
Cassini-Huygens	October 15, 1997	Data Storage	1400M bits	173.4
		Data Transmission Rate	249 kbps	2,150.1
		Power Generation	1,066 W	2,120.8
		Launch Payload Mass	5,712 kg	541.8

Table 4: Mission Cost Percentage Change.

Mission	Cost (\$, infl. Adjusted, 2020 dollars)	% Change
Mariner I, II	1.75B	N/A
Mariner III	1.75B	0
Mariner IV	1.75B	0
Mariner VI	1.52B	-13.1
Mariner IX	451M	-70.8
Viking I	2.44B	441
Galileo	2.96B	21.3
Mars Pathfinder	281M	-90.5
Cassini-Huygens	5.14B	1,729.2 (Pathfinder)/73.6 (Galileo)

While due to the limited number of data points available in Table 4, one cannot draw any trends in the actual cost increase or decrease from one mission to another. Though, one thing can be discerned: generally, mission cost went up over time, with the exception of intentionally lean programs like Mars Pathfinder.

III. Methodology

3.1 Chapter Overview

This chapter will outline the thought process behind, and development of the scientific inquiries and changes to various designs proposed in this thesis. It will outline the design of the launch vehicle, the payload to include the probe, the purpose behind the various subsystem construction methodologies, initial design schematics, and scientific and mathematical model justifications.

The launch vehicle, SpaceX's Falcon 9 Heavy, was chosen for its vastly superior payload capacity compared to any other launch vehicles of the modern era, as of 2017. This has since been superseded by the development of the Starship launch vehicle, also created by SpaceX, though Starship is not yet operational. Despite this, design improvements remain valid, if not even easier to accomplish. This will be further discussed later in this chapter.

Also to be discussed is the design of the probe to be launched into the Uranian atmosphere. Specifics as to its size, shape, scientific payload, environmental tolerances, overall size and weight will be elaborated upon. The design of the probe is relatively similar to that of the current probe for the design reference mission, only much larger and with potential for far greater instrumentation. The figure following this paragraph shows a preliminary and notably rudimentary schematic. With the greatly expanded payload capacity of the Falcon 9 Heavy, a much better payload fraction can also be attained from the mission due to proportionally less propellant required to achieve Uranian orbit as opposed to Earth atmosphere escape velocity.

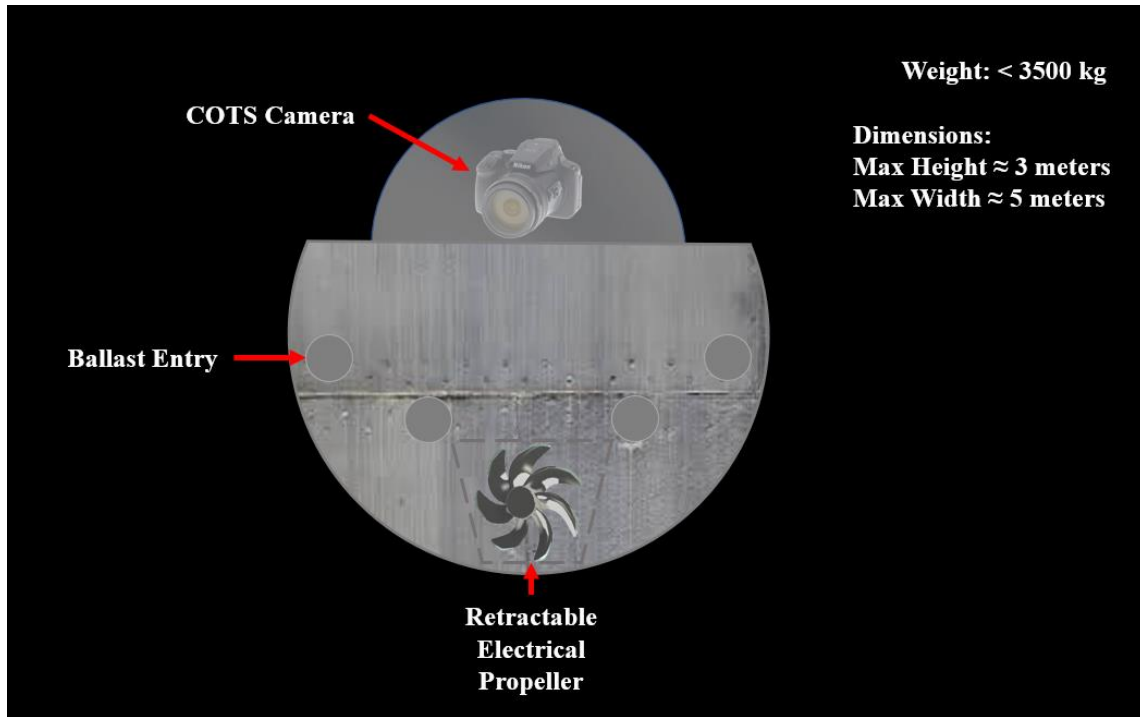


Figure 7: Initial Concept of Chiron Probe.

With the mission mass now being vastly increased, a constellation of satellites can be included, allowing for constant relay of data from the probe and back to Earth, with near 100% uptime. As discussed earlier, this also provides a proof of concept of such a mission construction. Each satellite in this constellation will have onboard its own Stirling-engine RTG (SRTG), producing enough power to keep said satellites operating for many decades.

And finally, the opus of this section will be an in-depth discussion on Doppler and collision broadening, how they will be measured within the Uranian atmosphere, and theoretical calculations thereof. A filtering algorithm was developed to produce a theoretical attenuation that could be expected depending on the input attenuation bands—which would be provided by an external data set, gathered from Uranian measurements and other sources—of a complex atmosphere.

3.2 Stirling RTGs

While SRTGs remain at a relatively low technological readiness level (TRL), new designs are developed and released to the public on a consistent basis. One such design that could be used for this design reference mission is the EU ASRG [44]. This model is compact, and relatively lightweight, boasting a 7 W/kg power density with a 40% efficiency power conversion.

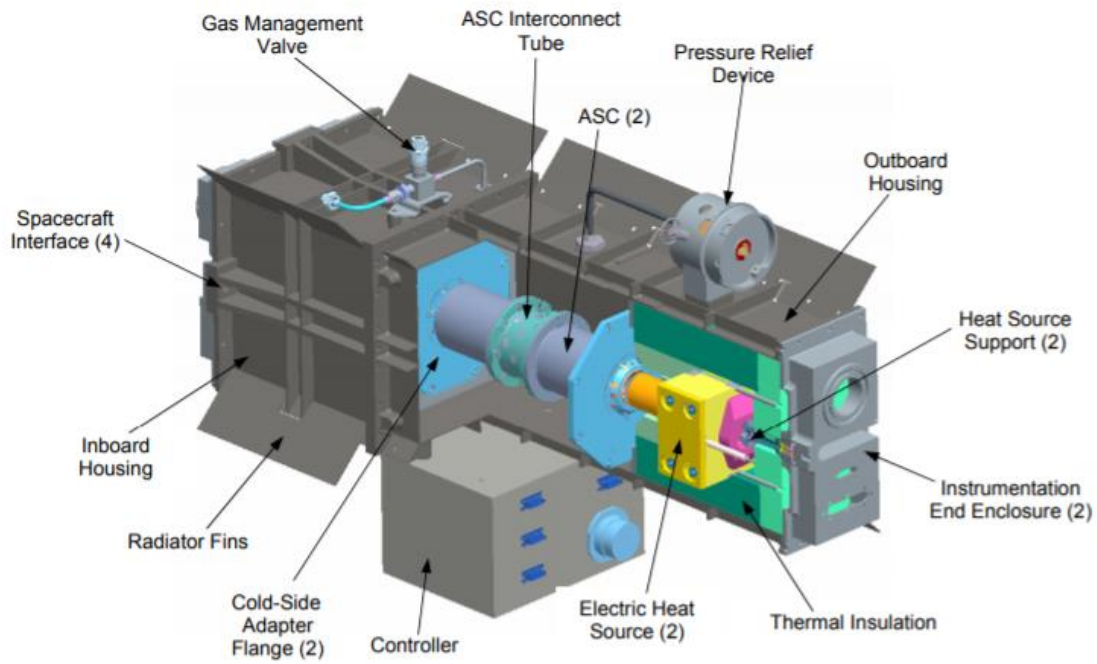


Figure 6: Sunpower Systems SRTG Schematic.

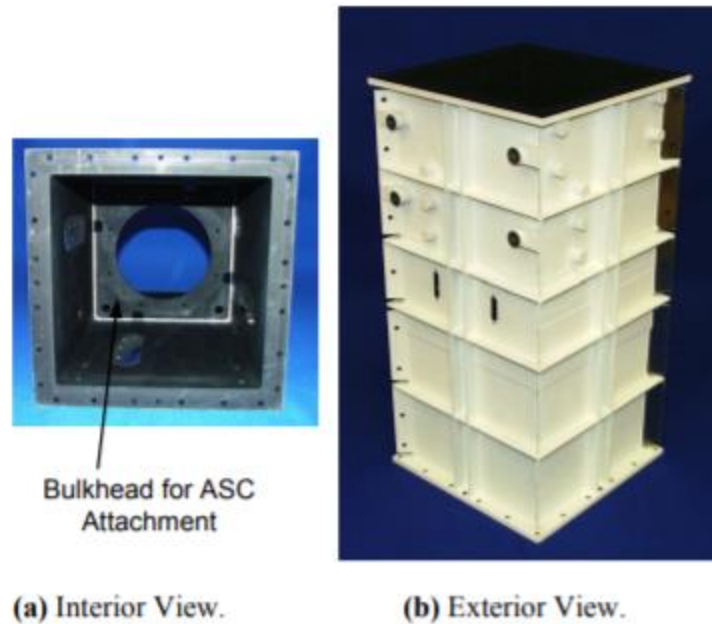


Figure 7: Engineering Scale Model of Stirling RTG.

This engineering model of an SRTG produces 140 W of electric power and 210 W of heat in a generator that can fit in a small satellite design envelope, but unfortunately, not a CubeSat envelope. Its dimensions are 73.4 cm in length, 45.7 cm in height, and 29.2 cm in width. The largest current cube satellite specification is 27U, or 34x35x36 cm. Therefore, this design is 2.3 times larger than the largest CubeSats. Part of what adds to the potential bulkiness of a SRTG is the Stirling piston system itself. A Stirling engine is a highly precise, machined metallic cylinder, made to move at high velocities with as little friction as possible.

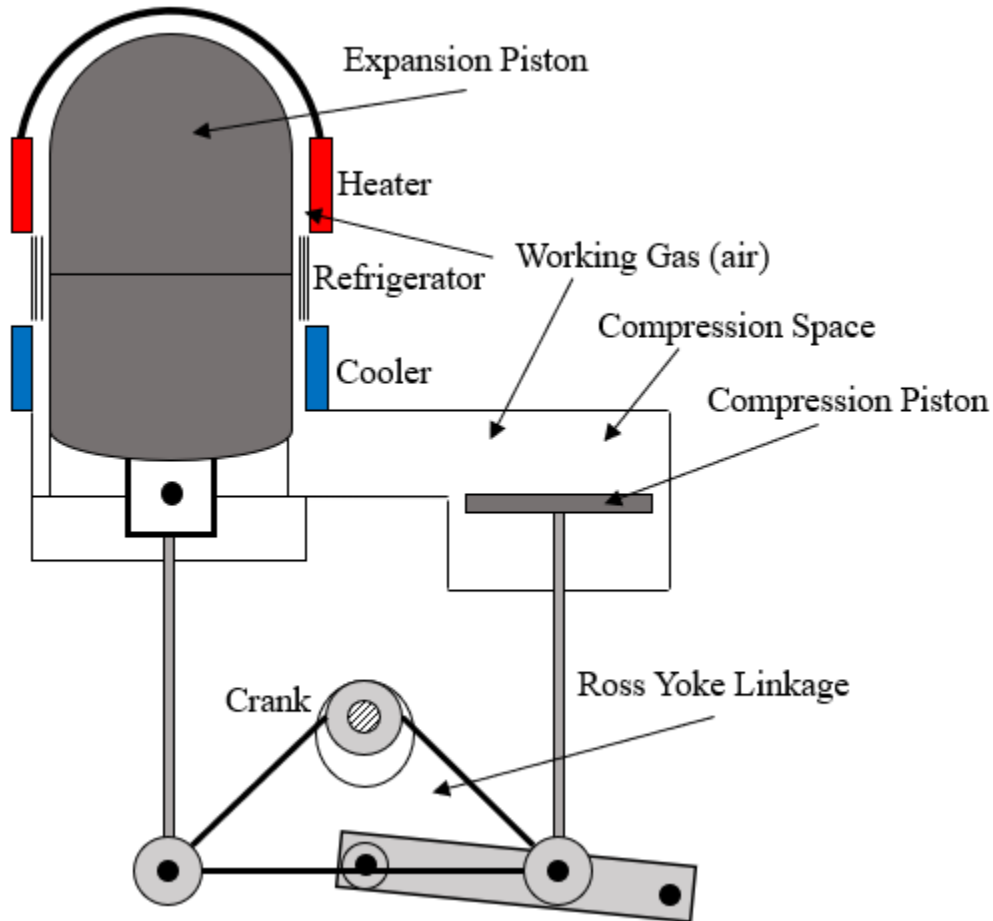


Figure 8: Schematic of a Stirling Engine.

The more precise the machining of the device, the greater the efficiency. The better insulated the device, the better the efficiency. That is, the more heat produced by the thermal process of the radioisotope that can be captured, the more of that heat differential can be used to alternate the Stirling piston. Using the vacuum of space and proper radiator sizing and coating schemes, the temperature differential can be maximized. Stirling turbines are a technology that on its own has been around for centuries, and therefore can be built efficiently, and with compact form factors.

3.3 Communications and Data Handling

The final chosen parameters of this design will be determined later, but for now, a few particular regimes were used for consideration. The chosen carrier frequency for signal propagation, both between CubeSats and back to Earth, was 100 GHz. This signal, if necessary, can be changed near Earth through orbiting satellite systems. Additionally, a transmitting antenna with a 6-meter diameter was selected. This is significantly larger than the Galileo spacecraft design of 4.8 meters [36], but considering the overall payload dimensions, mass, and fairing capacity, is well within the potential margin. In truth, using the most modern antenna design capabilities, it is possible to fit an antenna over 10 times this diameter into the space provided [45]. Considerations for this, however, are the pointing accuracy required with such a dish, and the mechanisms by which one may attain said pointing accuracies. Pointing accuracy, as a diffraction-limited Figure, can be derived as follows [46]:

$$Beamwidth = 70 \cdot \frac{\lambda}{D} \text{ (1)}^{11}$$

Where λ is the wavelength chosen in meters, and D is the antenna diameter in meters. The 70 is a number containing a scaling factor and a constant in order to output the final answer in degrees, rather than radians. The beamwidth, obviously, drives the pointing accuracy requirement. Therefore, pointing accuracy for this design is 0.035 degrees.

As can clearly be seen, increasing the antenna diameter drastically decreases the beamwidth. Nevertheless, there are mechanisms that are commonly used on spacecraft to

¹¹ Anywhere beamwidth is discussed, it is assumed to be half-power beamwidth.

attain such pointing accuracy. Control moment gyroscopes can produce pointing accuracy to within 0.01 degrees of specifications, contingent upon a pointing knowledge a factor of 10 more precise. Therefore, the chances of falling outside the 0.035-degree range required would be based upon a normal distribution with a standard deviation of 0.01. This yields a 0.18% chance of falling outside tolerances, which itself would lead to a greater than 3 dB decrease in antenna gain.

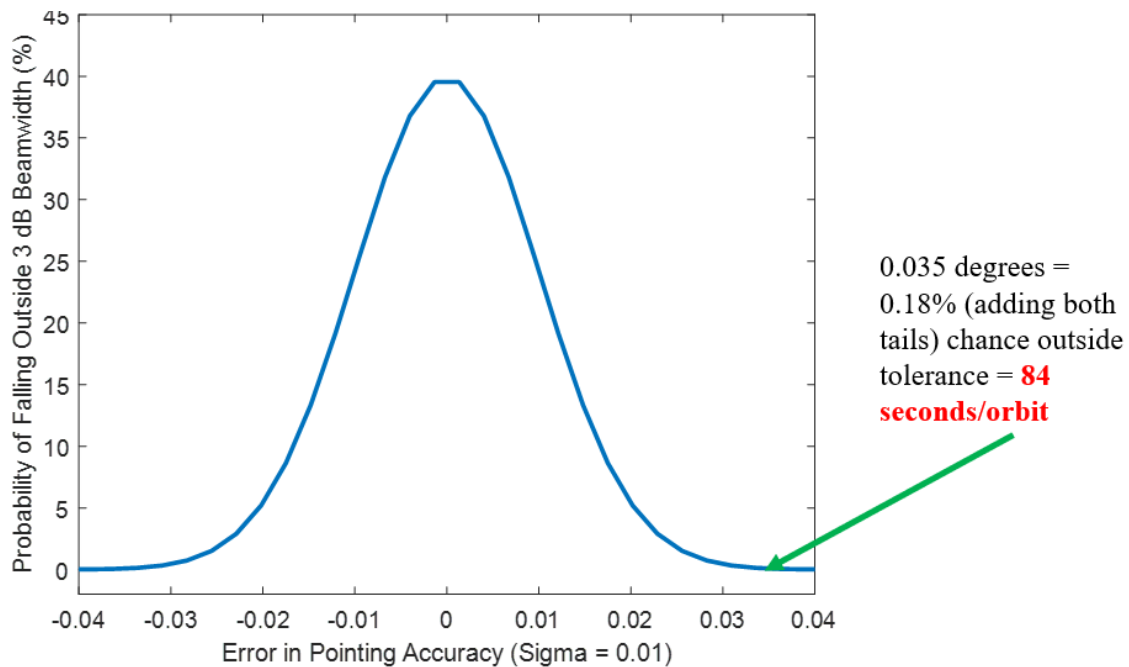


Figure 9: Normal Distribution for Beamwidth Error Probability.

If, for instance, a 30 GHz carrier frequency were used for this design, the beam width would be increased to 0.1457 degrees, rendering the chances of falling outside tolerance essentially to 0. Though, a possible benefit to decreasing the carrier frequency, and thus decreasing the pointing accuracy requirement, is that simpler, less power-hungry methods of providing that pointing accuracy can be implemented, such as stabilization jets or even gravity gradient methods [47]. While this may be appealing, the primary

limiting factor with regards to control wheels is their power requirements. Power is something that will in no way be in short supply over the course of this spacecraft's mission life. The limiting factor with stabilization jets, therefore, becomes propellant.

Using this regime, the probability of error as a function of wavelength is shown in the following figure.

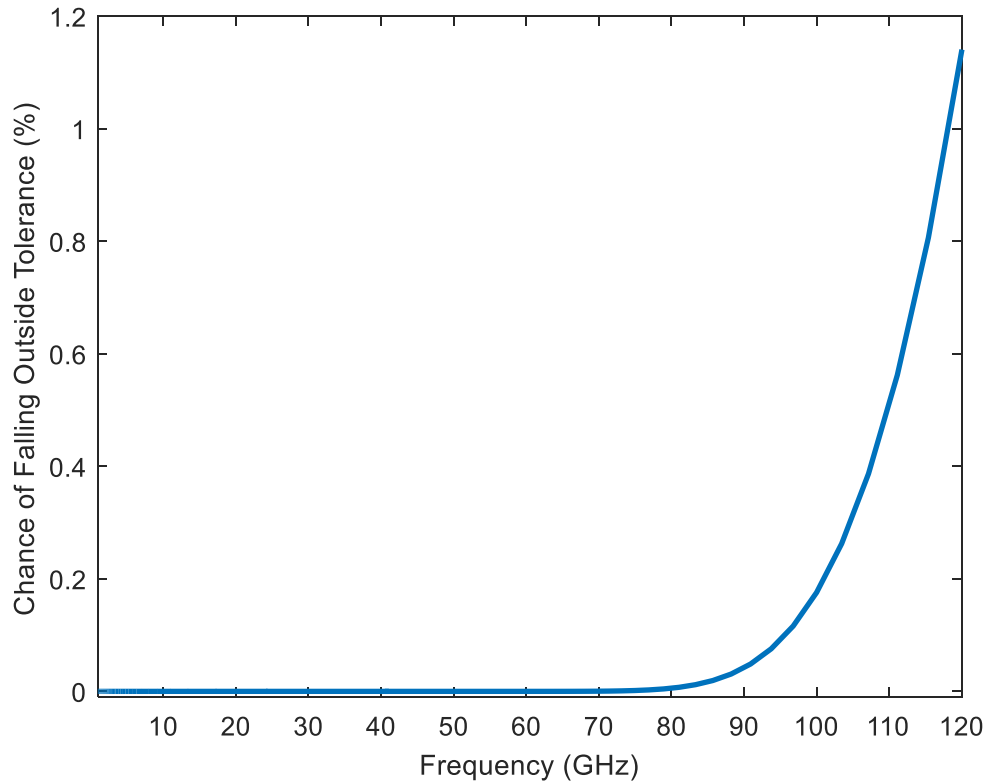


Figure 10: Probability of Error as a Function of Frequency.

The number of corrections required per day based upon that error probability is shown in the following figure.

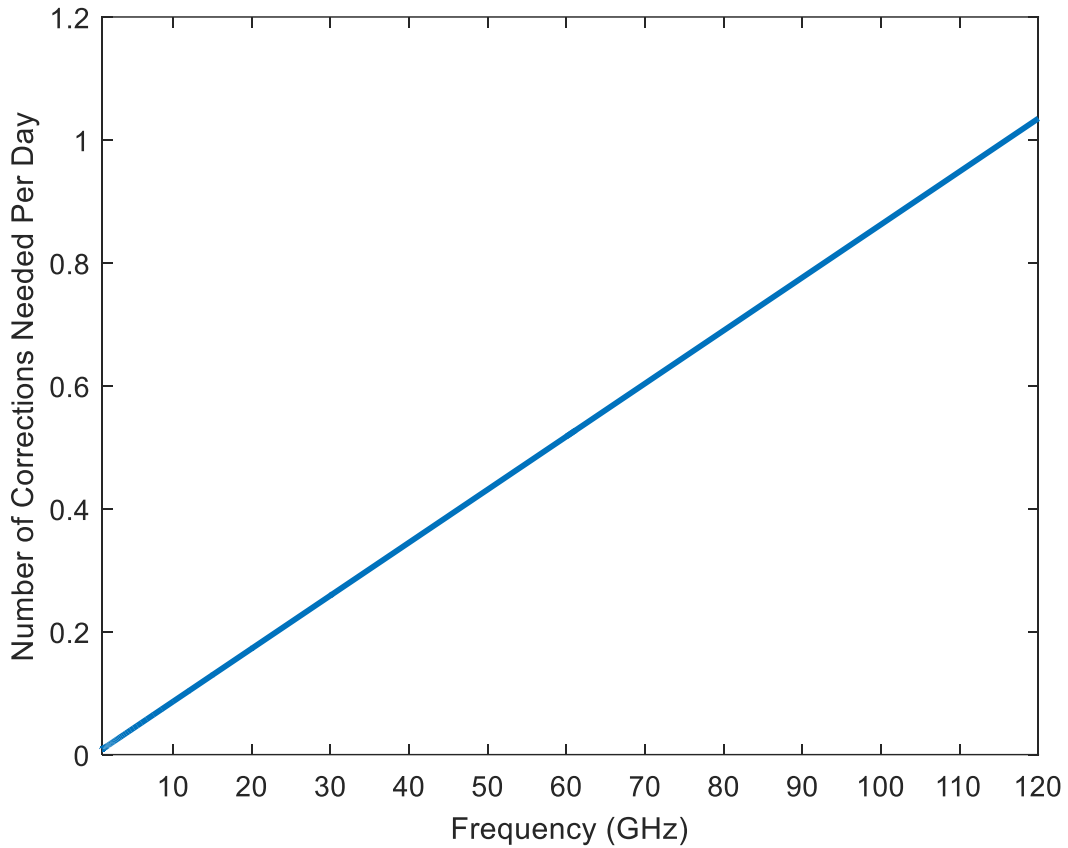


Figure 11: Number of Corrections Needed Per Day.

The number of corrections required per day is based upon wavelength (meters). This number is determined by calculating the total probability of error, and multiplying that by the total orbital period. Basically, it is the total number of times per day that the mothership's signal may fall outside the 3 dB beamwidth range.

The Bernoulli distribution showing the number of errors one can expect after 2,500 trials is shown in the following figure.

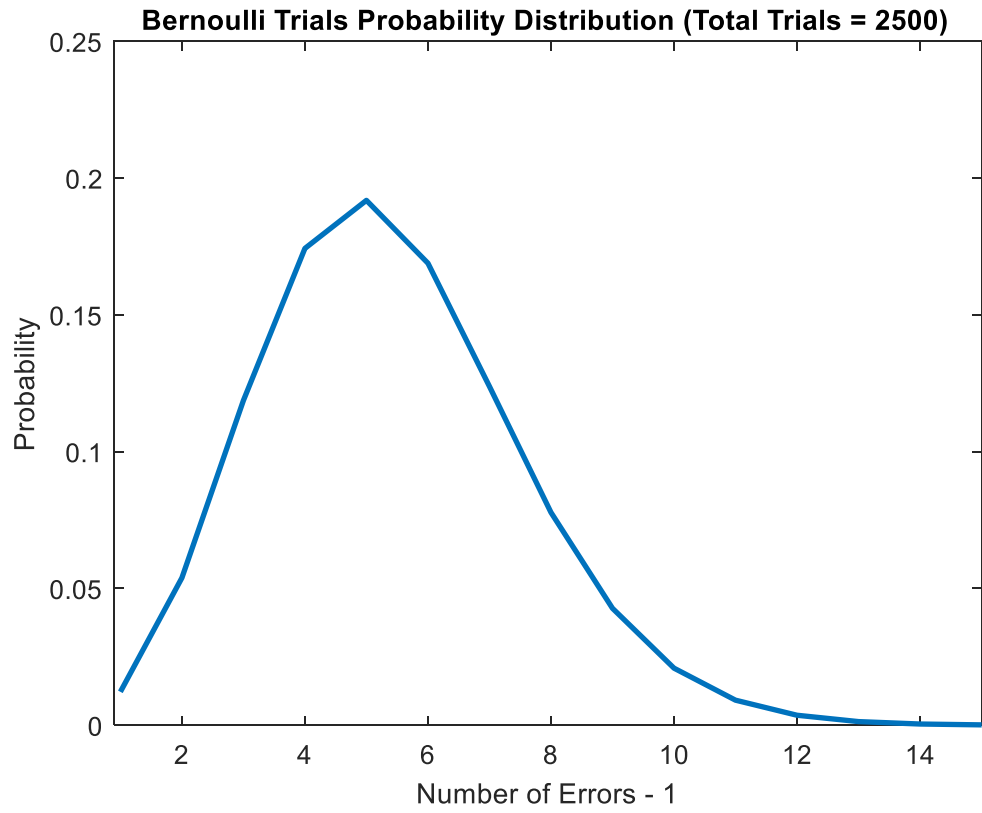


Figure 12: Binomial Distribution Expected Errors in 2,500 Trials.

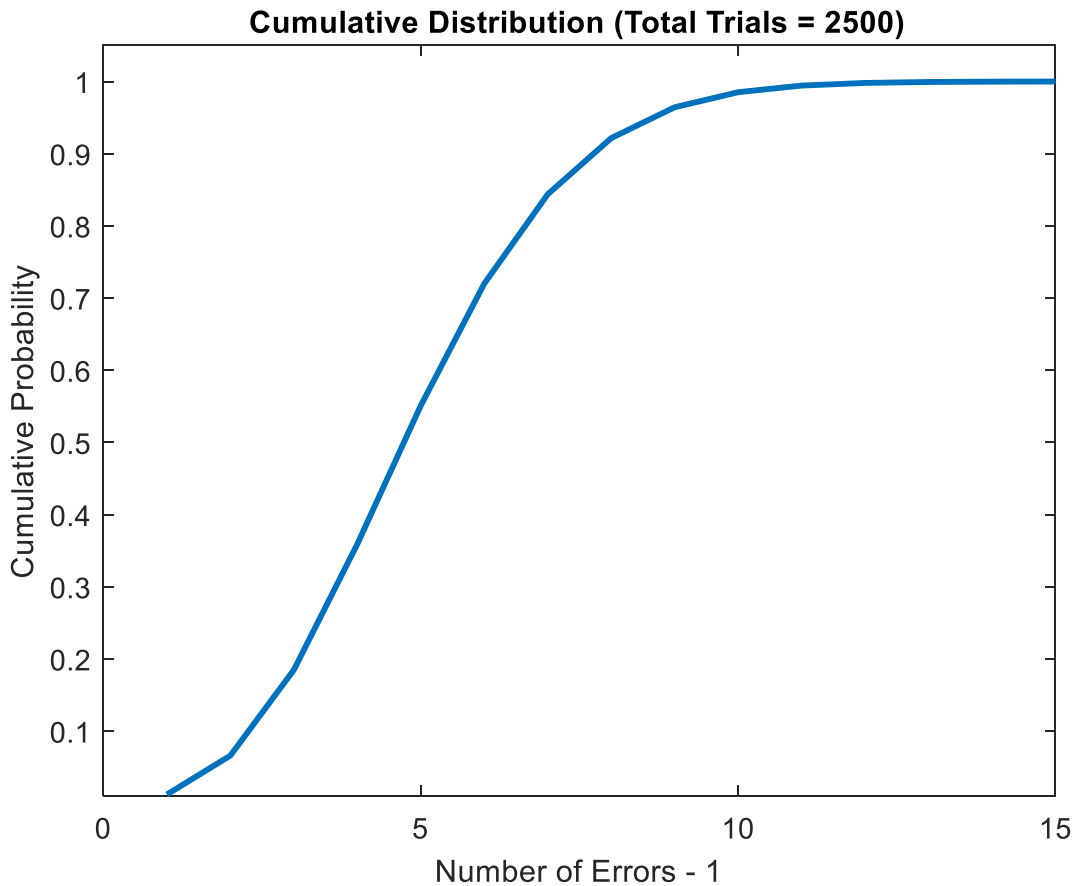


Figure 13: Cumulative Distribution Function for Errors.

The above cumulative distribution function shows the probability of a certain number of errors in attitude control after 2,500 trials. For example, there is a 99.9% probability of having reached the expected number of errors or more if the system experiences 15 or fewer errors.

Though there are other benefits to decreasing the carrier frequency. The first is that there is less potential for Earth-atmospheric interference, and thus increase the potential to beam the signal directly down to Earth's surface as opposed to using an orbiting satellite network, which will undoubtedly reduce the potential bit rate due to

decreased gain. A 30 GHz carrier frequency has some significant attenuation from the atmosphere, as shown in the Figure below, though not as drastic as 22 GHz or 60 GHz [46]. In these frequency regimes, it is a near certainty that a receiver will need to be placed somewhere in low-Earth orbit (LEO).

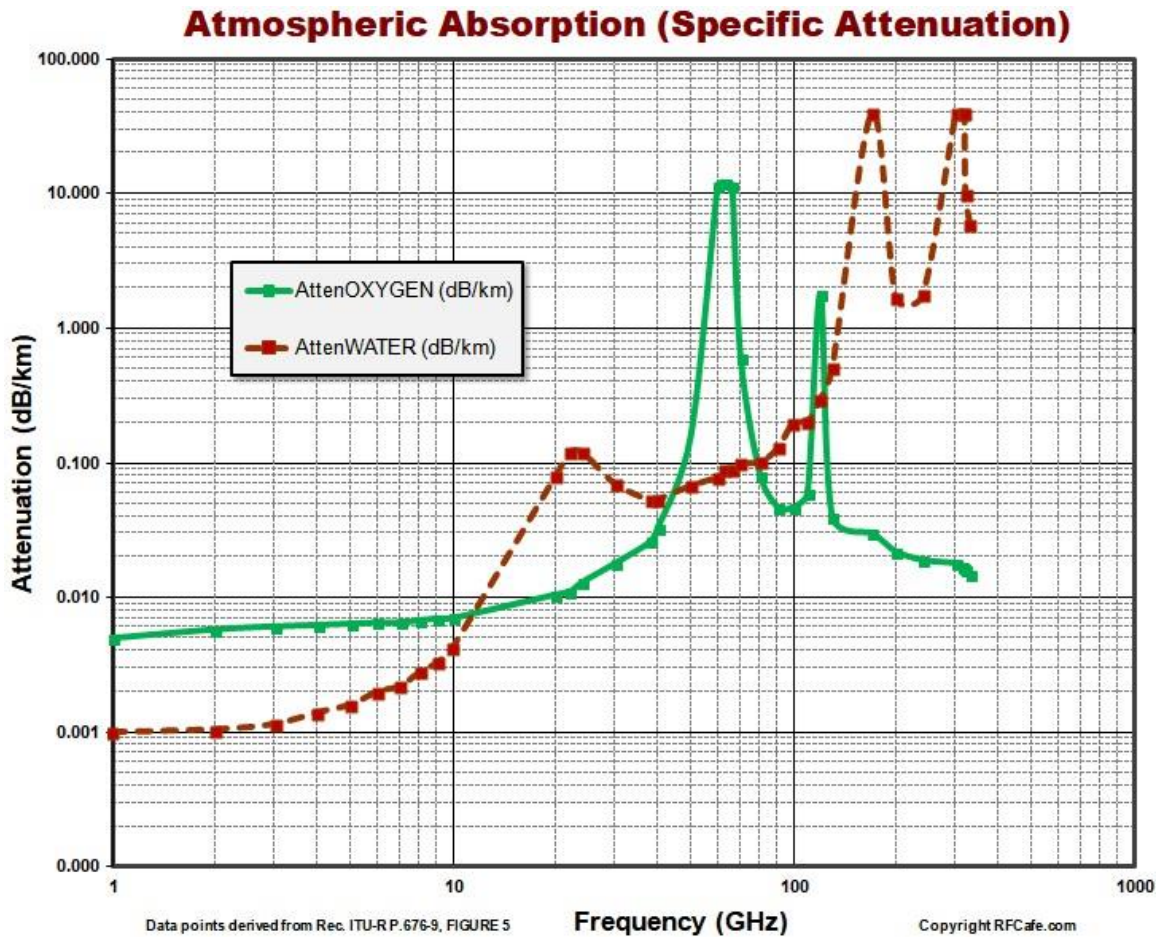


Figure 14: Frequency Attenuation Through Earth’s Atmosphere.

Another potential benefit to decreasing the carrier frequency is the ability to increase antenna diameter without overshooting pointing accuracy capabilities. The trick here is to find the optimization point that can be attained with current technology. If a beamwidth of 0.035 degrees can be maintained, the antenna diameter and frequency

parameters can be manipulated. It is indeed possible, with a large enough antenna, to send a signal with 0.035 degrees beamwidth back to Earth with a typical 15.4 GHz frequency. Such a possibility is elaborated upon in section 4.3. The following diagram shows the beamwidth of antennas with differing diameters and carrier frequencies.

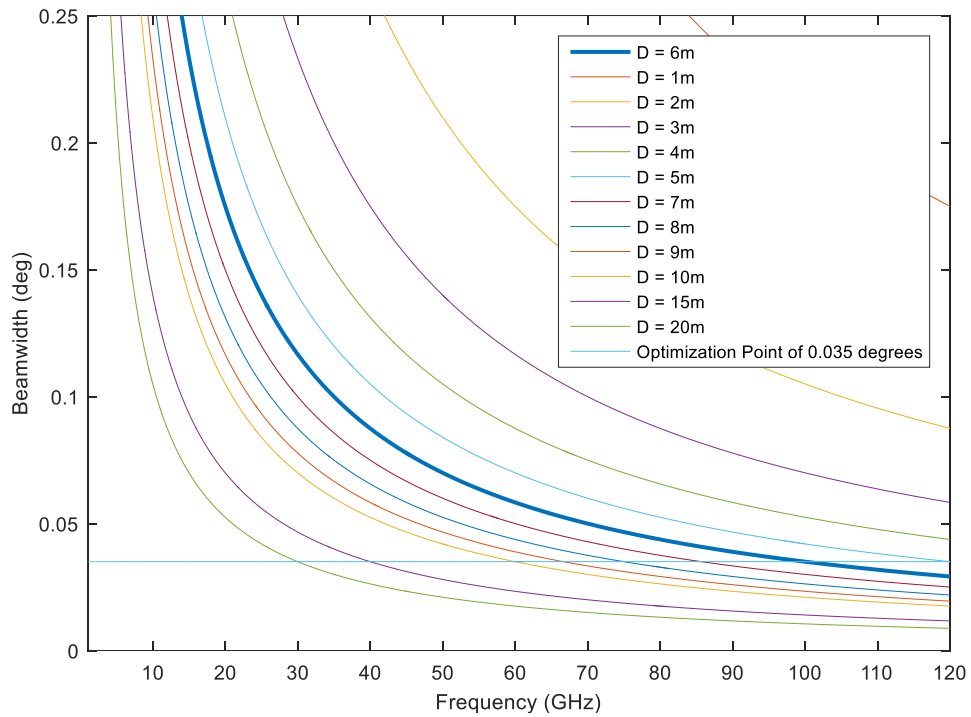


Figure 15: Beamwidth Versus Frequency for Different Antenna Diameters.

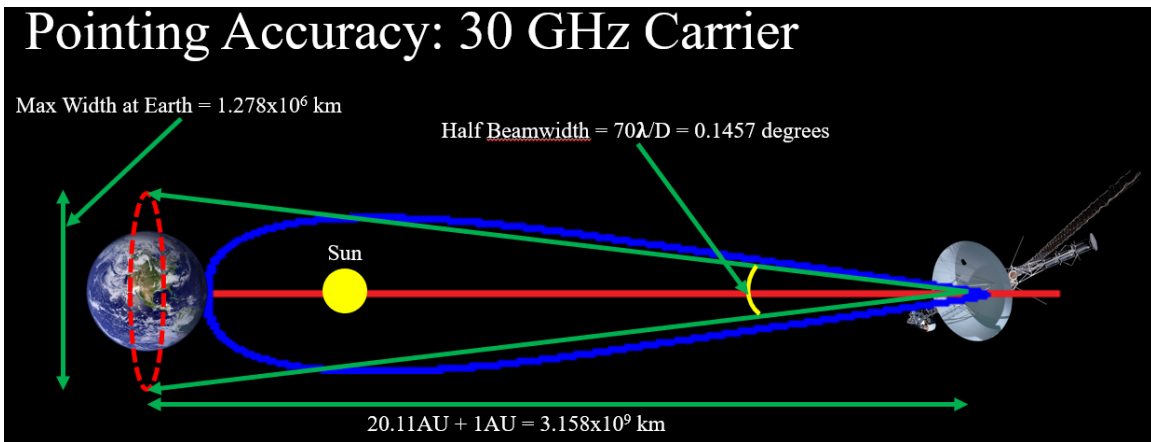


Figure 16: Mothership Signal Beamwidth to Earth.

Important to note is that in the previous figure, the diagram shows the 3 dB beamwidth. The signal may still reach Earth while falling outside this beamwidth. It would simply be attenuated more.

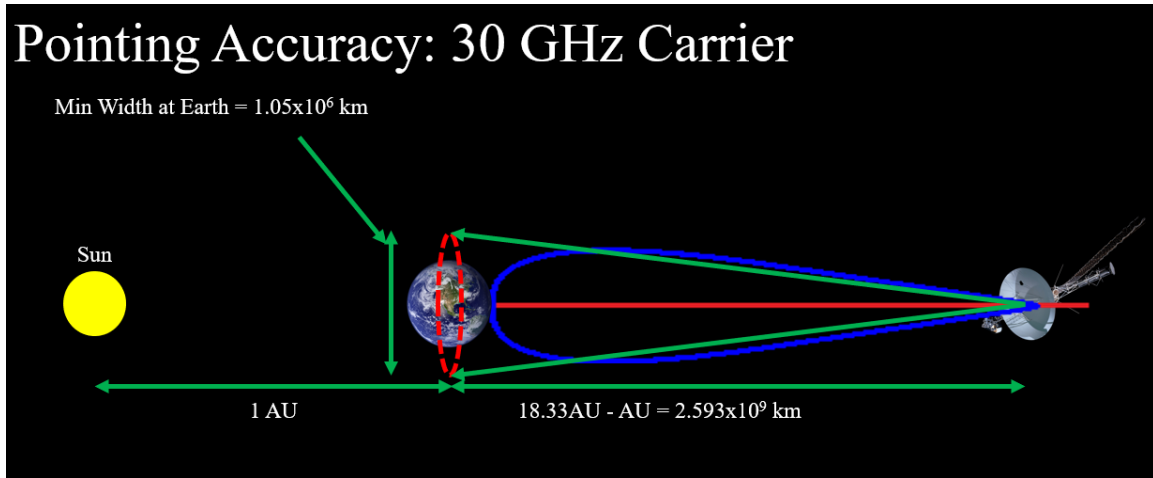


Figure 17: Mothership Signal Beamwidth with Earth Conjunction.

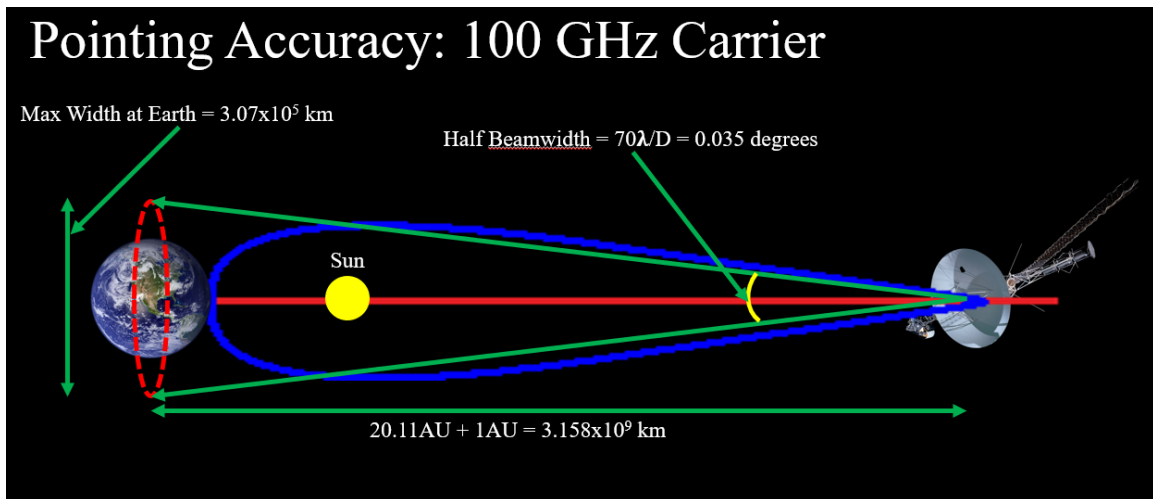


Figure 18: Mothership Signal Beamwidth with Earth Opposition (100 GHz Carrier).

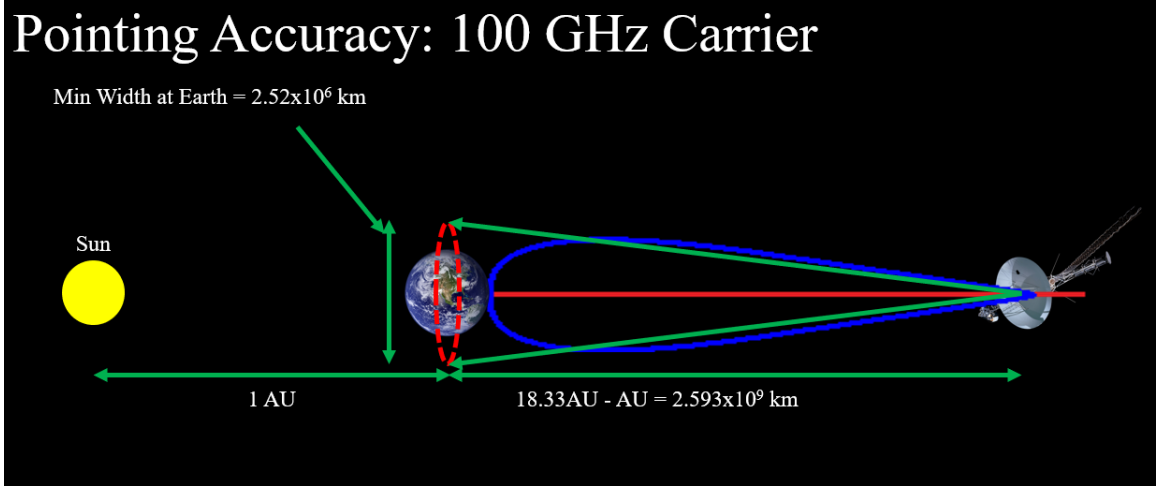


Figure 19: 100 GHz Beamwidth with Earth-Mothership Conjunction.

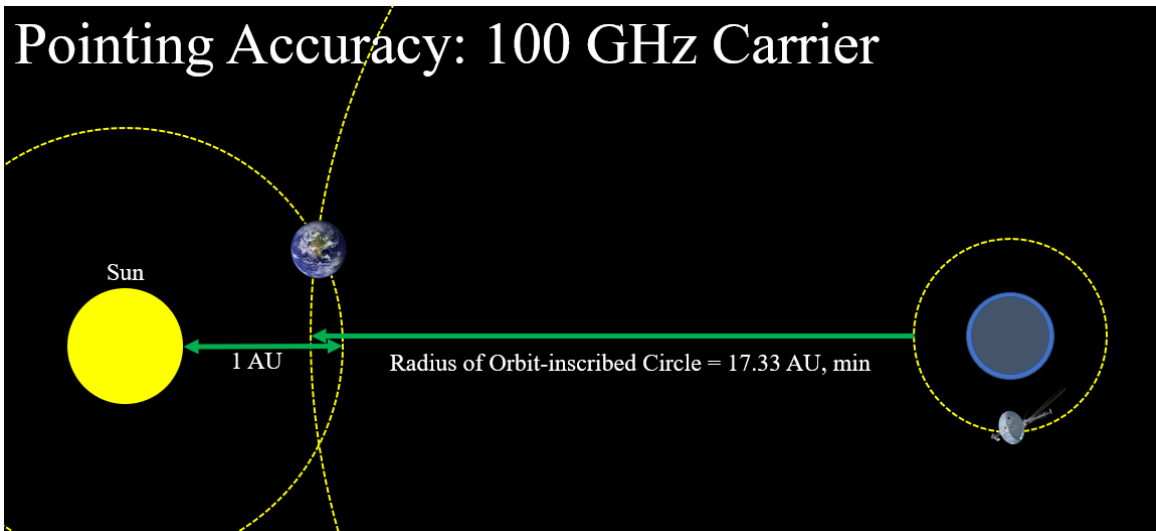


Figure 20: Inscribed Radii Between Earth and Uranus.

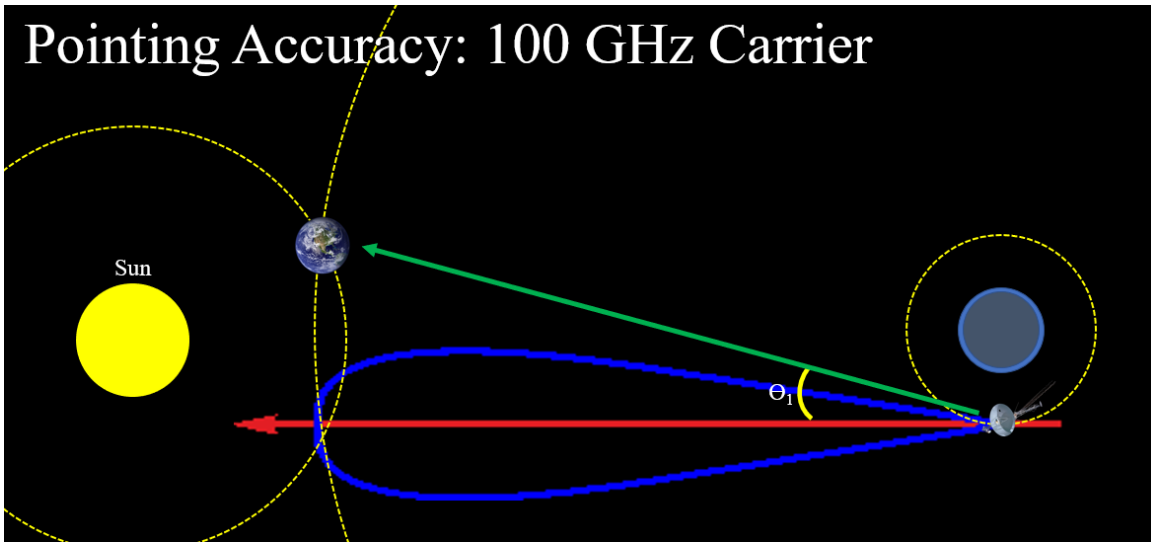


Figure 21: Maximum Apparent Angle Change Earth-Mothership (1).

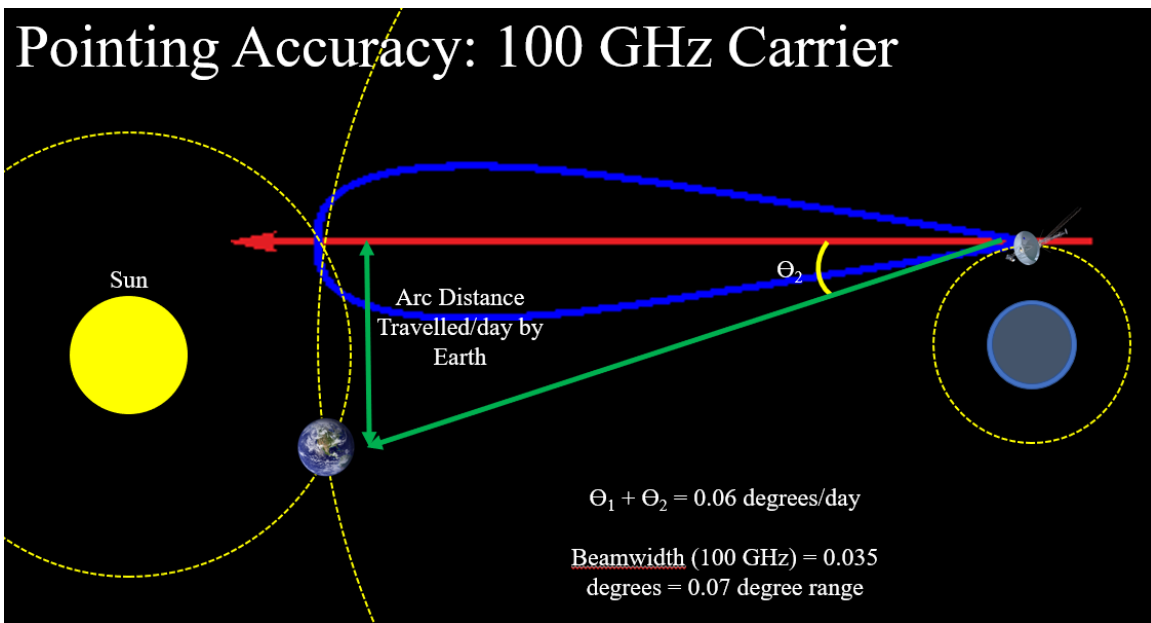


Figure 22: Maximum Apparent Angle Change Earth-Mothership (2).

The previous figure shows the absolute maximum change in apparent viewing angle between the mothership and Earth over the course of a single day. This figure is the

inscribed arc angle that the Earth travels through, plus Θ_1 and Θ_2 , and represents the maximum amount of error attitude correction would need to compensate for.

With the information derived from the previous figure, now the optimization of the gain can be derived. The relationship between the wavelength and the diameter of the antenna is linear, so this is a rather trivial calculation. Assuming the critical beamwidth cutoff point is 0.01 degrees, the maximum antenna diameter and carrier frequency possible is 21 meters and 100 GHz. This yields a gain of 84.25 dB, which can be calculated as follows [46]:

$$G_{tx} = 10 * \log_{10} \left[\left(\frac{\pi D_{ant}}{\lambda} \right)^2 \cdot \eta \right] \quad (2)$$

Where D_{ant} is the diameter of the antenna in meters, η is the efficiency of the antenna design¹², and λ is the wavelength of the carrier frequency in meters. The efficiency selected for this design was 0.55, though the actual number can be calculated later [46].

$$\begin{aligned} G_{tx} &= 10 * \log_{10} \left[\left(\frac{\pi(21 \text{ m})_{ant}}{0.003 \text{ m}} \right)^2 \cdot (0.55) \right] = 84.25 \text{ dB} \\ &= 266 \text{ Mbps possible} \end{aligned}$$

When compared to the specifications selected for this particular design, the gain is as follows:

$$\begin{aligned} G_{tx} &= 10 * \log_{10} \left[\left(\frac{\pi(6 \text{ m})_{ant}}{0.003 \text{ m}} \right)^2 \cdot (0.55) \right] = 73.3 \text{ dB} \\ &= 21.4 \text{ Mbps} \end{aligned}$$

¹² This value is usually between 0.5 and 0.6.

Therefore, the signal propagation of the 21-meter antenna is 12.43 times as powerful. Unfortunately, a 21-meter dish transmitting data with a 100 GHz carrier frequency would mean that the 0.01-degree beamwidth would cause the signal to be outside the 3-dB tolerance approximately 50% of the time, based upon a normal distribution curve with a standard deviation of 0.01 degrees. While this would still put the signal propagated at 81.25 dB upon reaching Earth (133 Mbps), consistent data transmission is of high importance in typical spacecraft design. Nevertheless, a 21-meter dish is a distinct possibility that may be considered going forward, especially since even with a 3-dB attenuation, the signal would remain 6.22 times as powerful as a 6-meter dish. Additionally, a 21-meter dish can relatively easily be fit into a 19.8-meter fairing, along with all other mission equipment. This is also important due to the uplink/downlink ratio between the probe and mothership, and the Earth and mothership. The probe, designed with a 300-watt RTG, has 25 watts allocated to signal propagation.

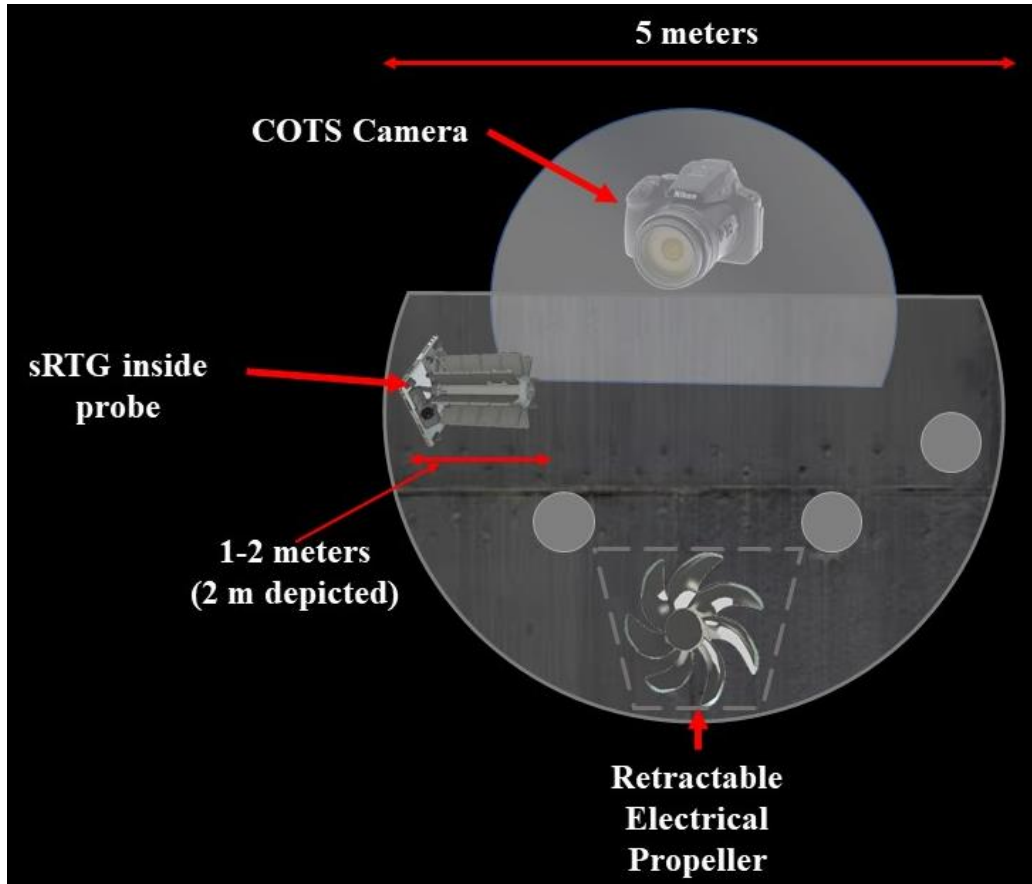


Figure 23: Probe with SRTG Embedded Inside.

With a 1-meter transmitter antenna on the probe, and a mothership orbit of 77,355 km above the Uranian hydrosphere at minimum, and 351,515 km at maximum,¹³ this yields a signal propagation strength as follows [46]:

$$R_{b,dB,P-M} = Power_{dBW} - \left(\frac{E_b}{N_0}\right)_{req,dB} - L_{FS,dB,mp} - N_{0,dB} + G_{tx,p-m} + G_{rx,p-m} \quad (3)$$

Where L_{FS} is free space loss, N_0 is the noise power spectral density, $Power_{dBW}$ is the transmission signal power, E_b/N_0 is the required signal-to-noise ratio, and G_{tx} and G_{rx} are the gains of the transmitting and receiving antennas respectively. All figures are in dB

¹³ $e = (r_{max} - r_{min}) / (r_{max} + r_{min}) = (351515 - 77355) / (351355 + 77355) = 0.6393$.

for this equation to work properly. There are also potential loss figures for Uranian atmospheric attenuation, pointing losses, and transmission line losses, but for now those will be omitted. Atmospheric attenuation of the signal may prove to be an issue due to Doppler and collisional broadening of the spectral lines of Helium, Hydrogen gas, and methane caused by the high temperature and pressure at the base of Uranus' troposphere, and those calculations will be done in a later section of this analysis.

$$L_{FS,dB,mp} = 10 * \log_{10} \left(\frac{4\pi D_{M-P}}{\lambda} \right)^2 \quad (4)$$

$$L_{FS,dB,mp} = 10 * \log_{10} \left(\frac{4\pi(351515 \times 10^3 \text{ m})_{E-U}}{(0.003 \text{ m})} \right)^2 = 243.37 \text{ dB}$$

$$Power_{dBW} = 10 * \log_{10}(25 \text{ watts}) = 13.98 \text{ dBW}$$

$$\left(\frac{E_b}{N_0} \right)_{req} = 10 \text{ dB};$$

$$N_{0,dB} = 10 * \log_{10}(kT_{sys}) \quad (5)$$

$$N_{0,dB} = 10 * \log_{10} \left(1.38 \times 10^{-23} \frac{\text{m}^2 \text{kg}}{\text{s}^2 \text{K}} \cdot [10,000 \text{ K}] \right) = -188.60 \text{ dB}$$

This is the noise of the system in dB.¹⁴ Next the gain of the transmitting and receiving antennas on the probe and mothership must be calculated.

$$G_{tx,p-m} = 10 * \log_{10} \left[\left(\frac{\pi D_{ant}}{\lambda} \right)^2 \cdot \eta \right] = 10 * \log_{10} \left[\left(\frac{\pi(1 \text{ m})_{ant}}{(0.003 \text{ m})} \right)^2 \cdot (0.55) \right] = 57.81 \text{ dB}$$

¹⁴ This was the selected system noise temperature, in Kelvin. 10,000 Kelvin is actually quite a conservative estimate (very high value), considering we will have access to high-quality equipment, and the black-body temperature at Uranus' orbit is roughly 65 Kelvin. A more appropriate estimate—and the one used for the calculations discussed in the abstract of this thesis—is 150 Kelvin. This is a very reasonably attained figure for system noise. The preceding calculations done in the body are with 10,000 Kelvin, however.

$$G_{rx,p-m} = 10 * \log_{10} \left[\left(\frac{\pi D_{ant}}{\lambda} \right)^2 \cdot \eta \right] = 10 * \log_{10} \left[\left(\frac{\pi (6 \text{ m})_{ant}}{(0.003 \text{ m})} \right)^2 \cdot (0.55) \right] = 73.37 \text{ dB}$$

From this figure, one can calculate a maximum data rate as follows:

$$R_{b,dB,p-M} = 13.98 - 10 - 243.37 - (-188.60) + 57.81 + 73.37 = 80.39 \text{ dB}$$

Or roughly 109.4 Mbps. These same calculations are done to accomplish the downlink bit rate from the mothership to Earth (1.045 Mbps). While increasing the antenna diameter on the mothership would also increase the bit rate between the probe and the mothership, the Earth-mothership/mothership-probe uplink/downlink does not change.

$$UD_m = \frac{R_{b,m-p}}{R_{b,m-E}} \quad (6)$$

$$UD_{6m} = \frac{(109.4 \times 10^6 \text{ bps})}{(1.045 \times 10^6 \text{ bps})} = 104.68$$

$$UD_{21m} = \frac{(266 \times 10^6 \text{ bps})}{(2.53 \times 10^6 \text{ bps})} = 104.68$$

This uplink/downlink ratio is an important consideration for data handling. For example, while it may be possible to transmit data from the probe to the mothership, in very short order, the memory storage space on the mothership will be filled up. Thus, data will either need to be overwritten, or sampled at a lower rate by the probe. For later consideration, the amount of power the probe allocates to signal propagation as well as the size of the probe's antenna can be reduced. For now, the graph below shows the antenna probe's diameter when optimizing for the appropriate uplink/downlink ratio.

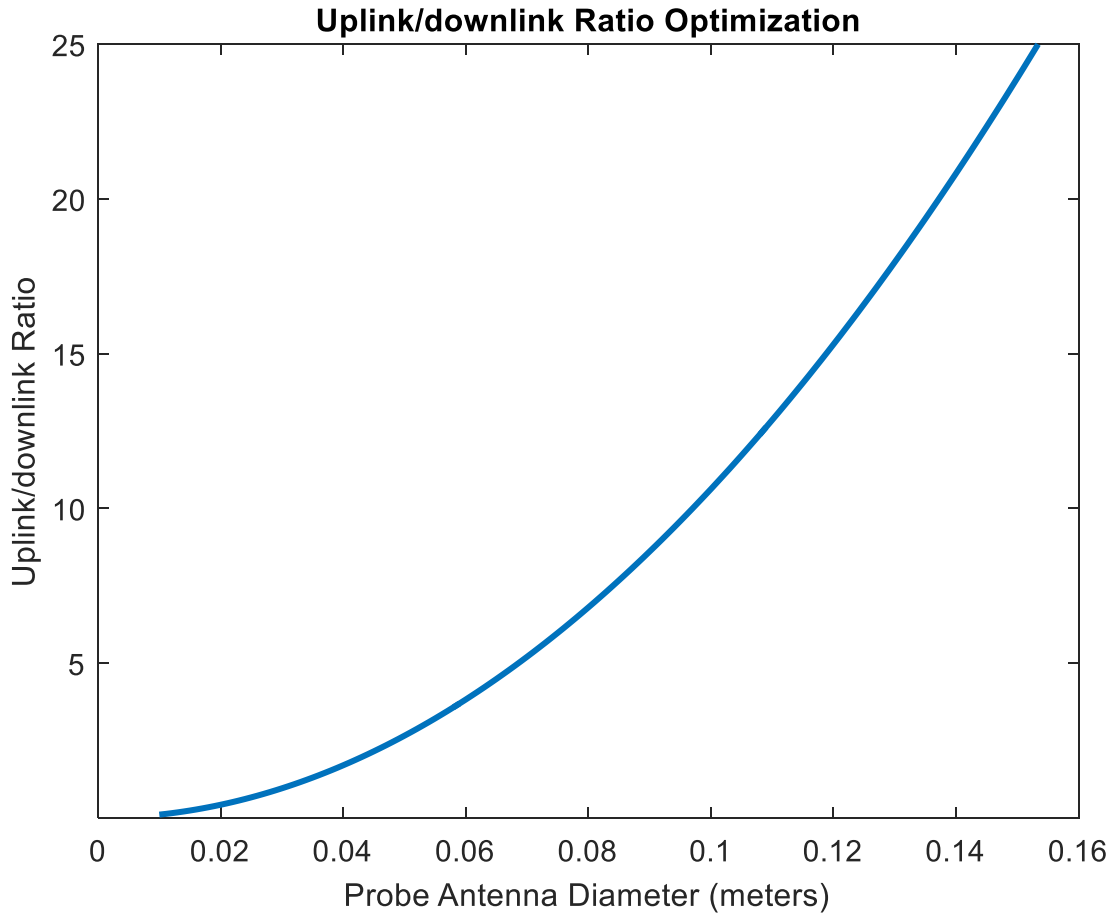


Figure 24: Uplink/Downlink Ratio.

The ideal probe antenna diameter to achieve a 1:1 uplink/downlink ratio is approximately 3 cm, as shown in the previous figure. As stated before, these calculations can be done for any particular uplink/downlink ratio that is desired. This ratio is driven by several factors. Principal among them is the total time that the mothership is in view of the Earth as opposed to the total time it is in view of the probe. Ideally, the probe will be aligned on the hydrosphere between Uranus' center and Earth, but one has to engineer for the worst-case scenario. Diagrams illustrating this are shown in Figure 26.

3.4 Traveling-Wave Guide Amplifier (TWTA) Calculations:

To determine the dimensions of the TWTA that will eventually be used in this design, a few assumptions must be made. First, the input impedance will be assumed at 50 ohms [48], and input voltage will be 200 volts. We will also assume that the electrons within the helix of the TWTA are travelling at 20% the speed of light. This is a relatively normal velocity for said electrons [49]. The equation for calculating the length of the TWTA is shown below:

$$L = \frac{[Gain(raw)+9.54](2\pi V_0)}{47.3 \cdot f_c \left(\sqrt[3]{\frac{IK}{4 \cdot V_{bus}}} \right)} \quad (7)$$

$$= \frac{(270030 + 9.54) \left(2\pi \left[6 \times 10^7 \frac{m}{s} \right] \right)}{47.3 \cdot (100 \times 10^9 \text{ Hz}) \left(\sqrt[3]{\frac{(1.33 \text{ Amps}) \cdot (50 \text{ Ohms})}{4 \cdot (200 \text{ Volts})}} \right)} = 50 \text{ cm}$$

Where Gain(raw) is the non-dB gain of the design, V_0 is the speed of the electrons in the system in m/s, f_c is the carrier frequency, I is the current of the system (1.33 Amps), K is the impedance, and V_{bus} is the voltage of the bus. Lower bus voltage will yield higher gain for a given length, and higher impedance will do the same. The constants of 9.54 and 47.3 have to do with the normalized voltage correction of frequencies typically transmitted through a TWTA. These corrections are necessary due to mass errors incurred by electron transmission speeds approaching the speed of light. For example, even at 5 keV, there is a 1% error in mass calculations for which the Equation must account [50]. These numbers can be changed as necessary. A gain of 25-30 dB is reasonable for a TWTA, but in order to attain a 50-cm length, the gain was selected as shown above (approximately 54.4 dB).

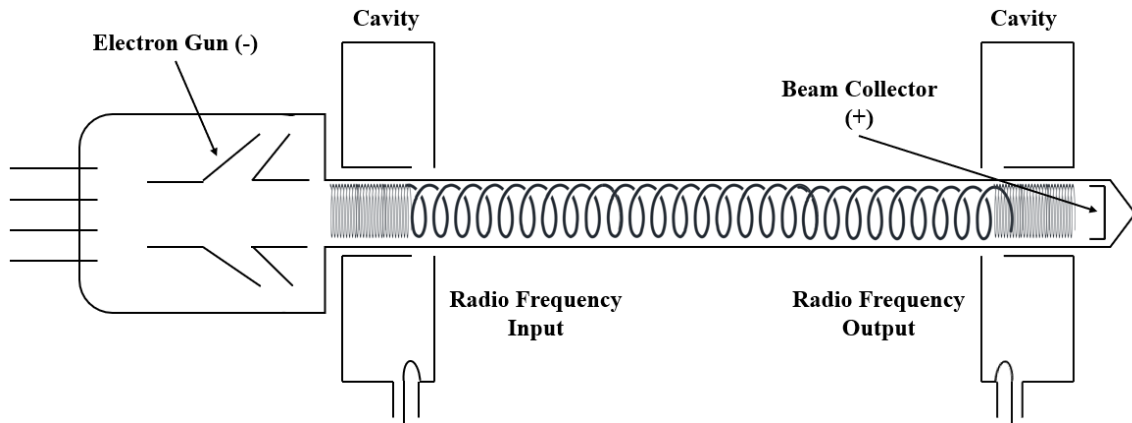


Figure 25: Diagram of a TWTA.

Though the system can operate at very high gain and requires minimal space, the question becomes whether it is possible to operate a TWTA in a reasonably efficient manner at the high frequencies of this design. In other words, are the equations describing the TWTA's signal amplification relatively linear? TWTAs, both experimental and operational, have been shown to operate nominally at or above 220 GHz [51].

3.5 Constellation Design

Another important note for this design, is that these calculations for pointing control are using control-moment gyros or better. What was not considered, was using star-trackers, which have pointing knowledge of 0.001 degrees or better [29]. This being the case, and combined with potentially far more accurate pointing accuracy devices, a much larger antenna size can be implemented in the design, which can also be accommodated for in the large fairing that will be used, upon the powerful launch vehicle used. A 21-meter antenna dish is not unreasonable if modern star trackers, gyros, and

actuators are implemented.¹⁵ Appropriate antenna folding could yield an antenna diameter of upwards of 70 meters [45]. This is similar in theory to the way that solar sail design concepts work [52]. In this light, the possibilities are nearly endless. The only limiting factor is the pointing accuracy, which constantly technically improving star trackers will be able to alleviate in the near-term.¹⁶

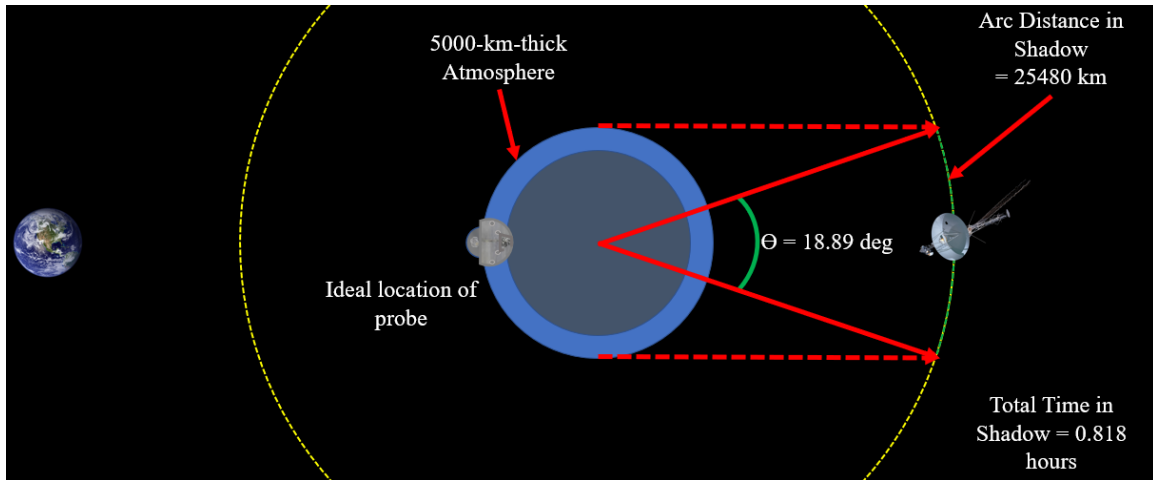


Figure 26: Ideal Location of Probe with Respect to Earth.

¹⁵ Or even much larger!

¹⁶ The effective data transmission rate would be roughly 3 Gbps for a 70-meter antenna operating at 100 GHz. Beamwidth would be roughly 0.003 degrees.

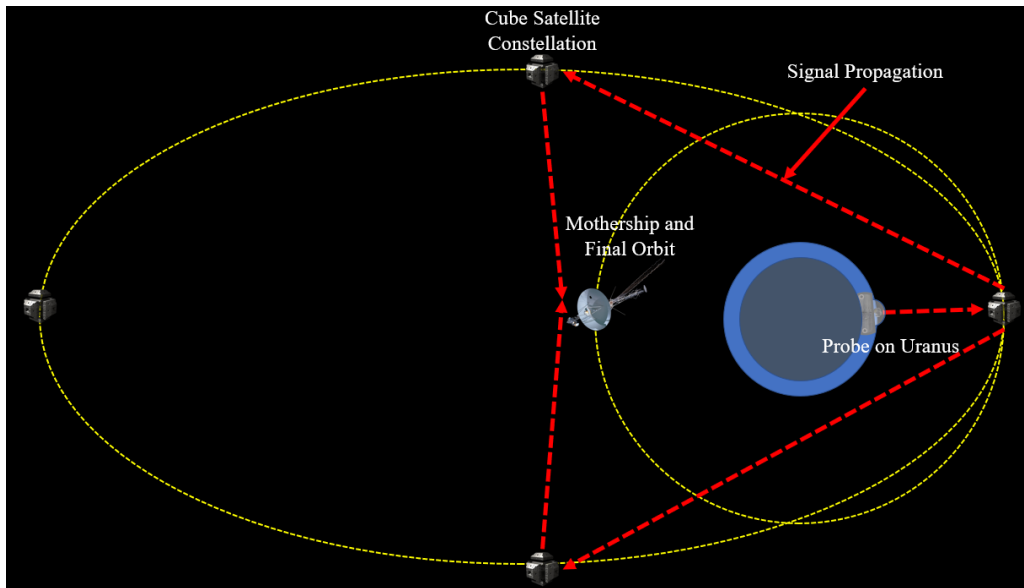


Figure 27: Illustration of Importance of Constellation Satellite System.

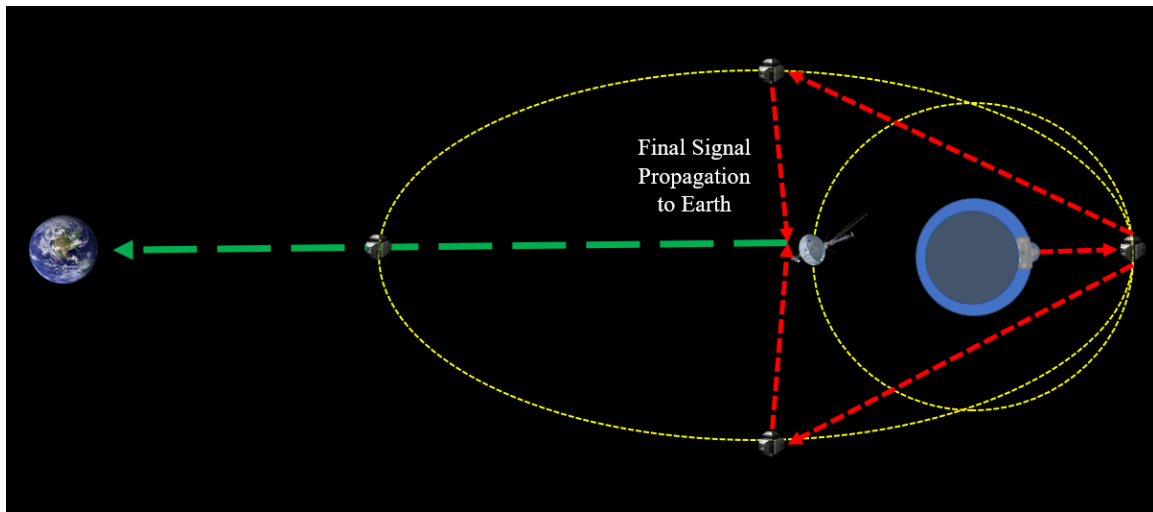


Figure 28: Worst-Case Scenario Probe Location with Respect to Earth and Mothership.

Either way, to calculate the total time that the mothership will be in the shadow of Uranus relative to Earth, one must find the arc length of Uranus' radial projection onto the mothership's final orbital distance of 77,355 km. This is illustrated in Figure 26.

$$a^2 = b^2 + c^2 - 2bc \cdot \cos(\theta) \quad (8)$$

All three sides are known. b and c are equal to one another (77,355 km), and a is simply the radius of Uranus (25,382 km). Therefore,

$$(25,382 \text{ km})^2 = (77,355 \text{ km})^2 + (77,355 \text{ km})^2 - 2(77,355 \text{ km})(77,355 \text{ km}) \cdot \cos(\theta)$$

$$\rightarrow \cos^{-1} \left[\frac{(25,382 \text{ km})^2 - 2(77,355 \text{ km})^2}{-2(77,355 \text{ km})(77,355 \text{ km})} \right] = 18.89^\circ$$

$$\rightarrow D_{arc} = \frac{(2\pi r) \cdot (18.89^\circ)}{360^\circ} = 25,477 \text{ km}$$

Determining the time in shadow is not as easy as finding the period of the mothership's orbit, and then multiplying by the ratio of the angle in darkness over 360 degrees, though that would be done as follows:

$$P_{orb} = 2\pi \sqrt{\frac{r_{orb}^3}{\mu_U}} \quad (9)$$

$$P_{orb} = 2\pi \sqrt{\frac{(77,355 \times 10^3 \text{ m})_{orb}^3}{\left(\frac{5.7938 \times 10^{15} \text{ m}^3}{\text{s}^2}\right)_U}} = 15.6 \text{ hours}$$

$$T_{shadow,U} = \frac{\theta}{360} (P_{orb}) = 0.818 \text{ hours}$$

Therefore, the total time the mothership is in the shadow of Uranus would be 18.07 times less than the time the mothership is in view of Earth, if this were the case, making the ideal uplink/downlink ratio for the mothership's orbit is 18-19 times. This yields a probe antenna diameter of approximately 13 cm. This, obviously, is contingent upon the mothership's final orbital semi-major axis and eccentricity.¹⁷ Though what is

¹⁷ Currently, this will be designed with 0 eccentricity and a radius of 77,355 km. This is subject to change in the future, when more fidelity on the Jupiter assist ΔV requirements is established.

being disregarded here is that the time the mothership is in the shadow is only a small sliver of the total portion of the orbit in which the probe is visible to the mothership. If we assume a minimum elevation angle of 10 degrees,¹⁸ determining the total visibility range is determined as follows [46]:

$$b = \cos^{-1} \left(\frac{r_{hyd}}{r_{orb}} \right) \quad (10)$$

This gives the maximum angle between the probe on the hydrosphere and the mothership, where they are in view of one another. r_{hyd} is the radius of the probe's final resting place from the center of the planet, and r_{orb} is the radius of the mothership's final orbit. Carrying out the calculation, the maximum angle is 74.74 degrees. Multiplying this by 2 in order to get the total angle in view yields 149.47 degrees. Determining the time in view, thus, is as simple as multiplying the total time of orbit by the ratio (149.47/360), yielding 6.48 hours of the 15.6-hour orbit. This yields an uplink/downlink ratio of

$$UD_{rat} = \frac{T_{orb,U} - T_{shadow,U}}{T_{view,p}} = \frac{15.6 \text{ hrs} - 0.818 \text{ hrs}}{6.48 \text{ hrs}} = 2.28$$

Yielding a probe antenna diameter of approximately 5 cm. Or more precisely:

$$d = \frac{\lambda}{\pi} \sqrt{\frac{10^{\frac{R_{b,req} - R_{b,probe} + G_{downlink}}{10}}}{\eta}} = \frac{0.003 \text{ m}}{\pi} \sqrt{\frac{10^{\frac{71.95 - 98.63 + 57.81}{10}}}{(0.55)}} = 0.0463 \text{ m}$$

$$= 4.63 \text{ cm}$$

This yields a beamwidth of 4.53 degrees by using Equation (E 1). As a result, the gain is then 31.13 dB for the probe's antenna.

¹⁸ A relatively conservative estimate, which is nevertheless a good idea due to the high atmospheric pressure, temperature, and overall thickness—which itself may lead to adverse effects upon visibility of the probe. Theoretically, there are no obstructing land masses, but possible tidal activity, to occlude vision.

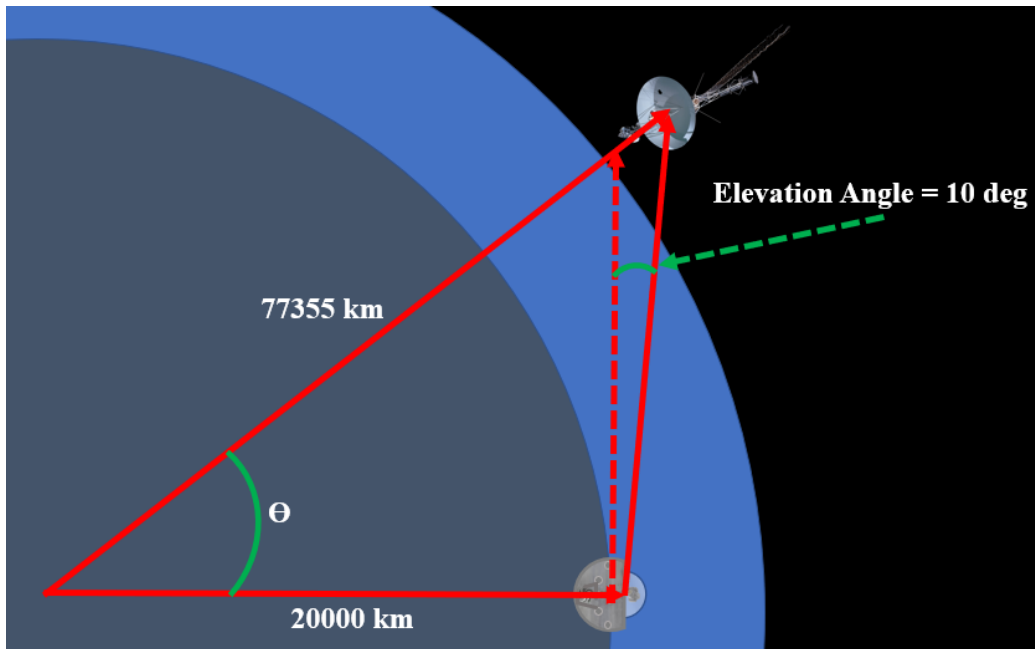


Figure 29: Elevation Angle and Range Between the Probe and Mothership.

3.6 Inclination Changes

It is important to note that Uranus rotates on its side relative to the ecliptic plane of the Solar System, and the majority of Uranus' satellites orbit about its rotational axis [5]. While it may be preferable for some mission concepts to attain this orbital inclination about Uranus, it requires extreme amounts of propellant and yields no significant benefits in terms of data handling/signal propagation back to Earth. While it is true that the probe could be placed at particular latitudes in which the mothership would attain nearly 100% contact at all times, with the CubeSat constellation acting as a signal repeater, this is not necessary.

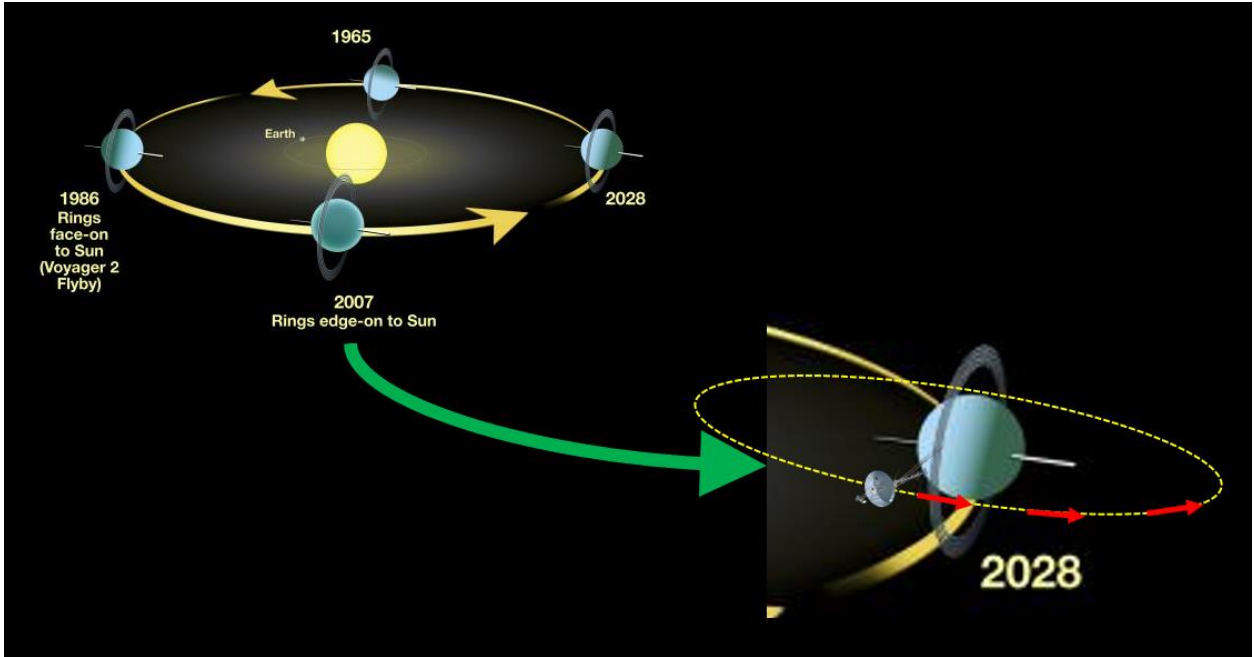


Figure 30: Uranus' Orbital Inclination Versus Mothership's Orbit.

It is unlikely that there will be any essential mission aspect that will require an inclination change to align the spacecraft with the rotational plane. If a simple inclination change is to be accomplished, calculations for the thrust requirement is accomplished as follows [46]:

$$\Delta V_{inc} = 2v \sin\left(\frac{\Delta i}{2}\right) \quad (11)$$

Where Δi is the inclination change in radians, and v is the orbital velocity. Uranus has an inclination of 97.7 degrees relative to its orbit. Thus, converting this number to radians, 1.7052 will be used for Δi . The point of slowest orbital velocity¹⁹ is attained upon first reaching aphelion of the proposed initial mothership orbit, 351,515 km altitude. Therefore, v would be as follows [29]:

¹⁹ And therefore, the best opportunity to accomplish an inclination change.

$$v_{ap} = \sqrt{\mu_{Uranus} \left(\frac{2}{r_{ap}} - \frac{1}{a_{orb}} \right)} = \sqrt{\left(5.7938 \times 10^{15} \frac{\text{m}^3}{\text{s}^2} \right) \left(\frac{2}{3.515 \times 10^8 \text{ m}} - \frac{1}{2.144 \times 10^8 \text{ m}} \right)}$$

$$= 2.438 \text{ km/s}$$

Thus, ΔV_{inc} is:

$$\Delta V_{inc} = 2 \left(2.438 \frac{\text{km}}{\text{s}} \right) \sin \left(\frac{1.7052}{2} \right) = 3.672 \frac{\text{km}}{\text{s}}$$

Using the ideal rocket equation, this would change our final orbiting mass from 2,400 kg down to 910 kg. The mission would effectively lose 62% of its payload for such a maneuver, best case. If this maneuver were to be accomplished, ideally it would be combined with other maneuvers, such as circularizing and elliptical burn to reduce the maneuver's impact.

3.7 Launch Window Design

One of the principle concerns with respect to sending a probe to Uranus is the means by which one can maximize the payload mass and dimensions that can be sent to the planet via current launch vehicles as well as orbital maneuvers. A common, well-tested method by which the mission can save on travel time, ΔV requirements, and increase mass, is to use other planets to “slingshot” the spacecraft toward its final destination. Jupiter tends to be the most sought-after destination for this purpose primarily because of its deep gravity well, due to the planet's exceptionally high mass of about 300 times that of Earth.

But there are many preliminary factors that must be sorted out before any such maneuver can even be considered. First of all, the orbits of Uranus, Earth, and Jupiter, must all be in an appropriate alignment in order to make such a maneuver possible.

Jupiter orbits the Sun with a period of 11.862 years, and Uranus with one of 84.02. If we take the time to orbit the Sun and combine that with the current true anomalies of the three planets, then it can be modelled where the planets will be over the course of one Uranian orbital period.²⁰ Any baseline date that is used can be extrapolated to determine where the planets will be in the future, in fact.²¹ Therefore, 29 January 2018 will be used for the purposes of this exercise. At that point, the true anomalies of the three planets were:

Table 5: Planetary True Anomalies.

Planet	True Anomaly (degrees)
Earth	102.937
Jupiter	14.331
Uranus	173.005

Based upon these true anomalies, with the Sun-centered orbit at the distance zero point, the following graphs of the planet's orbits can be built.

²⁰ Again, 84.02 years. This also omits precessions of each planet's orbit.

²¹ It is also important to note that these true anomalies are, of course, Sun-centered.

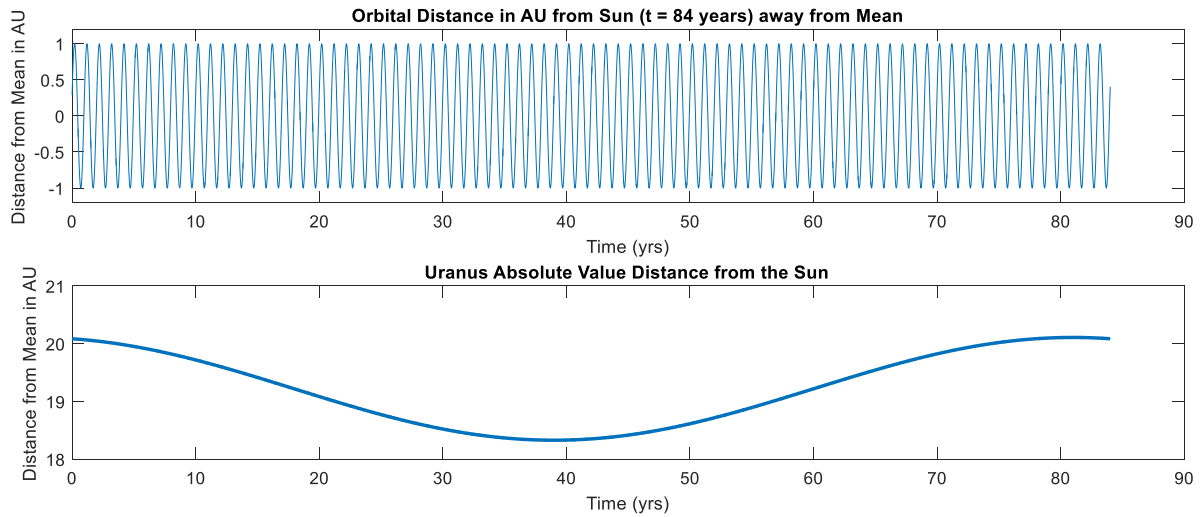


Figure 31: Orbital Periods of Uranus and Earth.

For Uranus’ orbital plot, since it is the end target, an absolute value distance is more appropriate for orbital optimization calculations, with the graph showing Uranus’ eccentricity effect on its absolute distance from the Sun. Because Uranus’ orbit is so large, its less than 5% orbital eccentricity yields a change in absolute distance from the Sun of nearly 2 AU. In order to better visualize this, the following plot should help:

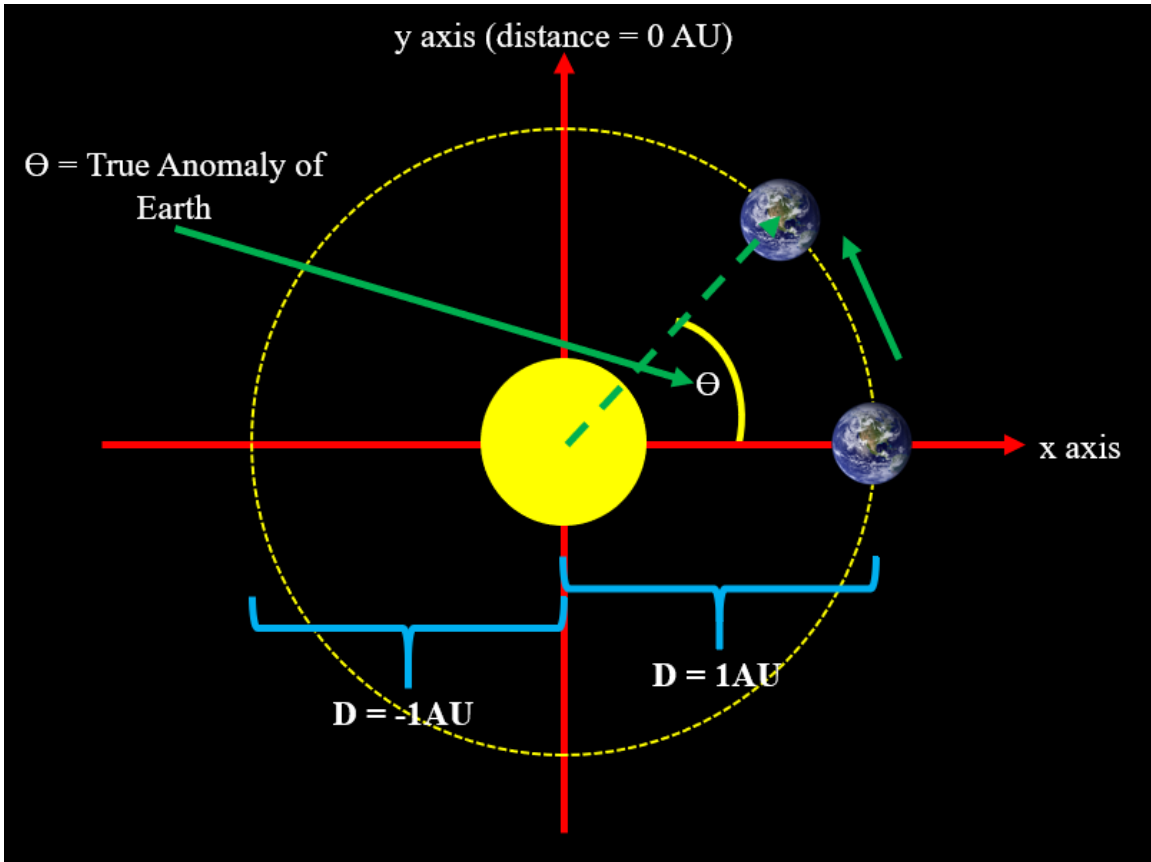


Figure 32: Schema Used for Launch Window Optimization.

With this explained, below is a graph of Jupiter's distance from the Sun with the Sun at the center of the axis plot.

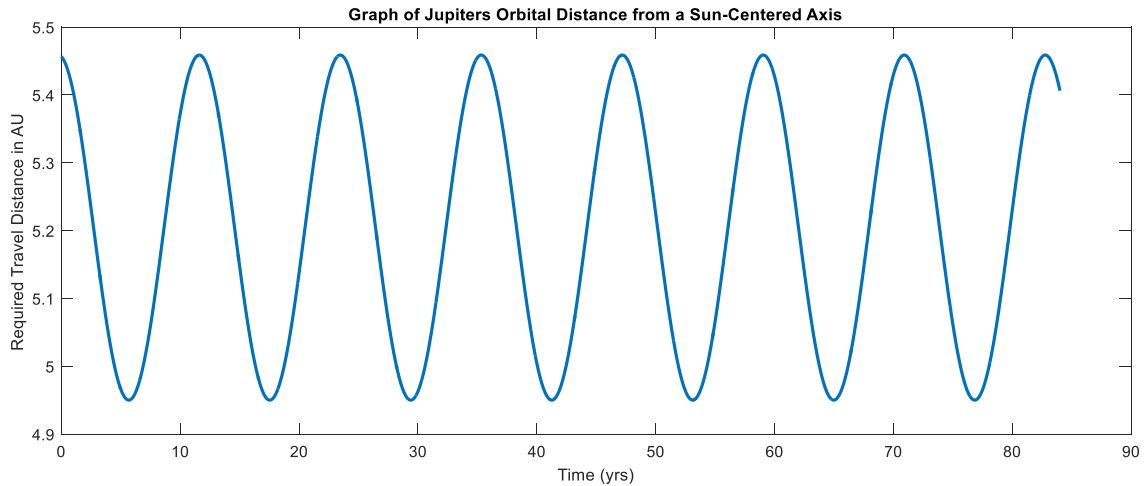


Figure 33: Jupiter's Orbital Period around the Sun.

From the previous figure we can glean many things, such as Jupiter's true anomaly based upon the starting (zero) point of the graph, as well as the number of orbital periods Jupiter will cycle through over the course of one Uranian orbit (~7). One can also determine Jupiter's eccentricity. This graph is approximate and does not account for precession, as is true with all of the graphs in this analysis. Taking these things into consideration, and superimposing the graph of Earth's orbital period on top of the graph of Uranus' orbital distance from the sun in absolute terms, a simplified version of the minimum and maximum distances required for travel between the two planets is yielded. This is shown in the following graph:

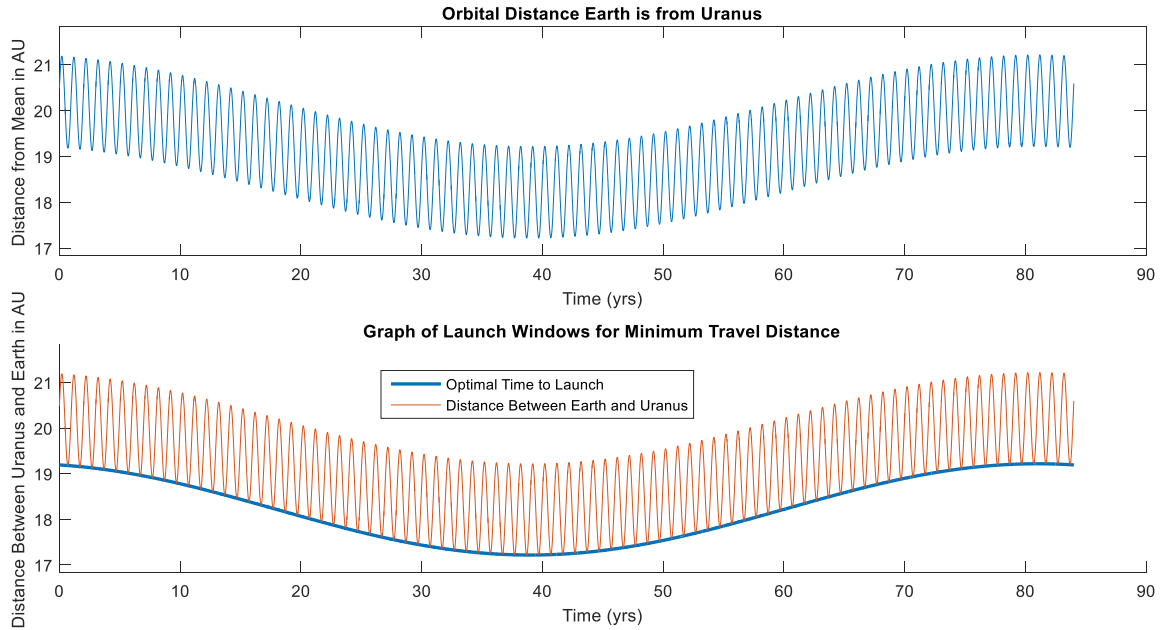


Figure 34: Orbits of Uranus and Earth Superimposed.

As can be seen from the previous graph, if we were to not utilize a gravity assist maneuver from Jupiter, the launch window for minimum travel distance would be in roughly 40 years' time, when Uranus and Earth are on the same side of the Sun.²² There is no difference between the top and bottom graph other than a minimum distance line superimposed on the bottom one. Following the same process for Jupiter and Earth's orbital resonance yields the graph below:

²² Of course, this assumes there will be no travel time. To actually achieve the minimum travel time, Earth launch would need to be baked into the numbers, meaning the ideal launch time will be $\sim 40 - (\text{travel time})$ years from now.

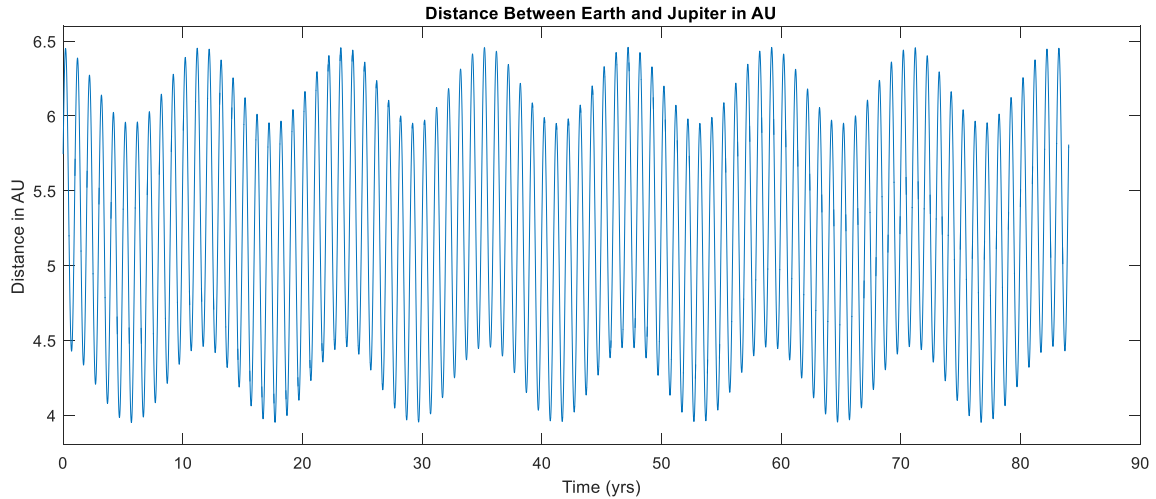


Figure 35: Jupiter and Earth Orbits Superimposed.

This graph shows the distance between Jupiter and Earth. Such a distance is important to glean if any efficient gravity assist is to be attempted. Earth will experience roughly 84 full orbits around the Sun over the course of a single Uranian orbit. Since Uranus is very near its maximum distance from the Sun, this grants ample time for design of this mission before the optimal launch window is attained. Utilizing Jupiter as a gravity assist mechanism requires one to superimpose the orbital period of Jupiter onto that of Uranus and Jupiter. The result is shown in the following graph. For better visualization, the Jupiter-Uranus distance graph is also included:

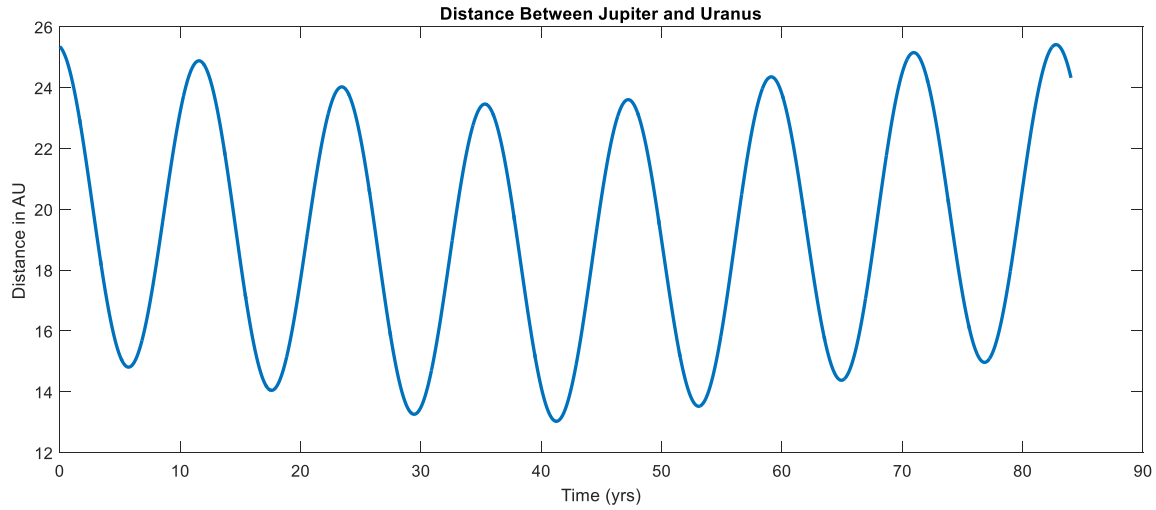


Figure 36: Jupiter and Uranus Orbits Superimposed.

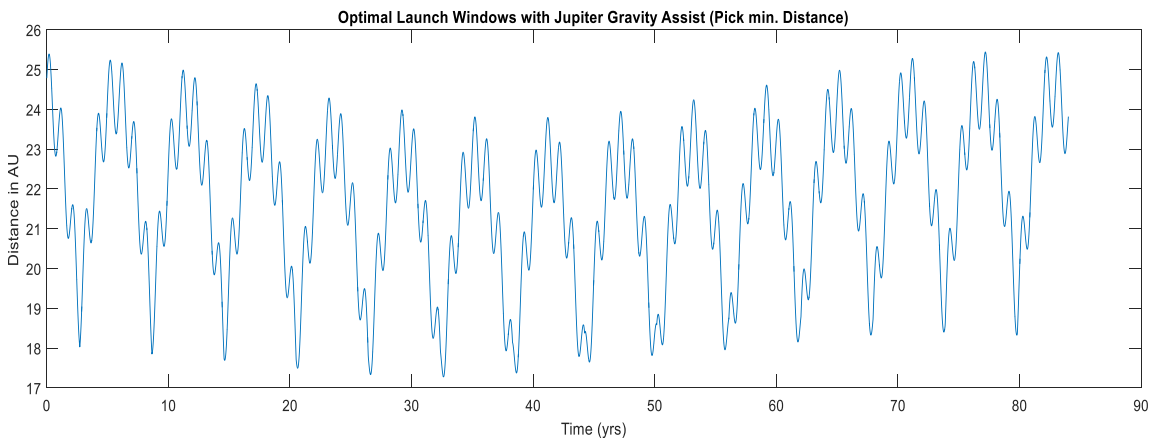


Figure 37: Earth, Uranus, and Jupiter's Orbits Superimposed.

As can be seen in the previous figure, the minimum distance would be roughly 33 years from 28 January 2018. Thus, considering travel time, the minimum travel distance would likely be roughly 20 years in the future.

As stated earlier, these graphs represent approximations of the orbits of Uranus, Jupiter, and Earth and their alignment, due to the fact that precession of orbits are not included, nor is Earth's eccentricity. Nevertheless, with Earth's eccentricity scarcely over

1%,²³ and including the fact that these eccentricity errors are imposed upon orbits with much smaller radii, the error can be assumed to be no more than a few tenths of a percent, or a few days of travel time. Calculations of this can be carried out later.

At the optimal launch window time, Jupiter's true anomaly will be approximately

$$TA_{J,obs} = TA_{J,19.5} + TA_0 + TA_{J,travel} \quad (12)$$

$$\begin{aligned} 19.5 \cdot \frac{\text{years}}{11.862 \frac{\text{years}}{\text{Jupiter Orbit}}} &= 1.6439 \text{ revolutions} \rightarrow (1.6439 - 1) * 360^\circ \\ &= 231.8058^\circ + TA_0 \\ &= 231.8058^\circ + 14.331^\circ = 246.1368^\circ \end{aligned}$$

Adding the travel time to Jupiter's true anomaly yields a true anomaly as follows:

$$\begin{aligned} 246.1368^\circ + \left(\frac{5 \text{ years}^{24}}{11.862 \frac{\text{years}}{\text{Jupiter Orbit}}} \right) * 360^\circ &= 246.1368^\circ + 151.75^\circ \\ &= 397.88^\circ = 37.88^\circ \end{aligned}$$

What this means is that Jupiter will have gone through roughly 42.15% of its orbit around the sun in the time it takes the spacecraft to travel to the planet.²⁵ Earth's true anomaly of 180 degrees at time of launch means that it must meet Jupiter at its 37.88-degree true anomaly. Knowing these numbers, we can then calculate the inscribed-triangle that will be made by this maneuver, from Earth's initial launch to rendezvous with Jupiter. With the angle separating Earth and Jupiter's true anomaly (at time of

²³ And this error in travel distance comes to only a few million km as opposed to a several billion-km journey. These calculations are meant to be within an order of magnitude.

²⁴ This calculation is iterative.

²⁵ A 5-year travel time is assumed based upon previous calculations. The process of determining this travel time will be iterative, as the ideal planetary locations for launch will constantly change based upon the numbers calculated.

rendezvous) being 142.12 degrees, the launch to Jupiter would look something like the following figures.

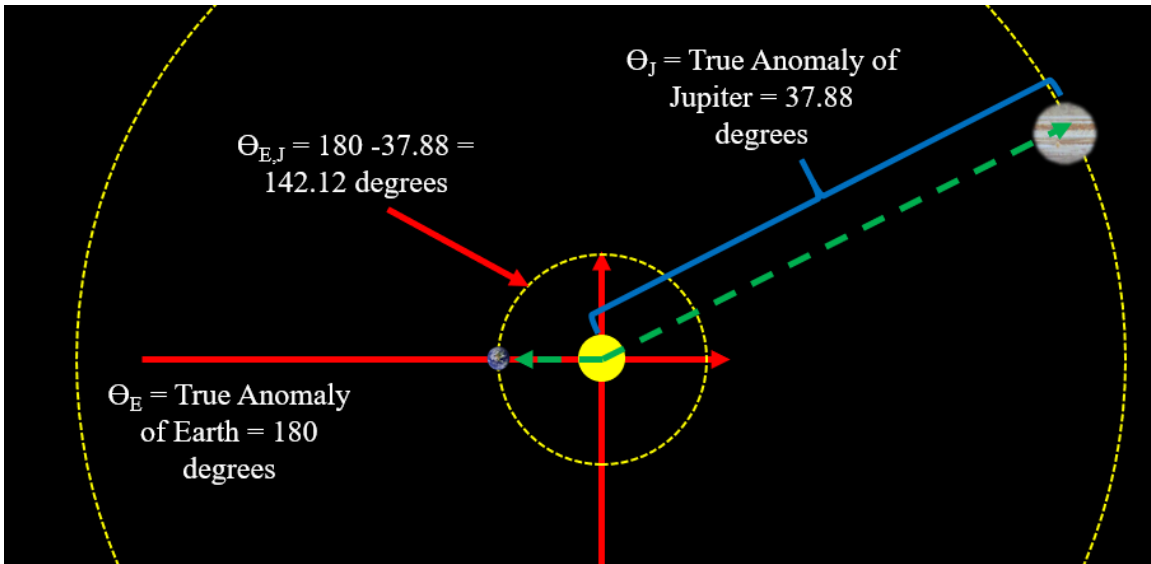


Figure 38: Orbital Locations at Time of Ideal Launch.²⁶

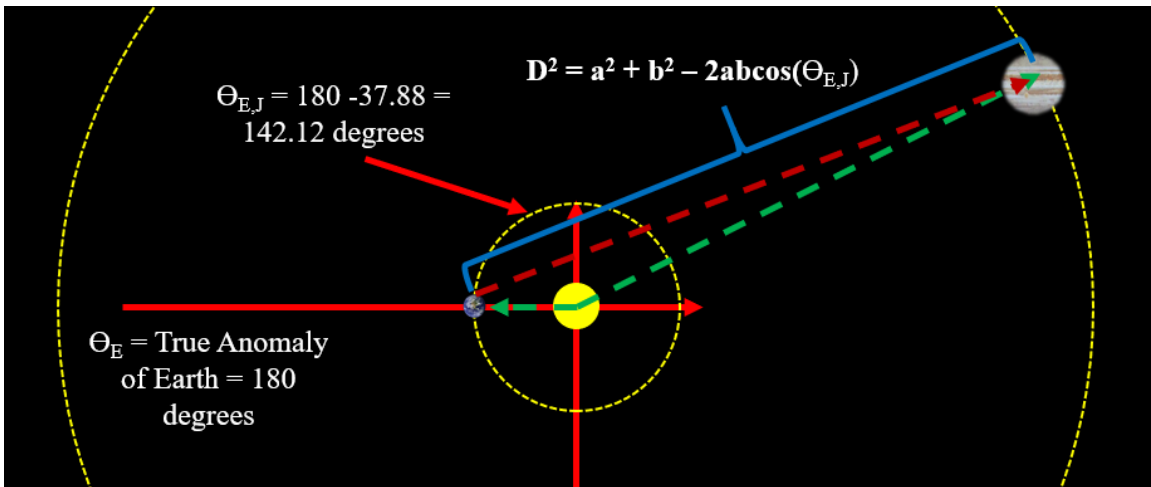


Figure 39: Means of Calculating Distance.

Now that the location and true anomaly at which Earth will rendezvous with Jupiter is known, one can determine the location of Uranus at time of rendezvous with

²⁶ Angles not exact.

Jupiter, as well as at time of spacecraft intercept (assumed to be 13 years from launch,²⁷ though this calculation is once again iterative). Uranus' true anomaly at time of spacecraft intercept will be:

$$\begin{aligned}
 TA_U &= TA_{U,0} + TA_{U,13} = \left(173.005^\circ + \left[\left(\frac{19.5}{84.02} \right) \cdot 360^\circ \right] + \left[\left(\frac{13}{84.02} \right) \cdot 360^\circ \right] \right) \\
 &= 173.005^\circ + 83.5515^\circ + 55.710^\circ = 312.2575^\circ
 \end{aligned}$$

This means that Jupiter will have to deflect the spacecraft 85.62 degrees. This means the spacecraft will need to fly within 2.5924 million km. This maneuver yields a velocity relative to the Sun of 20.54 km/s.

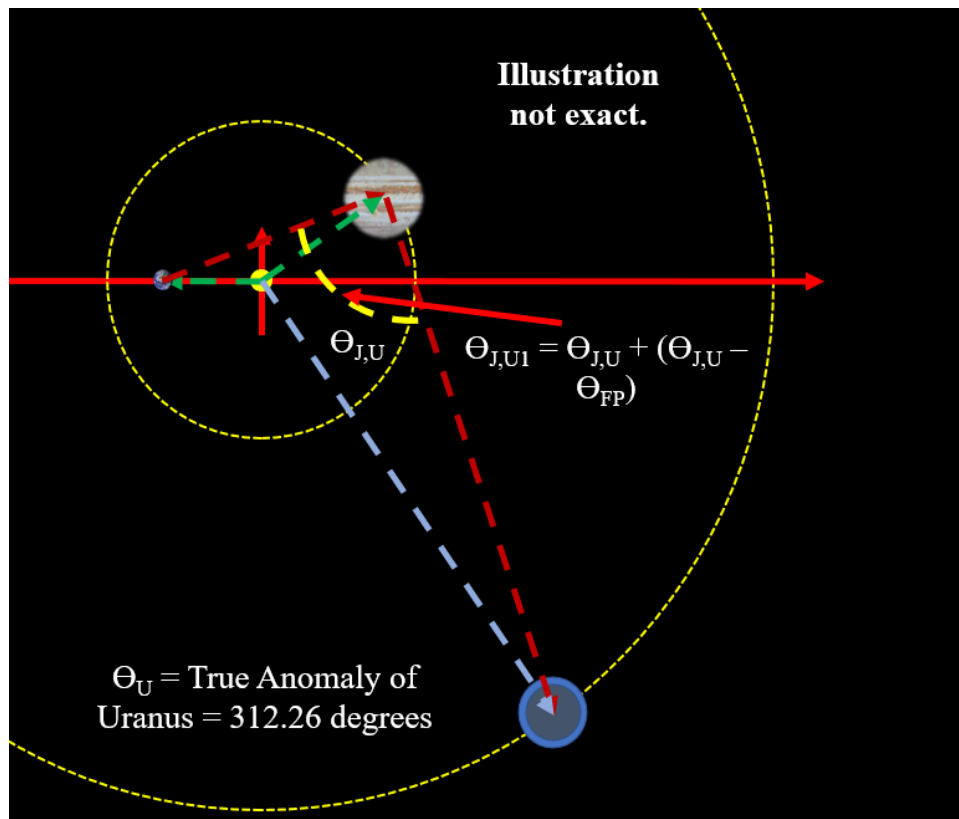


Figure 40: Flight Path Angles.

²⁷ This number is closer to 15 years, but for methodology purposes, 13 is placed here.

3.8 Tidal Force Effects

The next hurdle of overcoming the pointing accuracy requirements between the probe and the mothership can be somewhat tricky. In some ways, this is perhaps even more of a concern than the pointing accuracy between Earth and the mothership. This is due to the rapidly changing angle between the two systems via the mothership's orbit, as well as the significant movement that may be caused by the liquid surface upon which the probe will be floating. The total net effect on signal pointing accuracy²⁸ caused by tidal forces can be approximated by referencing Earth-based communications systems and determining the effects of tidal forces on them. Calculating tidal forces that may be experienced by the probe can be done as follows [53]:

$$q_{tid} = \frac{63(GM_P)^{3/2}M_P R_M^5 a^{-15/2} e^2}{4Q_M/2k_m} (13)$$

This calculation determines the total amount of internal heating affected upon a particular planet in Joules. This calculated number can be compared to that of Earth. With a ratio determined, the total potential "wave action," on Uranus may be discerned. In the Equation, G is the gravitational constant, M_P is the mass of a satellite orbiting the planet,²⁹ R_M is the radius of the planet, a is the semimajor axis of the satellite, e is the eccentricity of the satellite's orbit, Q_M is the planet's dissipation constant, and k_M is the planet's tidal love number. Q_M and k_m are calculated as follows [53]:

$$k_2 = \frac{1.5}{1 + \frac{19\mu}{2\rho g R}} (14)$$

²⁸ Potential degradation in terms of dB.

²⁹ Or in the case of the Sun's tidal forces on Uranus, Uranus would be the satellite of the Sun of course. This will carry through for every instance where a satellite of Uranus is mentioned.

Where μ is the rigidity of Uranus, ρ is Uranus' density, R is Uranus' radius, and g is the gravitational pull at Uranus' nominal surface.³⁰ While dissipation constants of planets are reliant upon direct measurements, it is known that the dissipation constants of large planets such as Uranus tend to be on the order of tens to hundreds of thousands. For perspective, the dissipation constant of Jupiter (Q_J) is 3×10^4 . Therefore, we will assume that Uranus' dissipation constant (Q_U) is 10,000. The rigidity of Uranus is based upon its composition and the rigidities of those different materials. Ice has a rigidity of 4×10^9 N/m², and rock has a rigidity of 3×10^{10} N/m² [54]. Since Uranus is proportionally 10/14.5 water-ice, 3/14.5 rocky core, and 1.5/14.5 gaseous atmosphere,³¹ the average rigidity of Uranus (not including the atmosphere) is as follows:

$$\begin{aligned} \mu_{rig,U} &= \frac{(\mu_{rock} \cdot 3) \cdot (\mu_{water-ice} \cdot 10)}{13} = \frac{\left(\left[\frac{3 \times 10^{10} \text{N}}{\text{m}^2}\right] \cdot 3\right) \cdot \left(\left[\frac{4 \times 10^9 \text{N}}{\text{m}^2}\right] \cdot 10\right)}{13} \\ &= \frac{1 \times 10^{10} \text{N}}{\text{m}^2} \end{aligned}$$

Gravitational pull at the nominal surface³² was calculated earlier (12.66 m/s²).

Therefore, the Tidal Love number of Uranus is approximately as follows:

$$k_{2,U} = \frac{1.5}{1 + \frac{19\mu}{2\rho g R}} = \frac{1.5}{1 + \frac{19(1 \times 10^{10} \text{N/m}^2)}{2(1,270 \text{ kg/m}^3)(12.66 \text{ m/s}^2)(2 \times 10^7 \text{ m})}} \approx 1.214$$

Now everything necessary to calculate the total tidal heating that may be expected on Uranus is available. Tidal heating caused by the satellites Miranda, Ariel, Umbriel,

³⁰ That is, the radius at which the probe will be floating.

³¹ This number is used for the purposes of tidal heating calculations. The actual number is less than 0.01%. The difference in final result is, however, negligible.

³² 25,382km – 5,000km \approx 20,000km.

Titania, and Oberon,³³ and the Sun will be calculated. These tidal forces will then be summed to find the overall tidal heating that Uranus experiences. As will be seen, the tidal forces caused by the Sun dominate all others.

$$\sum_{n=1}^N q_{tid,tot} = \sum_{n=1}^N q_{obj,n} = q_{tid,Sun} + q_{tid,Mir} + q_{tid,Ari} + q_{tid,Umb} + q_{tid,Tit} + q_{tid,Ob}$$

where $q_{tid,Sun} \gg (q_{tid,Mir} + q_{tid,Ari} + q_{tid,Umb} + q_{tid,Tit} + q_{tid,Ob})$

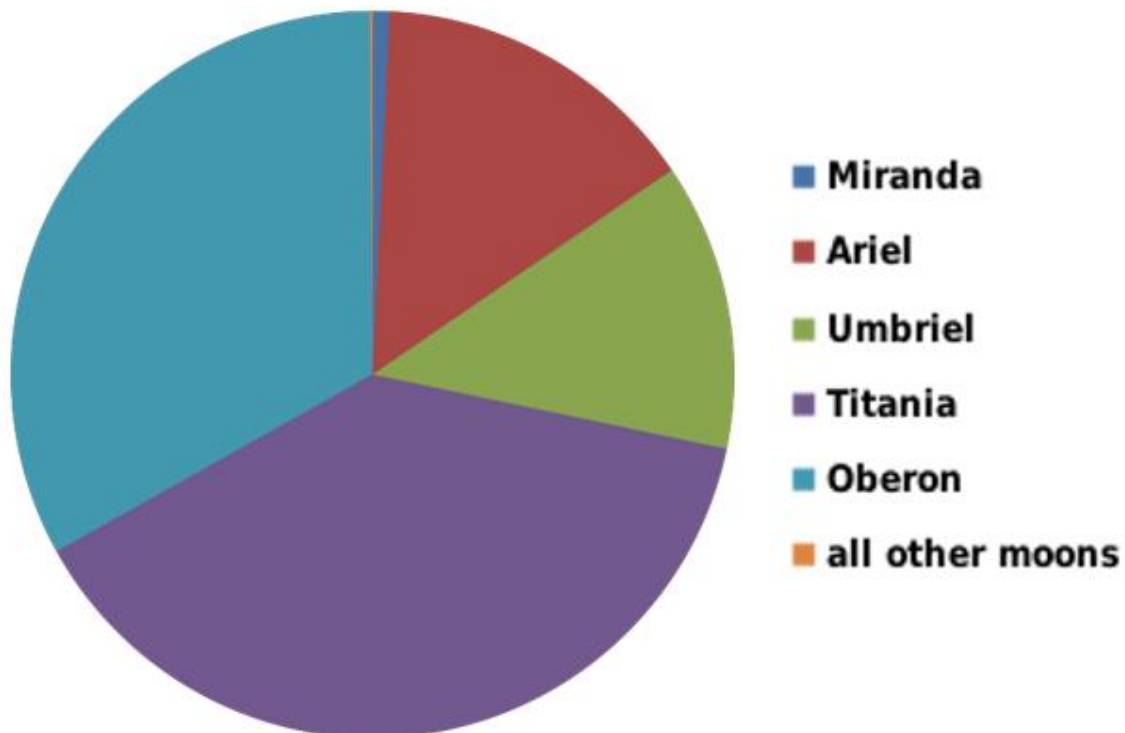


Figure 41: Mass Proportions of Uranus' Various Moons.

Despite the proximity of the moons to Uranus, the Sun's immense mass creates a tidal friction large enough to cause 7.051×10^{28} Joules of internal heating within Uranus.

The relative tidal force for Earth is 2.425×10^{31} Joules. This assumes an Earth dissipation

³³ These moons constitute 99.9% of the mass of all satellites orbiting Uranus, and therefore the bulk of the potential tidal heating.

constant of 100, and a tidal Love number of 0.3531. This is 343.86 times the tidal force that Uranus experiences. Thus, the waves caused by tides can be assumed to be roughly the same proportion less extreme on Uranus. The overall tide swells on Earth, assuming all separate elements,³⁴ is as follows [55]:

$$k_{tot} = M_2 + S_2 + N_2 + k_2 \quad (15)$$

$$k_{tot} = 384.83 \text{ mm} + 179.05 \text{ mm} + 73.69 \text{ mm} + 48.72 \text{ mm} = 0.6863 \text{ meters}$$

This, one can assume, is the average height of a wave on Earth. This indicates that the average wave height about the surface of Uranus' hydrosphere would be roughly 2 millimeters. This is therefore almost no disturbance. The surface of Uranus' hydrosphere should be *exceedingly* still, yet another paradox that this mission could demystify. In addition to these relative calculations, looking at Titan as a reference, this actually makes a lot of sense [56]. Titan's methane ocean waves are no more than a few millimeters in height at maximum. Though methane at temperatures observed on Titan tends to have a fairly high viscosity, accounting for these factors, relatively similar wave sizes, albeit markedly smaller within the same magnitude, can be expected on Uranus.

If we assume a lever arm of a 2-millimeter movement about the probe to be roughly 3,000 millimeters, this makes the angle change as follows:

$$\Delta A = \frac{h_{wave}}{2\pi l_{arm}} \cdot 360 \quad (16)$$

$$\Delta A = \frac{(0.002 \text{ m})}{2\pi(3 \text{ m})} \cdot 360 = 0.037 \text{ degrees}$$

³⁴ This is a highly conservative calculation (meaning bigger than expected), since it includes the tidal forces of the moon on Earth, which causes 54% of the tidal effects experienced [77].

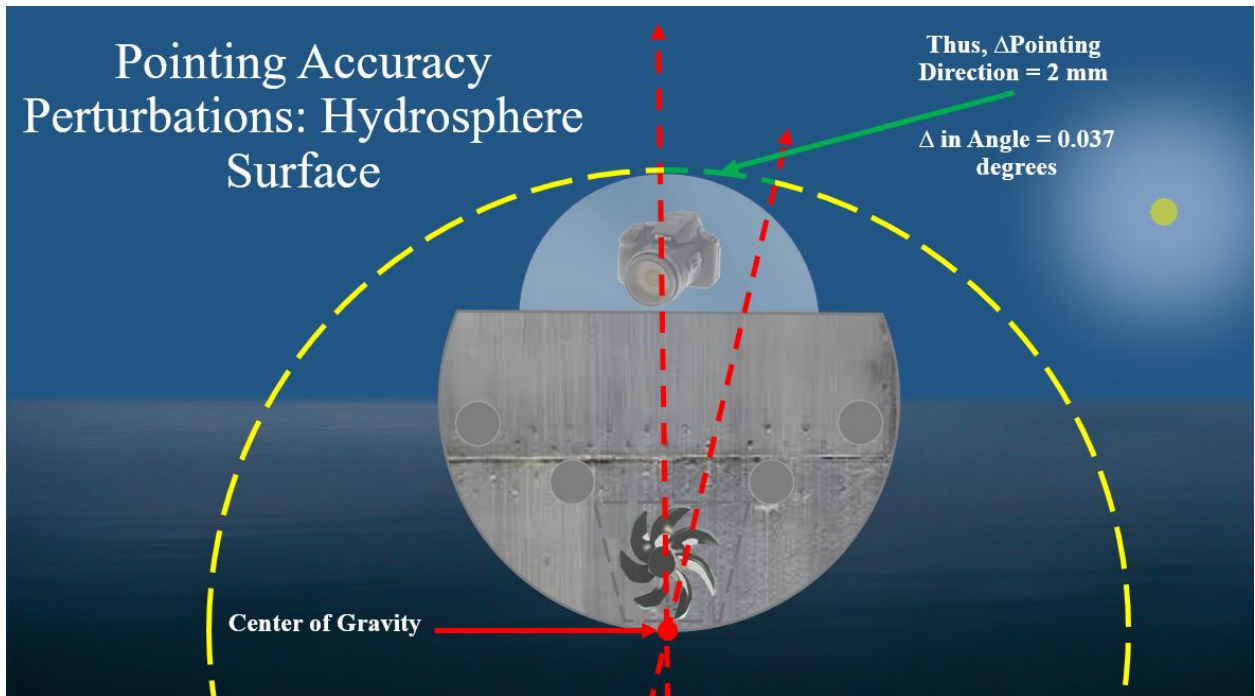


Figure 42: Change in Pointing Direction Due to Tidal Forces.

There are undoubtedly factors that have not been included, such as possible wind action upon the hydrosphere causing the waves to be slightly higher in maximum height, but this pointing direction change is 121.2 times smaller than the beamwidth. Therefore, the wave height would need to be 0.242 meters in height to be larger than the beamwidth. This margin is large enough to allow the propeller and mechanical arms of the camera to provide adequate attitude control.

This, however, is assuming the probe's center of gravity and center of buoyancy are the same, at the bottom of the probe. If, however, the center of buoyancy is moved closer to the antenna, the lever arm between the torque moment and the camera will be reduced, thus reducing the total perceived angle change in the antenna's direction.

3.9 Probe Design

The inclusion of ballast equalization capability—something already included in the current design reference mission’s probe [57]—could allow the probe to go under the surface of the hydrosphere and take further measurements, visually and otherwise. This would also increase the utility of potential cube/small satellites of the proposed satellite constellation construction in this mission set. This is because the ability to send radio signals through water is greatly diminished, and range amplification would be necessary. How deep the probe could submerge would be drastically augmented by overhead small satellites available for nearly 100% uptime to any outgoing signal of the probe. This, in addition to complex modern internal subroutines that prevent the probe from permanently losing signal or staying submerged indefinitely, would be implemented.

Ballast entry could serve a double purpose of also allowing for large material sampling chambers of any ballast liquid allowed in. Science experiments similar to those of the Mars Curiosity Rover could be used, measuring methane content, biological content, and the presence of hydrocarbons. Depth of submersion also changes the requirements for withstanding external pressures. This is a design limitation that must be strongly scrutinized, due to the already very high pressures at the base of the Uranian troposphere.

Probe size is limited by the absolute largest fairing that can be mounted upon the Falcon 9 Heavy. Additionally, any extra propellant that needs to be carried in order to attain Uranian orbit will take up extra space inside the fairing. As it stands, the Falcon Heavy’s payload capacity—not including embedded rocket engines inside the fairing—is

3,500 kg for the mission set. 3,500 kg is *not* generous, as will be seen later. This is something akin to a small submarine, rather than a simple submersible probe.

Harkening back to the previous section on tidal effects, one can begin discussing the antenna array design for the probe. Due to the expected tidal forces on the hydrosphere of Uranus, pointing angle change would be approximately instantaneous, and therefore the pointing accuracy would be required instantaneous as well. While this is an approximation, it nevertheless gives one insight into what can be expected for signal propagation. Referring back to missions such as those to Mars have significant simplifications in signal propagation, as the landers and rovers rested upon solid ground with minimal atmospheric perturbations. This presents difficulties, but none that are insurmountable.

Beyond this, such a small antenna is not typically mass-produced, though it can be otherwise made relatively easily. Usually, if a design calls for such a small diameter, the antenna will instead be made into a flat-panel. This type of antenna has a hemispheric beamwidth (180 degrees). The issue is attaining the required 31 dB gain from such an antenna. The gain of a flat-panel antenna is predicated upon the width of the panel to be used. All other factors being equal, finding the required width of such an antenna is as follows [58]:

$$\begin{aligned} W_{fp} &= \sqrt{\frac{G_{req}}{4\pi}} \lambda \quad (17) \\ &= \sqrt{\frac{1,297.1}{4\pi}} (0.003 \text{ m}) = 3.1 \text{ cm} \end{aligned}$$

Calculating this, one must then use the original number to iteratively determine the efficiency of said flat-panel antenna. This is because the efficiency of the antenna is contingent upon the antenna's width, which then changes the antenna's gain [58]:

$$\eta = 10^{\frac{\alpha}{10}} \quad (18)$$

$$\rightarrow \alpha = G(dB) - 21.5 - 20 \cdot \log_{10}[f(\text{GHz})] - 20 \cdot \log_{10}[W(\text{m})] \quad (19)$$

Using the two previous equations, the efficiency of the flat panel antenna with the above required width is 98.98%. Therefore, any iteration would yield minimal change and is not necessary. One way or another, this calculation does not yield a necessarily conservative estimate. Thus, the standard 0.5 to 0.6 antenna efficiency observed for antennas will be used instead [59]. Either way, this difference would only amount to a gain of approximately 3 dB, rather trivial in the grand scheme of the design. Therefore, the conservative value was chosen.

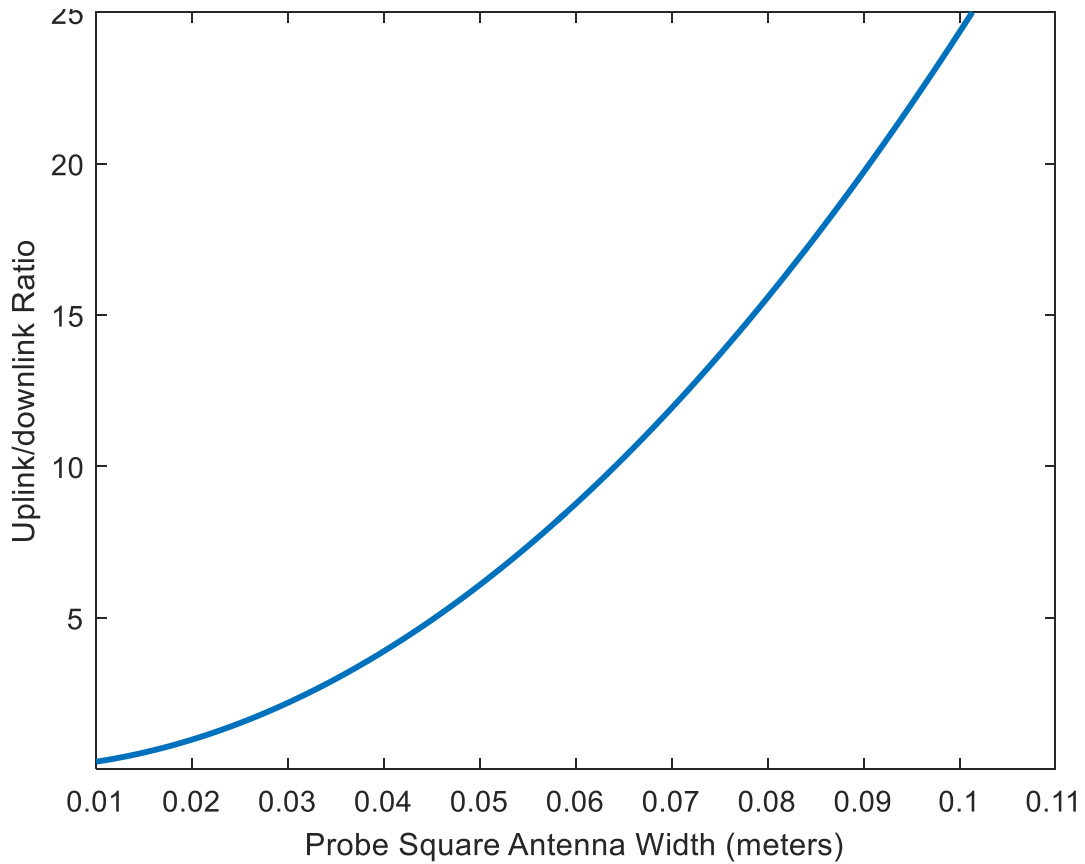


Figure 43: Uplink/Downlink Ratio with Flat-Panel, Square Antenna.

Once signal propagation from the probe to the mothership is sorted out, the next major feat is to determine the methodology and capability of sending the signal back to Earth. At closest approach,³⁵ it takes roughly 2.77 hours for a signal sent from Uranus to make it back to Earth.

³⁵ 18.33 astronomical units.

3.10.1 Doppler and Collision Broadening Science

One of the primary scientific inquiries of this thesis is an elaboration upon Doppler and collision broadening, and how this science can robustly be conducted upon arrival at Uranus. Doppler and collision broadening, or the broadening of attenuation spectra caused by increasing the density of a given medium is a frontier of contemporary communications science, with still much to be learned.

While long-term scientific studies can be conducted utilizing tabular matrices that allow for sifting through compounds, pressure regimes, temperature regimes, and more—much of which will be done in this thesis, only very specific portions of the electromagnetic spectrum have been analyzed with a great deal of scrutiny, and only very specific combinations of molecules and elements. With Uranus' 83% molecular hydrogen, 15% helium, and approximately 2% methane atmosphere, pressure variations much greater than Earth, and atmospheric thickness far greater as well, it offers up an opportunity to discern how these compounds attenuate frequencies. In truth, these types of scientific inquiries in the future should be conducted on any and all celestial bodies explored. How does a 100 picobar molecular hydrogen atmosphere attenuate frequencies at 300 GHz, for example? What about a three-bar CO₂ atmosphere attenuation of a 6 THz signal? As can be seen, the possibilities of inquiry are essentially endless.

For the purposes of this thesis, a theoretical look into Doppler and collision broadening was pursued, with an obvious limitation of not being able to conduct direct experiments on Uranus' atmosphere. The theoretical frequencies in question were between 1 and 100 GHz. Composition of the atmosphere in question was built to match

that of Uranus: 83% molecular hydrogen, 15% helium, and 2% methane. Theoretical attenuation data was gleaned from NIST et. al.

3.10.2 Collision Broadening Calculations Methodology

In MATLAB, the first step was to build vectors with known energy levels per molecule/atom of specific compounds. For testing, this was accomplished by gathering attenuation data for X-rays (not the frequencies in question) from NIST, and converting the data into the appropriate format. Data on the KeV potential of the compounds in question was also gleaned and vectorized in the same fashion.³⁶ All told, there were 165 lines of data per compound at 1 atmosphere pressure.

The next step was to attain a density-weighted average of the temperature of Uranus' atmosphere. This was accomplished by building two separate vectors—one with incremental mbar-logarithmic steps in pressure change, the other with empirically-measured temperatures at those pressures within the Uranian atmosphere. These two vectors were then multiplied together, the resulting magnitudes summed up, and then averaged by dividing by the total number of data points. MATLAB code accomplishing this is shown below:

```
pxmbar = [0.2 0.4 0.6... all the way to 100,000 mbar logarithmically];  
tempU = [92 112 91... all the way to 100,000 mbar pressure level];  
inttempU = pxmbar.*tempU;  
avgtempU = sum(inttempU)/sum(pxmbar);
```

³⁶ MATLAB line 539 is where this portion of the program starts.

Assuming each vector has an equal length, and data is scaled logarithmically, this should yield an average temperature of the entire atmosphere. Once this was accomplished and vectors transformed appropriately, the net effect each compound would have on the overall attenuation of the atmosphere is scaled by each respective compounds' overall composition of the atmosphere. For instance, molecular hydrogen's KeV data (called Hydrogen in the MATLAB code) was scaled in this way:

$$\textit{Hydrogen} = [0.454, 0.397, .297\dots];$$

$$\textit{Hydrogencomp} = \textit{Hydrogen}.*0.83;$$

The same process was followed for helium and methane. This resulted in the following logarithmic graphs for attenuation shown. Again, it is important to note that these graphs are purely for the methodology; the frequency range in question is that of X-rays.

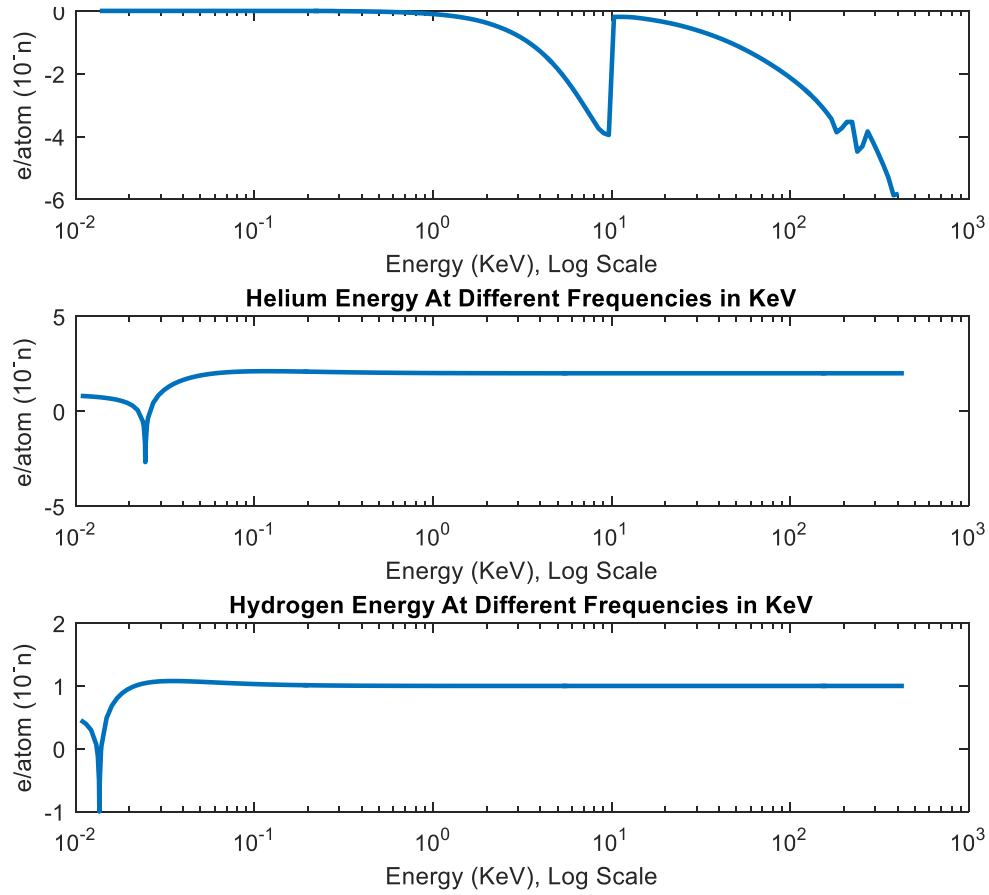


Figure 44: Attenuation Spectra of CH₄, He, and H₂ in the X-ray Band.

After this was accomplished, the atmospheric composition was derived by adding together the respective vectors, looking like this:

$$Atm_{comp} = Methane_{comp} + Helium_{comp} + Hydrogen_{comp} \quad (20)$$

The same process was conducted per unit of each compound. The weighted composite atmospheric attenuation for the Uranian atmosphere is as follows:

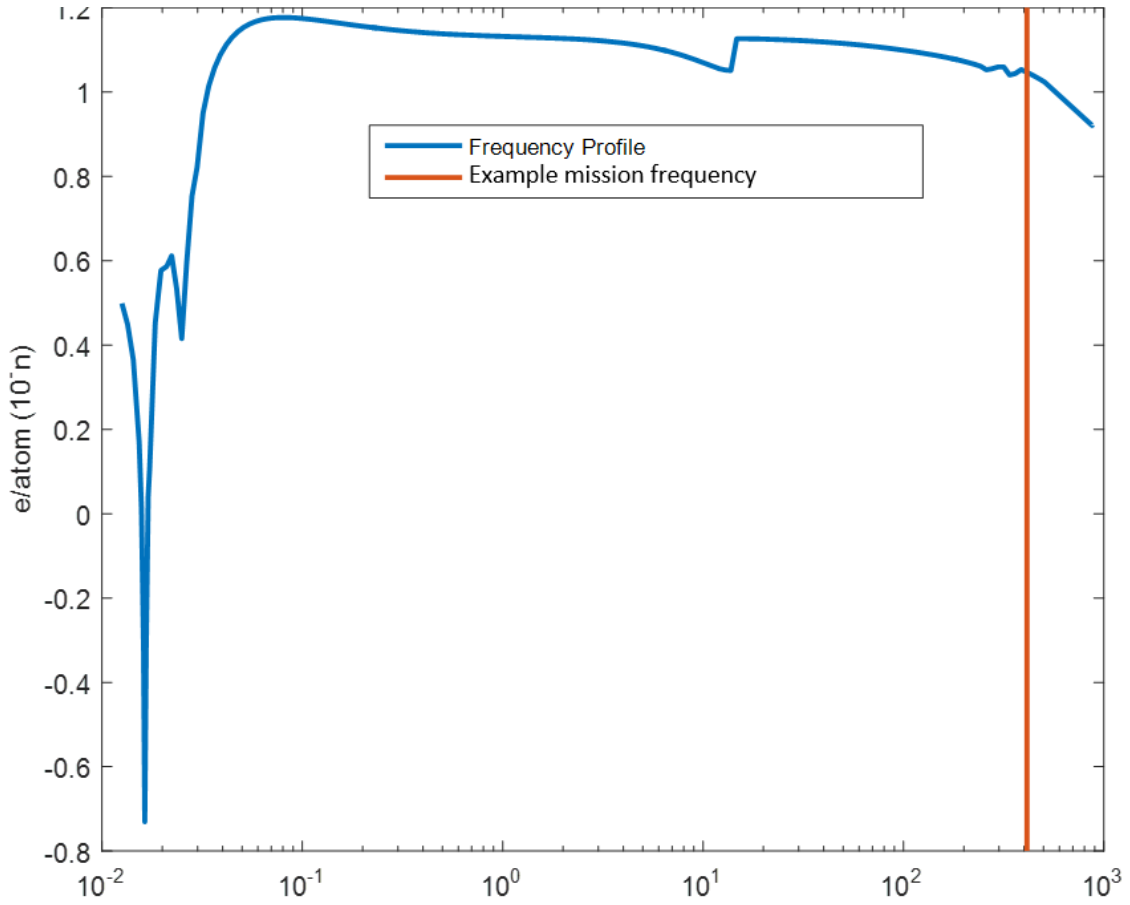


Figure 45: Attenuation of the Uranian Atmosphere.

Beyond this, a reduced mass molecular couple for each compound needed to be discerned. This required taking the average molecular mass of each compound and carrying out the following calculation:

$$\mu = m_{meth} - \frac{m_{meth}m_{H_2}m_{He}}{m_{meth}+m_{H_2}+m_{He}} \quad (21)$$

Where m_{meth} is the molecular mass of methane, m_{H_2} is the molecular mass of H_2 , and m_{He} is the molecular mass of helium. The above calculation must be accomplished with all three compounds. This calculation will expand depending upon the number of compounds in the gaseous mixture.

The next step is to find the self-broadening figure for each compound. The equation is as follows:

$$B_{S,Hyd} = \left(\frac{8kT}{\pi m_{Hyd,r}} \right)^{1/2} \quad (22)$$

Where $B_{s,Hyd}$ is the self-broadening factor of the compound—molecular hydrogen in the above example— k is Boltzmann’s constant, T is the temperature figure used for the medium in question,³⁷ and $m_{Hyd,r}$ is the reduced mass molecular couple of the compound. One then multiplies these figures by the partial pressure of each compound to get the self-broadening coefficient. From there, one finds the total effective pressure of the medium, as follows:

$$P_{eff} = P_{e,Hyd} + P_{e,He} + P_{e,meth} \quad (23)$$

Where P_{eff} is the overall effective pressure of the medium, $P_{e,Hyd}$ is the effective partial pressure of molecular hydrogen, $P_{e,He}$ is the effective partial pressure of helium, and $P_{e,meth}$ is the effective partial pressure of methane. One then must find the line half-width broadening coefficient of each compound. This is accomplished with the following equation:

$$C_{HW} = \frac{\left(\frac{2}{\sqrt{\pi}}\right) \cdot (D_{eff} \cdot 100)^2 \cdot P_{eff}}{c \cdot \sqrt{m_c k T}} \quad (24)$$

Where C_{HW} is the half-width broadening coefficient, D_{eff} is the effective diameter of the molecule or element, P_{eff} is the self-broadening-reduced effective pressure of the medium, c is the speed of light, m_c is the atomic mass of the molecule or element, k is

³⁷ In this case, we’re using the density-weighted average temperature of Uranus’ atmosphere.

Boltzmann's constant, and T is the temperature of the medium to be used. This equation must be calculated for each compound in question within the medium.

3.10.3 Doppler and Overall Broadening Calculations

With previous calculations, Doppler broadening numbers are now relatively straightforward to determine. To calculate Doppler broadening, it must be accomplished for all compounds in question within the medium, the same as with collision broadening, previously discussed. The equation to accomplish this is as follows:

$$B_D = \sqrt{\left(\frac{2kT}{m_c}\right) \cdot \log(2)} \quad (25)$$

Where k is again Boltzmann's constant, and B_D is the Doppler broadening end result.

Now that Doppler and collision broadening are discerned for each compound within the medium, it is a matter of simply adding the two numbers, which are overall coefficients to be utilized in the filtering methodology developed later.

$$B_{tot,c} = B_{D,c} + B_{C,c} \quad (26)$$

Where B_D is again the broadening of the spectral attenuation bands caused by Doppler effects, and B_C is the broadening of the spectral attenuation bands caused by molecular collisions. This will be accomplished for each compound in question, and the broadening coefficient provided for it. B_{Tot} is of course the total broadening coefficient to be theoretically observed.

3.10.4 Doppler and Collision Broadening Modelling Through Filters

The question then becomes how to accurately model these attenuation broadening effects in MATLAB, in a way that is visually simple and digestible. The way this was accomplished was by implementing a simple filtering method utilizing filtering assets native to the MATLAB computational engine.³⁸ Due to the high slope of the attenuation bands of all but methane in this methodology, notch filters were primarily used. Since methane had a steady logarithmic attenuation after the desired mission frequency, a basic filter was used for its filtering process. Filters used are shown as follows, before and after broadening effects are implemented.

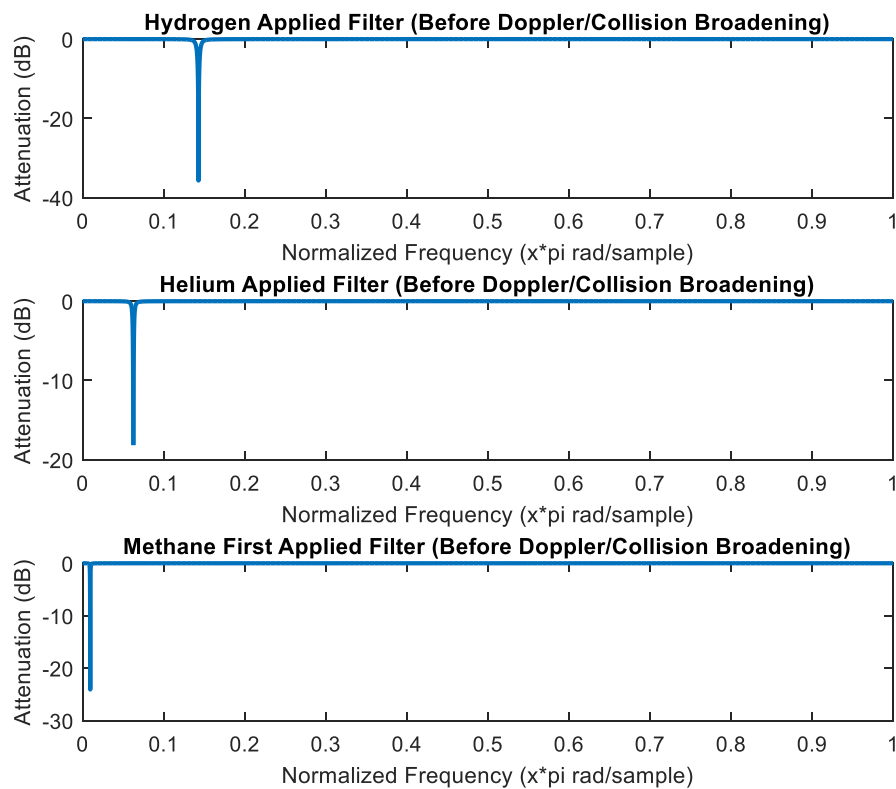


Figure 46: Selected Filters Before Broadening Effects.

³⁸ Line 671 of MATLAB code.

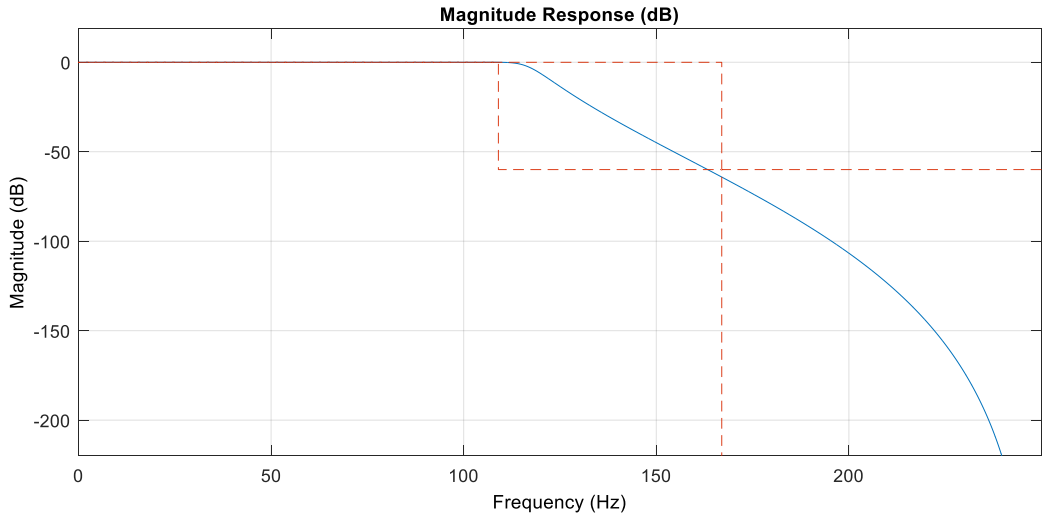


Figure 47: Filter for Methane's Higher Frequency Bands.

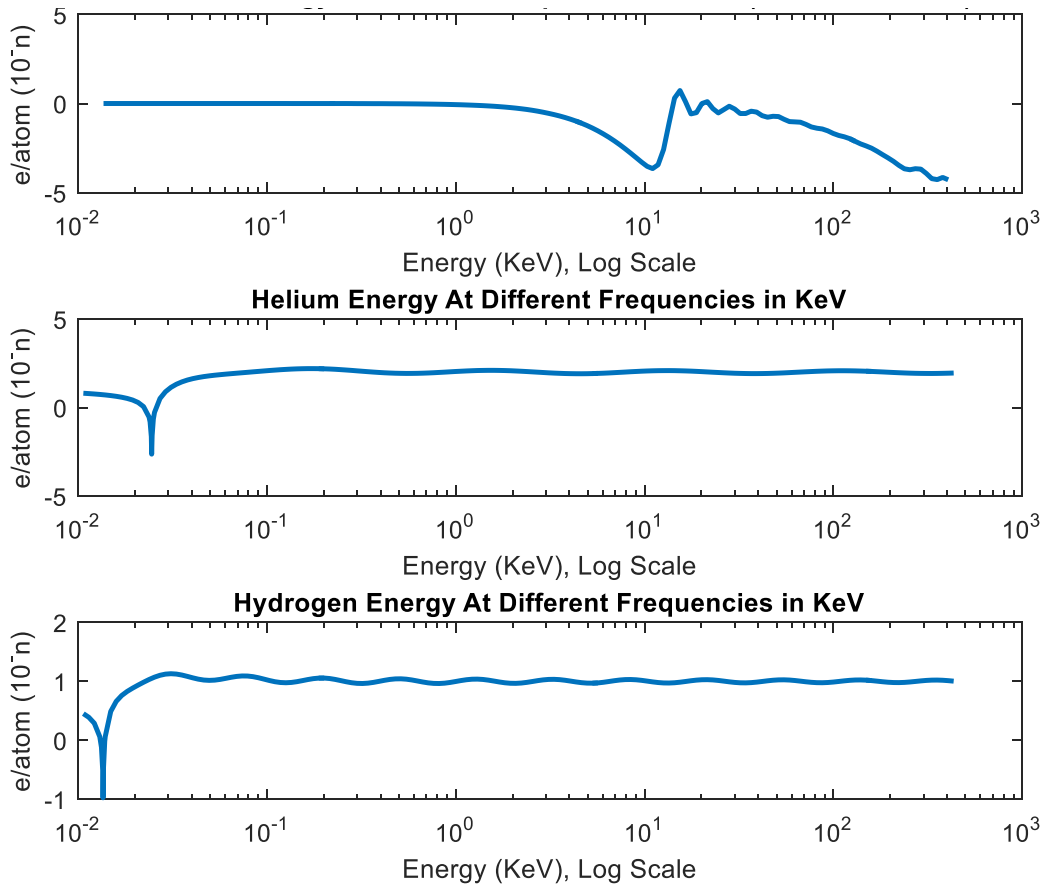


Figure 48: Attenuation Bands After Broadening Coefficients Implemented.

The final overall atmospheric attenuation with implemented broadening coefficients is shown as follows:

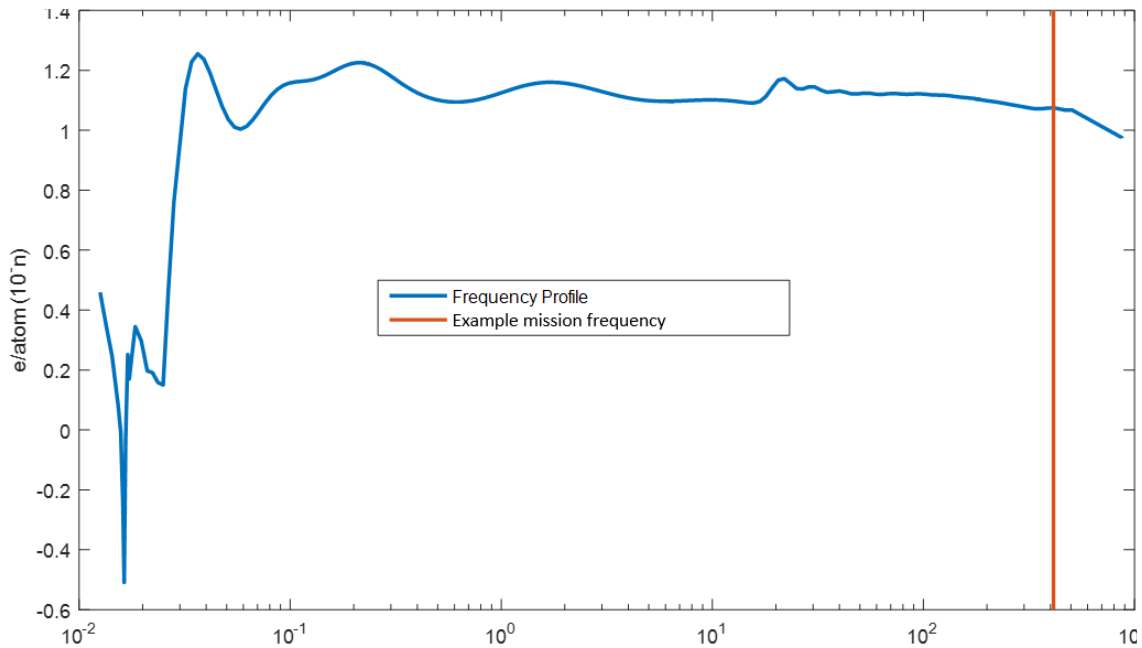


Figure 49: Final Uranian Atmospheric Attenuation for X-rays, After Broadening.

It must be noted that selected filter types can differ, leading to significantly altered final results. The filters used for this methodology led to a noticeable ripple in the pass band that, if another filter type were selected, may or may not be present. This is merely meant to be a representation for a potential method by which collision broadening can be successfully taken into account in scientific models.

3.11 Falcon 9 Heavy Launch Vehicle

Using the Space Shuttle (STS) missions as a reference [60], the payload fairing of the Falcon 9 Heavy has roughly half the volume [61]. Though it must be noted that the Shuttle was a bay, not a fairing. While the mass margin for this design may be significantly improved upon from other launch vehicles, this proves to be useless if those

massive payloads cannot fit into the fairing. Nevertheless, fairings are a relatively easy thing to choose/design. For reference, the maximum size fairing currently available is a Delta IV fairing, which is 19.82 meters in length [62].

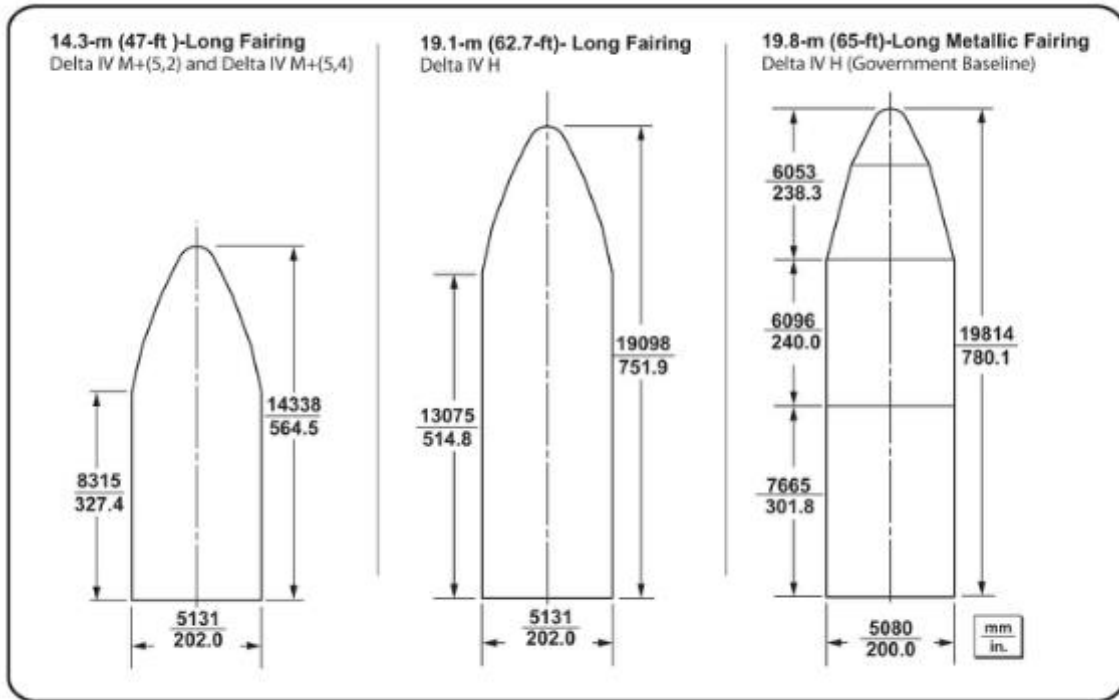


Figure 50: Possible Payload Fairings of the Delta IV Rocket.

This table shows mass what can be launched upon the Falcon 9 Heavy launch vehicle, not volume in the fairing [61].

Table 6: Falcon 9 Heavy Payload Capacity Versus Mission Distance Desired.

Destination	Falcon Heavy			Falcon 9
	Aug 2013 to Apr 2016	May 2016 to Mar 2017	Since Apr 2017	
LEO (28.5°)	53,000 kg	54,400 kg	63,800 kg	22,800 kg
GTO (27°)	21,200 kg	22,200 kg	26,700 kg	8,300 kg
Mars	13,200 kg	13,600 kg	16,800 kg	4,020 kg
Pluto	--	2,900 kg	3,500 kg	--

3.12 Orbital Dynamics

Among the first tasks at hand is to calculate the total ΔV that will be needed in order to get the spacecraft from Earth to Uranus. Beyond this, various different gravity assist regimes and other manipulations can be carried out. The ideal—or cheapest—scheme to use, seeing as how the Falcon 9 Heavy is to be used as the launch vehicle, is to determine the ΔV requirements starting from a Geo-Transfer Orbit at low altitude, and boost from there to the next destination in a patched conic manner; 180 km above the surface is a common initial reference frame. The ideal rocket equation, shown in Equation (27), yields the ΔV for the regimes in question. As mentioned, a patched conic will be used, which provides sufficient accuracy for the purposes of this analysis.

$$\Delta V = I_{SP} g_0 \ln \left(\frac{m_i}{m_f} \right) \quad (27)$$

I_{SP} is the specific impulse of the propellant used for this design. This varies with every stage of the flight path, based on the propellants and the engine involved. g_0 is

Earth's gravitational acceleration at standard sea level, 9.80665 m/s^2 . This value does not change, no matter where the spacecraft is in the Solar System and beyond. It acts as a constant. m_i is the initial mass of the system, including propellant, payload, and the rocket itself, and m_f is the dry mass of the system. m_i and m_f can be further manipulated by splitting up the rocket's launch profile into several stages. For initial analysis, this was not done. The I_{SP} selected was 285 seconds for the first stage, 465 seconds for the geosynchronous transfer orbit to Earth escape portion of the flight profile, and 285 seconds for the Uranus orbital insertion portion of the flight profile. This corresponds to the specific impulses of a kerosene propellant, an $\text{H}_2\text{-O}_2$ propellant, and a solid propellant respectively.

To determine the ΔV required based upon the mass of the Earth and the spacecraft's initial and final orbits, we used the patched conic ΔV equation shown in Equation (29).

$$V = \sqrt{\frac{2\mu_1}{a_1} - \frac{\mu_2}{a_2}} \quad (28)$$

Initially, the Falcon 9 Heavy will achieve a semimajor axis in this patched conic calculation of 24,363.5 km above the surface of Earth, but it will have an initial, non-circularized radius above Earth of 6,563 km. This also corresponds to when the first stage of the rocket will be discarded, is tangent to a geosynchronous orbit, and the ideal rocket equation variables will change. This is therefore a_1 . Geostationary orbit resides at 42,164 km, which yields an a_2 of 24,363.5 km [29]. The reason for this is that the perigee of the orbit is still the same. The geostationary orbit is not a completed Hohmann transfer at this point. It will not be completed, as the semimajor axis is intended to reach Uranus. μ_1 and

μ_2 are the same. They are the μ of Earth, which is the mass of Earth multiplied by the gravitational constant.³⁹ Thus,

$$V = \sqrt{\frac{2\mu_1}{a_1} - \frac{\mu_2}{a_2}} = \sqrt{\frac{2\left(3.986 \times 10^{14} \frac{\text{m}^3}{\text{s}^2}\right)}{(6,563 \times 10^3 \text{ m})} - \frac{3.986 \times 10^{14} \frac{\text{m}^3}{\text{s}^2}}{(24,363.5 \times 10^3 \text{ m})}} = 10.25 \frac{\text{km}}{\text{s}} \quad 40$$

The next step is to calculate the velocity the spacecraft must attain near Earth in order to attain a Uranus-orbit semimajor axis apogee. That is, the spacecraft will boost itself up to an “altitude” equivalent to the orbit of Uranus. Therefore, r_E (the radius at Earth before the transfer burn) is 1 astronomical unit (AU) = 1.496×10^{11} m, and $r_U = 18.33 \times (1 \text{ AU}) = 2.742 \times 10^{12}$ m. The μ of the Sun will be used during this transit, a transit that assumes that the spacecraft has escaped Earth’s gravity well, and has not entered Uranus’ gravity well.

$$a_{EU} = \frac{r_E + r_U}{2}$$

$$V_{near \ Earth} = \sqrt{\frac{2\mu_S}{a_E} - \frac{\mu_S}{a_{EU}}}$$

$$= \sqrt{\frac{2\left(1.32712828 \times 10^{20} \frac{\text{m}^3}{\text{s}^2}\right)}{(1.4964034 \times 10^{11} \text{ m})} - \frac{1.32712828 \times 10^{20} \frac{\text{m}^3}{\text{s}^2}}{(1.4458846 \times 10^{12} \text{ m})}} = 41.1 \frac{\text{km}}{\text{s}} \quad 41$$

In order to determine the excess velocity required to reach Uranus, one must determine the orbital velocity of Earth, which is a well-known figure of 29.78 km/s. This means that a hyperbolic excess velocity of 11.23 km/s is required. With this hyperbolic

³⁹ $G = 6.67408 \times 10^{-11} \text{ m}^3/\text{kg}\cdot\text{s}^2$.

⁴⁰ Line 46, “Geo-transit Orbit Given by Falcon Heavy.”

⁴¹ Line 48, “Geo-transit Orbit Given by Falcon Heavy.”

excess velocity, a hypothetical semimajor axis can be found, which then will be used to determine the required total delivered ΔV near Earth, in order to attain Earth escape and Uranus transfer.

$$a_U = -\left(\frac{\mu_E}{V_{HE}^2}\right) = -\left(\frac{3.986 \times 10^{14} \frac{\text{m}^3}{\text{s}^2}}{\left(\frac{11.23134 \times 10^3 \text{m}}{\text{s}}\right)^2}\right) = -3,159.91 \text{ km} \quad 42$$

Thus, the required delivered velocity near Earth is

$$V_{del} = \sqrt{\frac{2\mu_E}{a_E} - \frac{\mu_E}{a_{HE1}}} = \sqrt{\frac{2\left(3.986 \times 10^{14} \frac{\text{m}^3}{\text{s}^2}\right)}{(6,563 \times 10^3 \text{ m})} - \frac{3.986 \times 10^{14} \frac{\text{m}^3}{\text{s}^2}}{(-3,159.91 \times 10^3 \text{ m})}} = 15.735 \frac{\text{km}}{\text{s}} \quad 43$$

This means that the total velocity that must be delivered by the second stage of the spacecraft is 5.483 km/s. With this, one can use the ideal rocket equation to get an achievable mass ratio at the edge of Earth's Hill Radius. The Hill Radius can be calculated using the following equation:

$$r_H = a(1 - e)^3 \sqrt{\frac{m_{Earth}}{3m_{Sun}}} \quad (29)$$

Where e is the eccentricity of Earth's orbit, m_{Earth} is the mass of Earth, and m_{Sun} is the mass of the Sun. Carrying out this calculation, the Hill Radius of Earth is found to be approximately 1.45 million kms. Using the ideal rocket equation, the mass ratio to this radius is

$$\Delta V = I_{SP} g_0 \ln\left(\frac{m_i}{m_f}\right) \rightarrow \frac{\Delta V}{I_{SP} g_0} = \ln\left(\frac{m_i}{m_f}\right) \rightarrow e^{\frac{\Delta V}{I_{SP} g_0}} = \frac{m_i}{m_f}$$

⁴² Line 50, "Geo-transit Orbit Given by Falcon Heavy."

⁴³ Line 51, "Geo-transit Orbit Given by Falcon Heavy."

$$\rightarrow e^{\frac{5483.4 \text{ m/s}}{(465 \text{ s})(9.80665 \frac{\text{m}}{\text{s}^2})}} = \frac{m_i}{m_f} = 3.328 \quad 44$$

Thus, if 26,700 kg can be sent to geostationary orbit by the Falcon Heavy, 8,022 kg will reach Earth escape. Assuming that we have a 10% loss, this mass becomes 6,154 kg.

This process is iterated again for Uranus insertion. However, there is another step that will be placed in between Earth escape and Uranus insertion, and that is using Jupiter for a gravity assist maneuver. In order to determine to what effect Jupiter can be utilized for such a maneuver, first, one must determine spacecraft state upon reaching Jupiter. That is, what will the excess potential of the spacecraft be (hyperbolic excess velocity)? Assuming the orbital radius of Jupiter is 7.78567×10^8 km, one can find the velocity of the spacecraft near Jupiter.

$$V_{near \text{ Jupiter}} = \sqrt{\frac{2\mu_s}{a_j} - \frac{\mu_s}{(1\text{AU} + 5.204\text{AU})}}$$

$$= \sqrt{\frac{2 \left(1.327 \times 10^{20} \frac{\text{m}^3}{\text{s}^2} \right)}{(7.785 \times 10^{11} \text{ m})} - \frac{1.327 \times 10^{20} \frac{\text{m}^3}{\text{s}^2}}{(1.496 \times 10^{11} \text{ m} + 7.785 \times 10^{11} \text{ m})}} = 9.729 \text{ km/s}$$

With this velocity, one can determine the deflection angle, based upon a pre-selected minimum altitude above the surface of Jupiter when the spacecraft flies by the planet. This number will vary depending upon the time of launch, and the amount of propellant one is willing to use to get the spacecraft to align with any specified altitude. The equation for determining the spacecraft's deflection angle is shown in Equation (30).

⁴⁴ Line 54, "Geo-transit Orbit Given by Falcon Heavy."

$$\delta = 2 \sin^{-1} \left[\frac{1}{1 + \left(\frac{r_p |v_{\infty}|^2}{\mu_{Jupiter}} \right)} \right] \quad (30)$$

$$= 2 \sin^{-1} \left[\frac{1}{1 + \left(\frac{(2.5 \times 10^9 \text{ m}) \left| 9.279 \times 10^3 \frac{\text{m}}{\text{s}} \right|^2}{(1.266 \times 10^{17} \frac{\text{m}^3}{\text{s}^2})} \right)} \right]$$

$$= 42.46^\circ$$

This being a hypothetical example, the altitude over Jupiter can be changed in order to change the deflection angle. This can be a very useful tool in lowering the overall ΔV requirement upon Uranian orbital insertion.

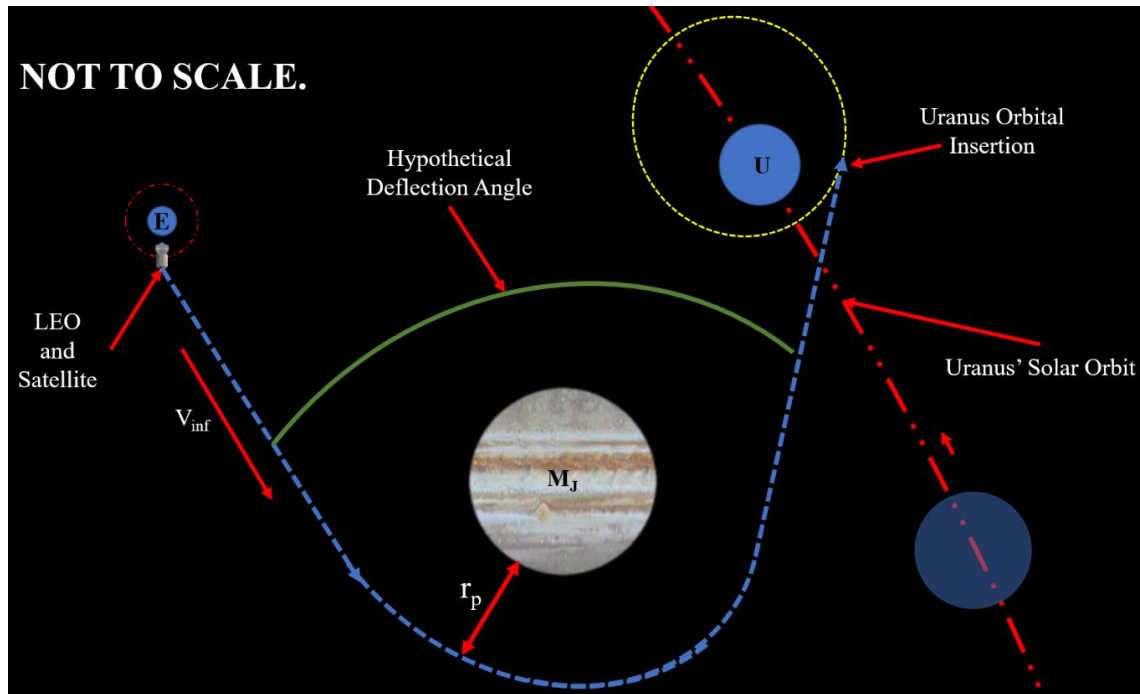


Figure 51: Hypothetical Jupiter Gravity Assist Maneuver.

Therefore, the velocity upon exiting Jupiter's influence⁴⁵ is as follows:

$$V_{exit} = V_J + V_{near\ Jupiter} \cos(\delta) \quad (31)$$

$$= \left(13.07 \frac{\text{km}}{\text{s}}\right) + \left(9.73 \frac{\text{km}}{\text{s}}\right) \cos(40.81^\circ) = 20.43 \text{ km/s}$$

Based upon the ΔV delivered, and the distance that the spacecraft must travel in a Hohmann transfer orbit, the total time for the trip is calculated as follows:

$$T_{flight} = \pi \sqrt{\frac{a^3}{\mu_{Sun}}} \quad (32)$$

Where a is the semimajor axis of the Hohmann transfer orbit, and μ_{Sun} is the mass of the Sun multiplied by Newton's gravitational constant.

$$= \pi \sqrt{\frac{(1.5042 \times 10^{12} \text{ m})^3}{\left(\frac{1.327 \times 10^{20} \text{ m}^3}{\text{s}^2}\right)}} = 15.95 \text{ years}$$

Based upon the 16-year travel time and the radioactive decay of plutonium, the power that will be delivered at Uranus is significantly different when compared to the beginning of the mission. The mission design calls for five to ten SRTGs, utilizing plutonium as the primary power source. This is required due the extended distances at which the mission will take place. The overall power delivered by the Sun at this distance, assuming $S = 1,353 \text{ W/m}^2$ at Earth, is inversely proportional to the square of the distance away from the Sun. That is, with Uranus currently 19.5 times farther away from the Sun than the Earth is, the total power delivered if solar panels at 25% efficiency were used would be:

⁴⁵ In reference to the Sun.

$$P_{delivered} = S \left(\frac{1}{r^2} \right) e_{sp} A_{sp} \quad (33)$$

Where S is the reference solar flux taken at Earth's distance from the Sun, r is the radius (in astronomical units) of the orbit, e_{sp} is the efficiency of the solar panels, and A_{sp} is the area of the solar panels.⁴⁶ The total usable surface area of a CubeSat in this design would be roughly 0.0929 m^2 ,⁴⁷ which means that the total power that could be delivered to a CubeSat from solar panels would be

$$\begin{aligned} P_{delivered} &= \left(1,353 \frac{\text{W}}{\text{m}^2} \right) \left(\frac{1}{(19.5)^2} \right) (0.25)(0.0929 \text{ m}^2) = 0.0935 \text{ watts} \\ &= -10.291 \text{ dBW} \quad 48 \end{aligned}$$

For a cellphone, 94 milliwatts may be sufficient transmission power, but the distances traveled from one repeater to another on Earth are typically on the order of a few dozen km. The loss due to free space alone, from one CubeSat to another in the proposed constellation assuming a 90-degree orbit separation is at a minimum⁴⁹

$$L_{FS} = \left(\frac{4\pi D_{cubes}}{\lambda} \right)^2 = 1.893 \times 10^{22} = 222.77 \text{ dB}$$

Where D_{cubes} is the distance between the CubeSats (orbital radius $\times \sqrt{2}$), and λ is the wavelength of a 30 GHz carrier. Therefore, the received power at the mothership, which is designed for a signal amplification of 80 dB would be (at best) -153 dBW, or 4.9422 attowatts. This also assumes 100% of the power received from the Sun is used for the communication system *and* is transmitted with 100% efficiency. Assuming an

⁴⁶ This calculation does not take into consideration the degradation of the solar panels over a 13 to 16-year transit time.

⁴⁷ This does not include the reduction in efficiency due to surfaces not facing the Sun.

⁴⁸ Line 449, "Cube Satellite Signal Capabilities."

⁴⁹ This calculation also assumes a circular orbit, which is not the case.

omnidirectional antenna, an efficiency of the TWTA of 19%, a total CubeSat-mothership system noise temperature of 150 Kelvin, and a minimum acceptable signal-to-noise ratio of 10 dB, the bit rate in this system would be as follows:

$$R_b = \frac{P_r}{10N_0} = \frac{P_r}{10kT}$$

3.13 Launch ΔV Estimations

Running a simple routine of mathematical calculations, one can determine a Pareto optimal front for mass and launch ΔV for this mission set. If the following launch characteristics are assumed, then a simple manipulation of the launch mass can determine the overall ΔV available for the mission.

Table 7: Top-Level General Figures.

Falcon Heavy		
Lift off mass	1420788	kg
Payload to GTO	63800	kg
deadweight fraction	0.05	
Mean Throttle position	0.949252	

Table 8: Interim Calculations.

Boosters	2	First Stage	1	2nd Stage	1
Engines	9	Engines	9	Engines	1
F sea level	7600000 N	F sea level	7600000 N	F sea level	
F vacuum	8200000 N	F vacuum	8200000 N	F vacuum	934000 N
Isp sea level	282 s	Isp sea level	282 s	Isp sea level	
Isp vac	311 s	Isp vac	311 s	Isp vac	348 s
mass flow sea level	2748 kg/s	mass flow sea level	2748 kg/s	mass flow sea level	
	2688		2688		273 kg/s
Burn time	154 s	Burn time	187 s	Burn time	397 s
Mass Propellant	397389 kg	Mass Propellant	397389 kg	Mass Propellant	103138 kg
Mass Dead	18923 kg	Mass Dead	18923 kg	Mass Dead	4911 kg
Mass Boosters	832625 kg	Mass 1st stage	416312 kg	Mass 2nd stage	108049 kg

Table 9: ΔV Figures.

Mass on Pad	1361988 kg	ΔV
Booster+1st stage		
Effective Isp	296 s	
Starting mass	1361988 kg	4831
Final Mass	258544.5028 kg	
1st stage post booster		
effective Isp	311 s	
Starting mass	220697 kg	1591
Final mass	130990 kg	
2nd stage		
effective Isp	348 s	
starting mass	112067 kg	8277
Final mass	9911 kg	

Implementing a MATLAB code that iterates the above system of inputs based upon a changing mass from 100 kg to 10,000 kg yielded the following Pareto front graph:

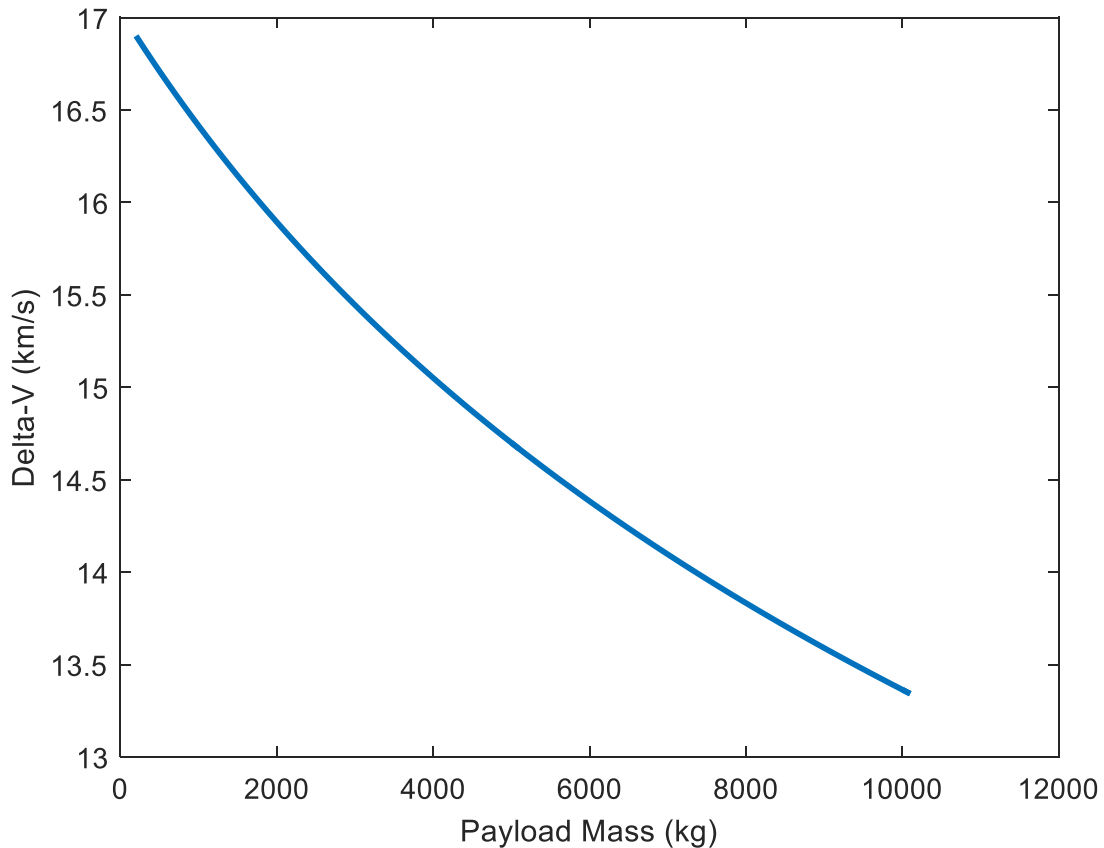


Figure 52: Pareto-Optimal Front of Payload Mass Versus ΔV .

This methodology can be applied in conjunction with a desired ΔV in order to determine the type of flight path trajectory that can be implemented in the thesis design for maximizing efficiency and minimizing travel time. If it is, for instance, determined that the mission can be accomplished with the desired technological improvements while only requiring a mission payload mass of 3,000 kg, that would mean a maximum ΔV of approximately 15,500 m/s could also be accomplished. This number can then be used to inform calculations on a Jupiter gravity assist, which can then inform models for determining travel time and desired launch dates.

3.14 Atmospheric Insertion Dynamics

It is important to understand that the atmosphere of Uranus is 5,000 km thick, and therefore, upon entry, the probe can be expected to be travelling through said atmosphere for a significant amount of time. Huygens, for example, spent roughly 40 minutes travelling through the atmosphere of the giant moon, Titan, before it finally landed upon its frozen surface [63]. This was in an environment with roughly 20% Uranus surface gravity, and a maximum surface pressure about 70 times less than when compared to the base of Uranus' troposphere.⁵⁰ This not only means the friction that can be expected upon entry into the Uranian atmosphere will be far greater, but also that the terminal velocity to which the probe will slow in the Uranian atmosphere will in all likelihood be far less, further broadening the regime in which the probe must be expected to slow down, thus further increasing the total amount of heat necessary to dissipate.

Assuming an exponential atmosphere, the drag force the probe will experience is as follows [64]:

$$D = \frac{1}{2} C_d A V^2 \rho_0 e^{-H/H_0} \quad (34)$$

Where C_D is the drag coefficient. This number, due to the shape of the proposed probe, can be assumed to be 0.45. A is the cross-sectional area of the descending object. Since the design preliminarily calls for a 5-meter diameter of a roughly spherical probe, the cross-sectional area is 19.625 m^2 . V is the velocity at which that object is moving, which will change from the initial entry velocity of 8.654 km/s , until it reduces to the

⁵⁰ The atmospheric pressure at Titan's surface is roughly 1.45 bar, compared to the 100 bar at the surface of Uranus. $100/1.45 = 68.965$ times the pressure.

terminal velocity at the base of the atmosphere of 13.84 m/s. The terminal velocity is calculated as follows [64]:

$$V_t = \sqrt{\frac{2mg}{\rho AC_d}} \quad (35)$$

Where g is the gravitational pull of Uranus at the termination point of the descent (5,000 km below the top of the atmosphere). This gravitational pull changes significantly over the course of travelling through the atmosphere, starting from 0.886 g's at the top, and increasing up to 1.425 g's.⁵¹ Nevertheless, calculating this number out, the terminal velocity proves to be negligible when compared to the entry velocity.

$$g = \frac{M_U G}{r^2} = \frac{(8.681 \times 10^{26} \text{ kg})(6.67408 \times 10^{-11} \text{ m}^3/\text{kg} \cdot \text{s}^2)}{(25,362 \text{ km} - 5000 \text{ km})^2} = 13.97 \text{ m/s}^2$$

It was originally thought that this number was an overestimate due to the total mass that will be below the probe when compared to that which the probe will have already traveled through. The atmosphere of Uranus might be thought of as a significant portion of Uranus' overall mass,⁵² but it amounts a relatively trivial difference. While a more accurate measurements can and will be conducted by the probe, for now it can be assumed that the gravitational pull at the base of the troposphere will be 13.97 m/s².

$$V_t = \sqrt{\frac{2(500\text{kg}) \left(13.97 \frac{\text{m}}{\text{s}^2}\right)}{\left(8.256 \frac{\text{kg}}{\text{m}^3}\right) (19.625 \text{ m}^2)(0.45)}} = 13.84 \text{ m/s}$$

⁵¹ The terminal velocity remains low enough to remove the necessity of a parachute, or any other means of slowing the probe's descent.⁵¹ Typical under-canopy descent speeds for humans on Earth are between 10 and 15 m/s [78].

⁵² The atmosphere is $m_{atm,U} = \frac{4\pi R_U^2 P_{S,U}}{g_U} \approx 5.69 \times 10^{21} \text{ kg} = 0.0066\%$ of Uranus' overall mass.

ρ_0 is the density of the atmosphere at its base, and H_0 is the atmospheric scale height. The density of the atmosphere at its base is calculated as follows [65]:

$$\rho_0 = \frac{p_0}{RT} \quad (36)$$

Where p_0 is the surface pressure in Pascals,⁵³ R is the specific gas constant of the Uranian atmosphere at its base, and T is the temperature at the base of the troposphere in Kelvin (320.4 K). This yields an atmospheric density of 8.257 kg/m³. The scale height of Uranus is a fairly commonly known figure—27 km—but a more exact calculation can be carried out through the following equation [65]:

$$H = \frac{RT}{mg} \quad (37)$$

Where R is the universal gas constant, T is the temperature in Kelvin of the atmosphere, m is the mean molecular mass of one atmospheric particle, and g is gravitational acceleration of the celestial body.⁵⁴

The primary issue that must be solved upon Uranian atmospheric entry, is the means by which the heat will be dissipated, as well as the total heat that needs to be dissipated. With a change in velocity of 8.633 km/s, the instantaneous drag force at -300 km is

$$\begin{aligned} D &= \frac{1}{2} C_d A V^2 \rho_0 e^{-\frac{H}{H_0}} = \frac{1}{2} (0.45) (19.625 \text{ m}^2) \left(8,636 \frac{\text{m}}{\text{s}} \right)^2 \left(8.257 \frac{\text{kg}}{\text{m}^3} \right) e^{-\frac{300 \text{ km}}{27 \text{ km}}} \\ &= 40,639 \text{ Newtons} \end{aligned}$$

⁵³ 101,325 Pa*100 = 10.0 MPa.

⁵⁴ For Uranus, this is 8.69 m/s², or 0.886 g's. However, this is at the top of Uranus' atmosphere. At the base of the troposphere, this number changes to 13.97 m/s².

Converting this to temperature in degrees Celsius temperature change of the surface of the descending probe is not as straightforward, as data on the matter tends to be highly empirical. However, referencing the graph below, it can be assumed that the maximum surface temperature the probe would experience upon descent would be roughly 3,800 Kelvin. This temperature is well within the nominal operating range of current, inexpensive, known technologies that could be utilized for the descent [66]:

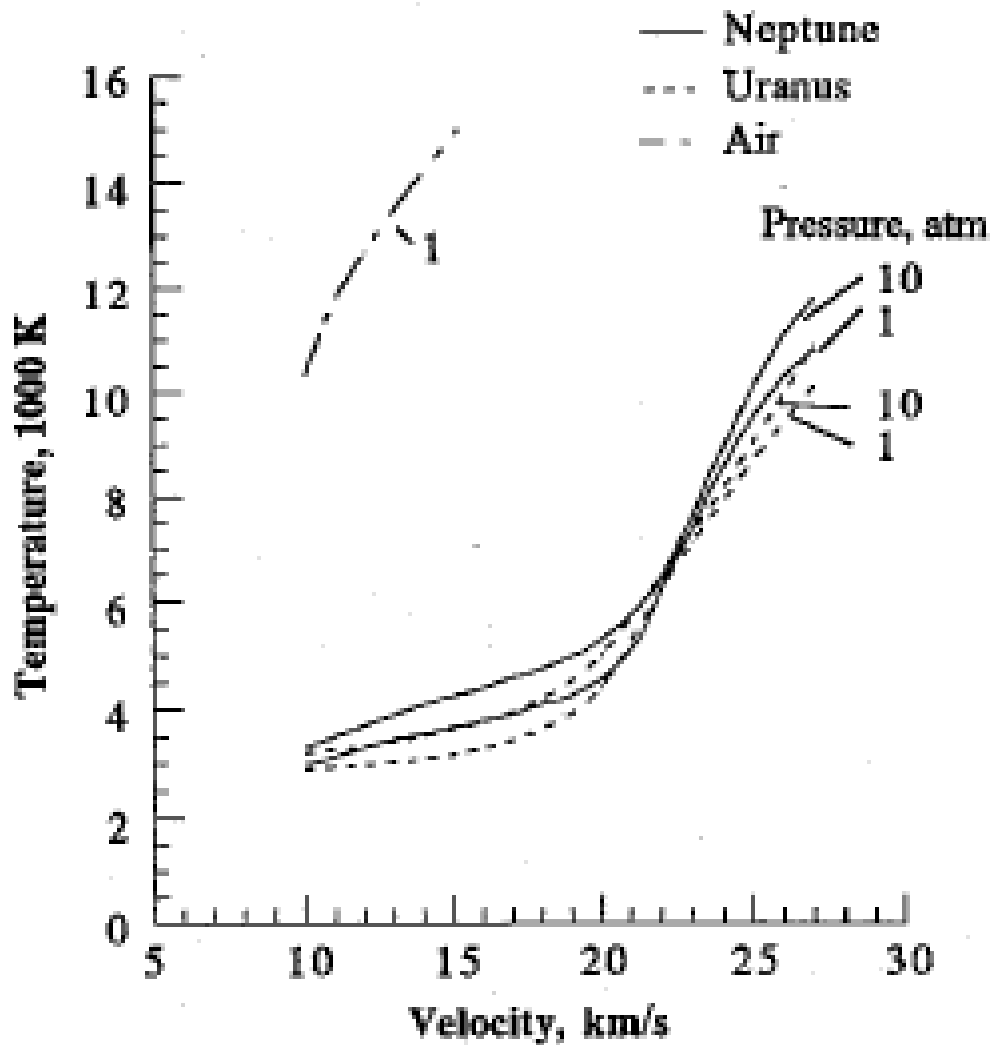
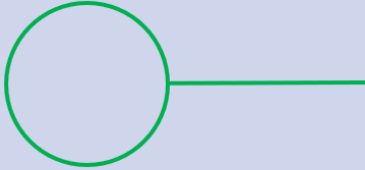



Figure 53: Temperature Behind Normal Shock for Uranus.

Entry velocity is expected to be roughly 8.5 km/s, assuming the probe reaches Uranus with nearly no hyperbolic excess velocity remaining. In order to be conservative, a 10 km/s entry velocity is thus assumed, providing the 3,800 Kelvin number.

Table 10: Ballistic Coefficients of Probe Shapes [67].

SHAPE	COEFF. OF DRAG	WIND DIRECTION
	0.47	→
	2.30	→

IV. Analysis and Results

4.1 Chapter Overview

This chapter will be discussing the following:

1. The final Doppler and collision broadening models used.
2. A discussion on the final SRTG design and its efficiency in a Uranian atmosphere.
3. The antenna and frequency parameters chosen for the final mothership satellite design.
4. The final probe model settled upon for the thesis.
5. The settled upon space probe launch design—how it will be stored in the launch vehicle fairing. This will include the final overall mass, ΔV , Jupiter assist calculations, and the selected launch date.

4.2 Results of Doppler and Collision Broadening Models

Of the three species taken into account in the Doppler and collision broadening calculations, only methane has any attenuation bands or properties of significance within the frequency band of 1 to 100 GHz. Over this frequency span, from maximum signal propagation to minimum, the difference is 1% at most. Helium exhibited similar properties. This is discerned from data sets of HITRAN [68]. The data desired was exceptionally difficult to find, as it generally is assumed that attenuation within the frequency band in question is negligible for the compounds analyzed. The models developed in section 3 were for methodological purposes only, but that methodology, specifically with respect to the species, could be adapted very readily to the visible

spectrum. Additionally, in atmospheres with different constituents, there would undoubtedly be attenuation bands within the frequency ranges used for signal propagation. While some attenuation was present in the desired frequency range of between 1 and 100 GHz, it was not of significant enough interest for scientific inquiry in the HITRAN database.

4.3 Settled Upon Frequency Range

The frequency range settled upon for this design relied on one critical design component: the development and deployment of a receiving antenna outside of Earth's atmosphere. The primary purpose of this is to mitigate the extreme signal attenuation properties of Earth's atmosphere in particular frequency ranges, referenced in section 3 extensively. The development and deployment of such a space-borne antenna, while likely costing on the order of \$500 million to upwards of \$1 billion USD, would undoubtedly have a very large customer base, as ground-based receivers are limited due to the crippling effects of Earth's atmosphere on propagation of higher signal frequencies. This is good for the health of biological life, but not good for information gathering. Therefore:

1. Assuming a space-borne signal receiver can be placed in orbit or at a Lagrange point of Earth perhaps, the frequency band selected for this design would be 100 GHz. Another possible location for the receiving antenna could potentially be the International Space Station, though possibly more prudent, a constellation of said satellites could also be deployed. The latter is more expensive, but the sunk cost of the venture and potential future uses would likely justify it. Beyond being able

to receive higher frequencies from space, limitations from weather erosion typically seen at ground-based sites would be eliminated, which then may open the door for the testing of mylar solar sail design concepts. Solar sail deployment concepts retrofitted properly for use as an antenna would work wonders as a rapidly deployable system, having potentially unlimited frequency range. Though most importantly, if a mylar solar sail transmitter were placed upon the mothership of large enough diameter,⁵⁵ then frequencies within the typical reception bands of the ground-based DSN could be sent with satisfactory beamwidth for the gain desired. Additionally, concepts exist using mylar solar sails to create virtual Lagrange points by utilizing solar wind to maintain a satellite's stationary position relative to Earth [69].



Figure 54: Solar Sail Design Concept [70].

⁵⁵ 40 meters would perhaps be sufficient when looking at Figure 15.

- Assuming purely ground-based receivers are to be utilized, then the typical 15 GHz transmit signal would likely be used, though some flexibility does exist in this range.
- Below are Tx-Rx diagrams for the signal propagation between Uranus and the Earth.

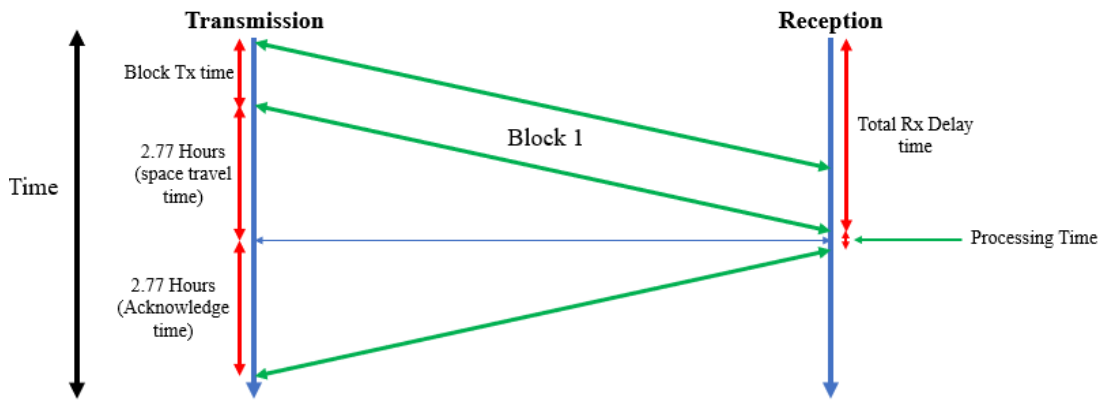


Figure 55: Single Transmission-Reception Timeline.

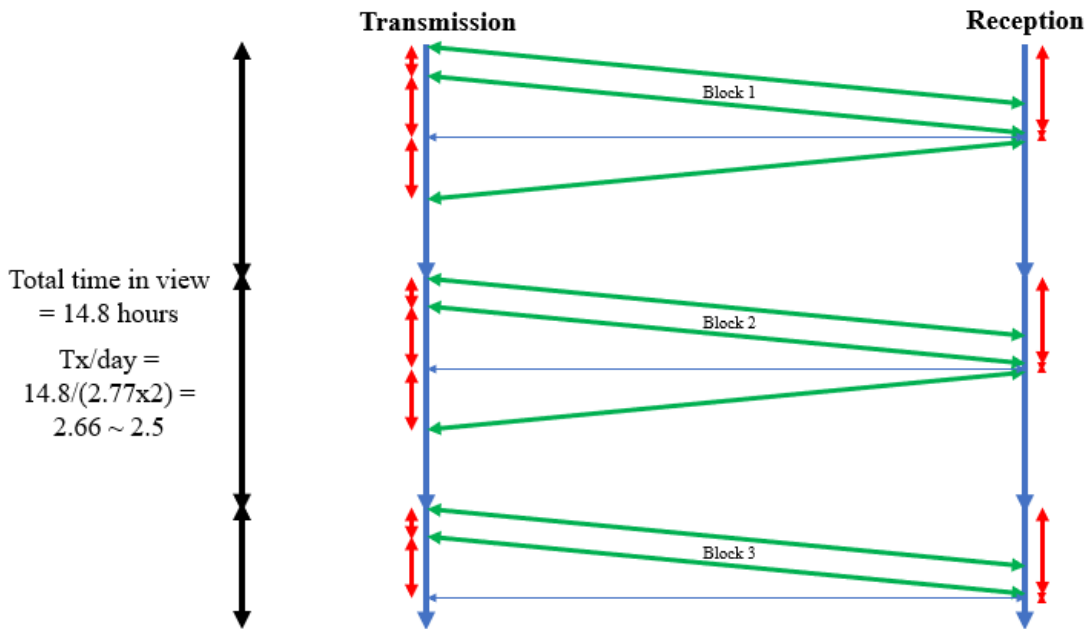


Figure 56: Daily Transmission-Reception Timeline.

4.4 Settled Upon General Probe Design

One of the most prominent issues that came about with the overall probe design was how to store the power generation systems. Initially, the desire was to have a completely self-contained, sealed probe vessel with ballast bays, in order to provide sufficient buoyancy where required, and sufficient density when submersion into the liquid ocean was desired. However, the SRTG power systems to be used for the probe would produce a very large amount of unutilized heat, that would then dissipate in the surrounding environment. Therefore, they would not be storable within the vessel itself. Instead, a design like the one shown in the following diagram would be more appropriate. Note that there is a total of five SRTGs, providing a total of 1200 W of usable power.

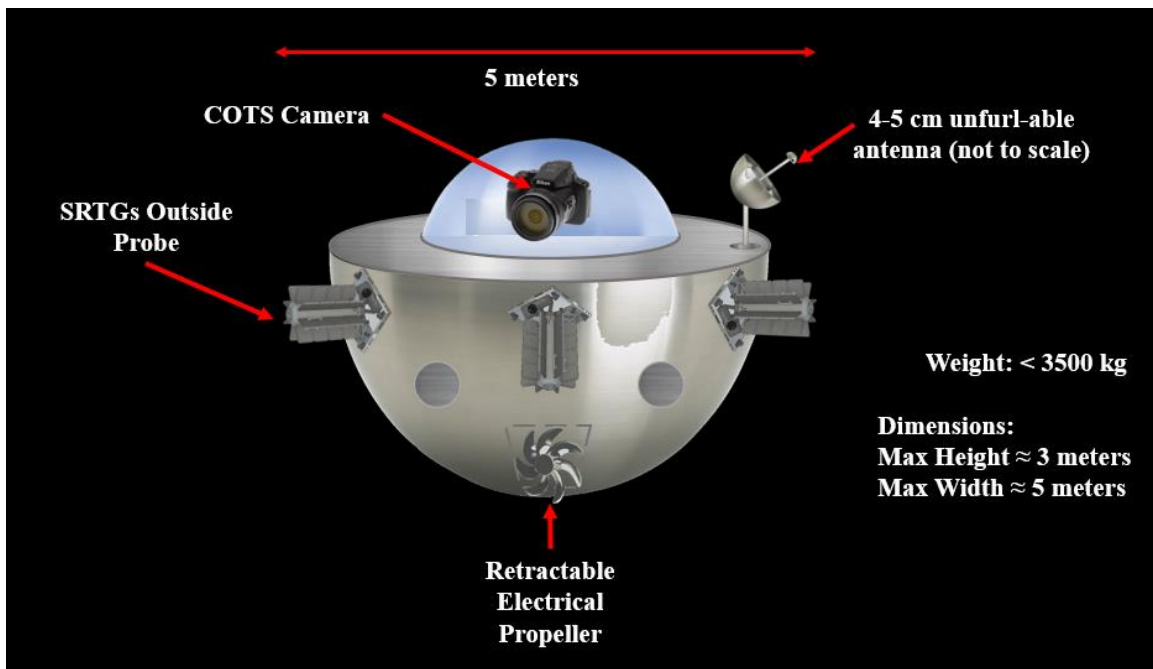


Figure 57: Side View of Probe Design.

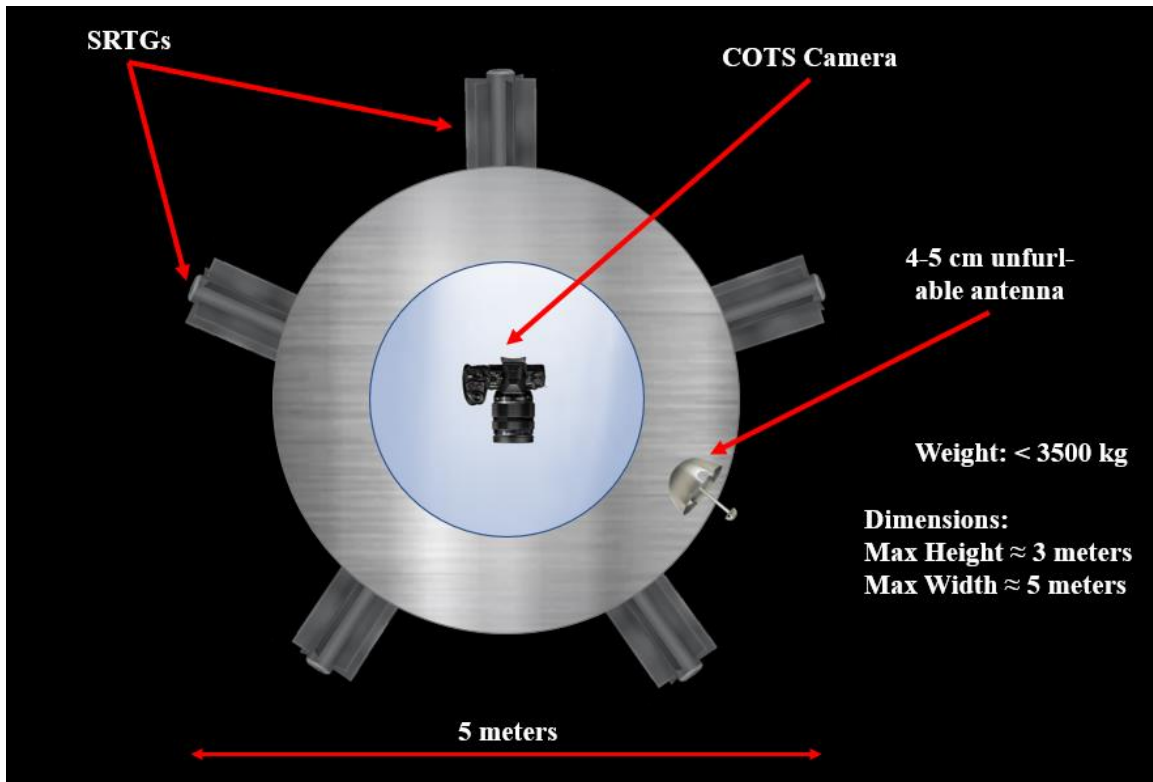


Figure 58: Top-View of Probe Design.

Also important to note, while this diagram shows perhaps an ungainly design by other power production standards, it is a scheme that is very similar to that of Galileo, except Galileo not only had the power system separated from the rest of the spacecraft, but by a vast distance. The satellite had an extended boom for its RTG. To that point, once the probe has safely landed upon the Uranian surface, the RTGs can be extended into the surrounding environment with deployable booms, something like what is shown in the following diagram.

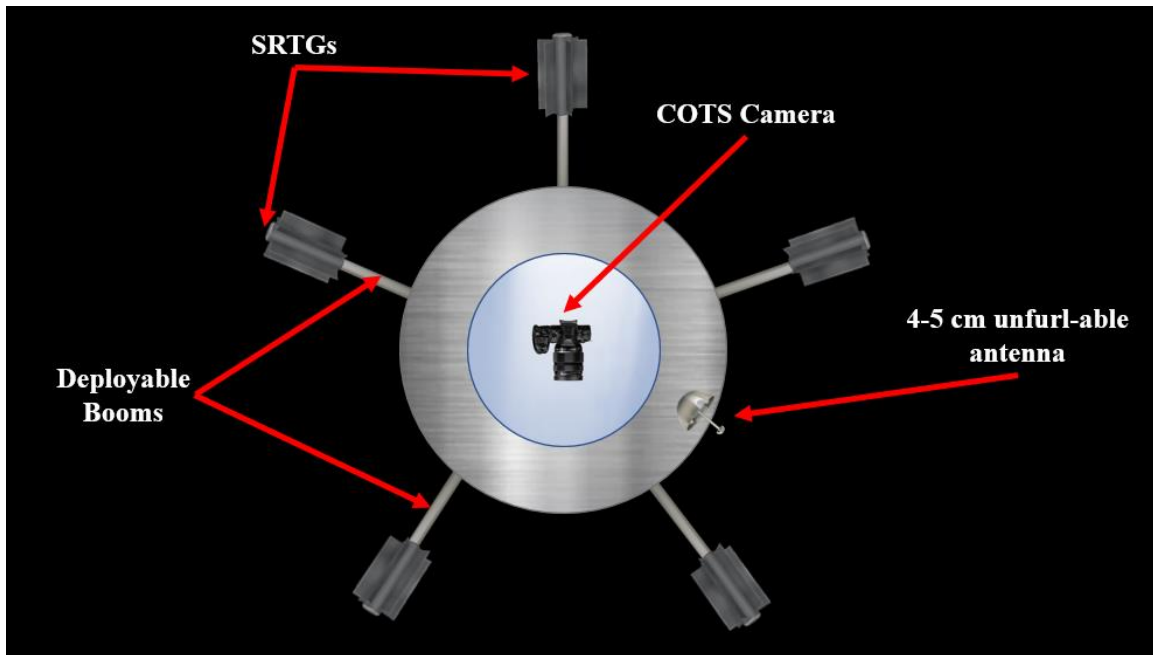


Figure 59: Probe Design with Deployable SRTG Booms.

This design would drastically increase the efficiency of the RTGs by allowing them to submerge into the liquid ocean more readily. It would also drastically increase the stability of the probe, preventing excessive bobbing in the water—though as stated earlier in this thesis, this would be a marginal problem at best due to the presumed calm seas of Uranus.

In much the same way that the SRTGs can be deployed once the probe lands upon the ocean, so too can the small antenna dish atop it. Only 4 to 5 cm. in diameter is all that is needed for the probe to send the required signal to the mothership with the desired data rates. The signal frequency settled upon is 100 GHz, which does not experience any attenuation through the helium-hydrogen-methane atmosphere, while providing much greater directionality of the signal and therefore greater expected gain. Additionally, as only approximately 300 W of power will be necessary for the various scientific

experiments that would be onboard the probe, the rest of that power can be used for signal propagation. Assuming the temperatures can be kept to within reasonable limits on such a signal transmitter, the remaining 900 W of usable power could go towards sending signals out. This would greatly improve the data rate, which would have only the limiting factor of data storage on the mothership. But ultimately, only the amount of power necessary for adequate signal transmission is required.

Since the probe will be floating in water, rather than putting all remaining 900 W of power towards the signal, 300 W can be put towards signal transmission, and the remaining 600 W can be put towards the propeller, allowing the probe to move much more rapidly in the Uranian sea. The probe will not be restricted to the 1 m/hour crawl of designs like the Mars Curiosity Rover [71].

Nevertheless, this still remains a non-ideal build. Having the SRTGs partially submerged in the liquid ocean changes the optimal operation temperature range due to the high convection coefficient of liquid water. Additionally, having multiple moving parts made to operate nominally after what would be approximately 13 to 16 years in storage is non-ideal. Therefore, the final design, one that would not necessitate booms, nor would it change the SRTG temperature ranges to unacceptable levels, would be to place the SRTGs around the camera dome, as shown in the following diagram.

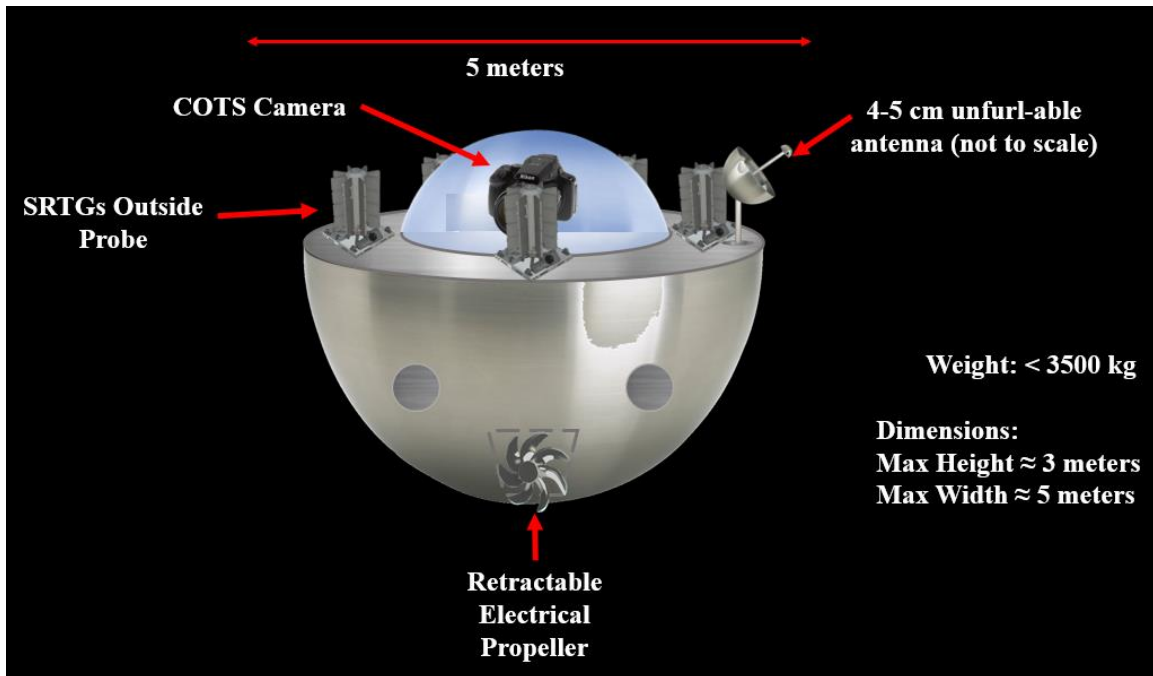


Figure 60: Final Probe Design.

In the previous figure, it is important to note that, while the camera would have some obstruction in its view, it would be simple to correct, moving a mere 15 degrees to get a view of the environment once more. This is also made easier by the fact that the probe will be floating on water as opposed to on a solid surface. In addition, building the probe in this way will allow for much more effective storage within the fairing of the launch vehicle, as a simple water-filled cylinder could be placed around the probe in storage, until it is in space.

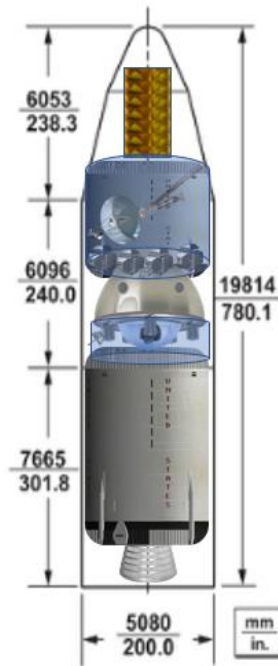
4.5 Settled Upon Launch Specifications

This mission design implements a large number of high-powered, very hot subsystems, to include at least ten SRTGs, seven high-powered signal transceivers, and many other devices. As such, considering many of these devices produce copious

amounts of heat whether in use or not, a means by which they can effectively be stored in the launch phase must be devised. The following figure shows the concept of water-cooling the devices while in the fairing using cylindrical water-cooling cells.

Delta IV Fairing
Maximum Size:
19.8x5.1 meters

- Propellant Length/engine: 7.3 meters
- Probe Length: 3 meters
- Antenna Length: 2 meters



$$7.3 + 3 + 2 = 12.3 \text{ meters}$$

$$-19.8 - 12.3 = 6.5 \text{ meters left for mothership and cube satellites (4)}$$

-Water-cooling cells

For Scale

Figure 61: Final Launch Vehicle Fairing Setup.

This has been done many times in the past and is not necessarily a new concept. The way in which the idea will be implemented, however, is on a larger scale. The final design will implement four repeater small-satellites, the Uranus Probe dubbed Chiron, and the mothership dubbed Chronos. The unfurled transceiver dish will be connected to the other mothership subsystems via boom to allow for maximum size.

The final selected mission mass of the payload will be 3,500 kg, to include approximately 2,000 kg for the probe. Using a gravitational assist from Jupiter with the massively increased payload capacity of the Falcon 9 Heavy launch vehicle, this will mean that the spacecraft will reach Uranus in approximately 15 years from the date of

launch. Ideally, this launch date will be roughly around the year 2040, when the conjunction between Uranus and Earth place the two planets at their minimum distance from one another. Additionally, Jupiter will be properly aligned for said gravitational assist. This will require an overall ΔV provided by the propulsion systems of roughly 16 km/s. This included 15.1 km/s from the launch, and 0.9 km/s to slow the spacecraft upon reaching Uranus. The remaining ΔV will be provided by the Jupiter gravitational assist. This will yield an overall ΔV on the order of 20 km/s.

4.6 Settled Upon SRTG Dynamics

It is important to take into consideration that current models of the efficiency and power generation of Stirling RTGs and regular RTGs are generally derived from environments either (a) similar to that of Earth, or (b) at or near a space vacuum. The primary mechanism that allows for power generation through a Stirling or thermal processes is the leveraging of a temperature differential between systems. In space, there is no actual temperature, as a temperature requires some type of medium such as a gaseous atmosphere through which to travel, which is absent in space. On Earth, the atmospheric pressure and temperature are far different from Uranus. Below are diagrams illustrating the power generation process through thermal leveraging.

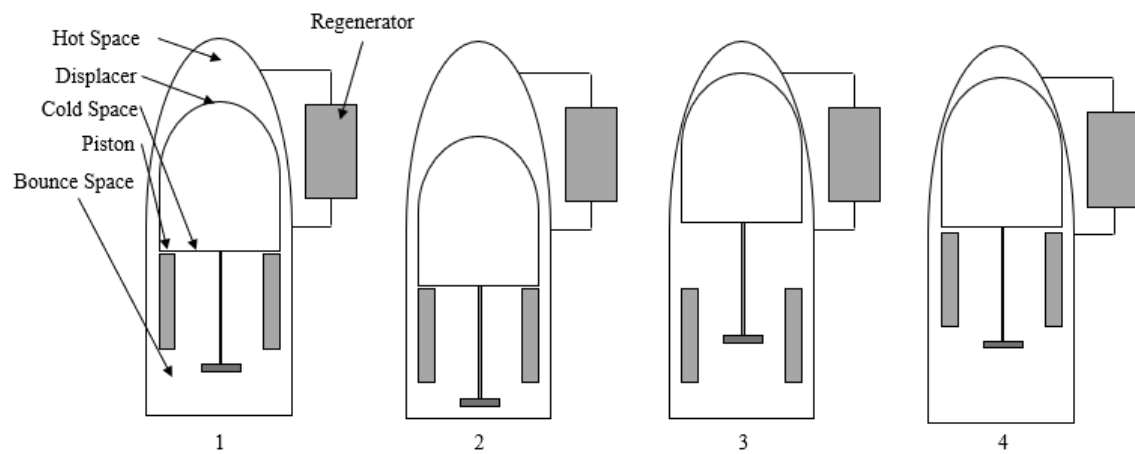
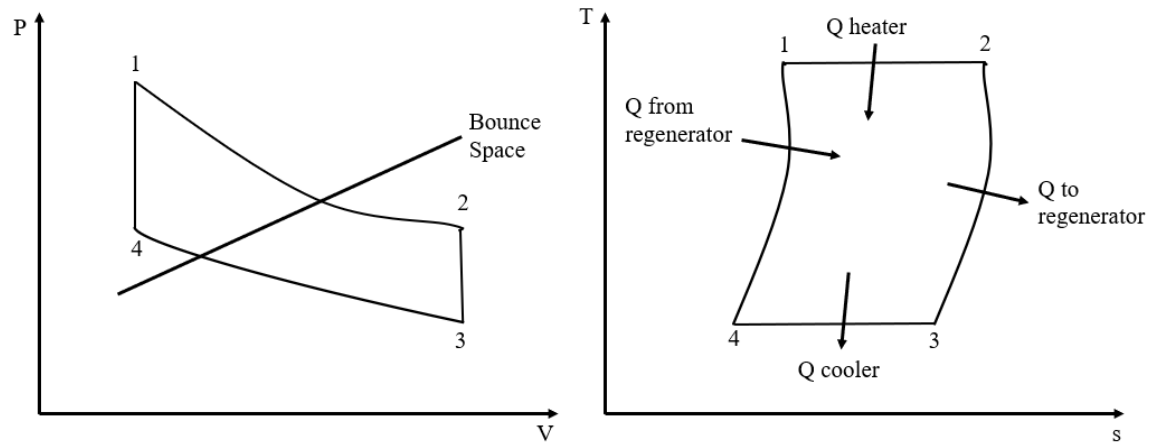


Figure 62: Ideal Stirling Cycle [72].

Since thermal difference is so vital to power production in these cycles, the higher temperature of Uranus, combined with the relatively high viscosity of the atmosphere, will yield a potentially much less capable system. If the system steady state is equated to a circuit, it would appear as follows:

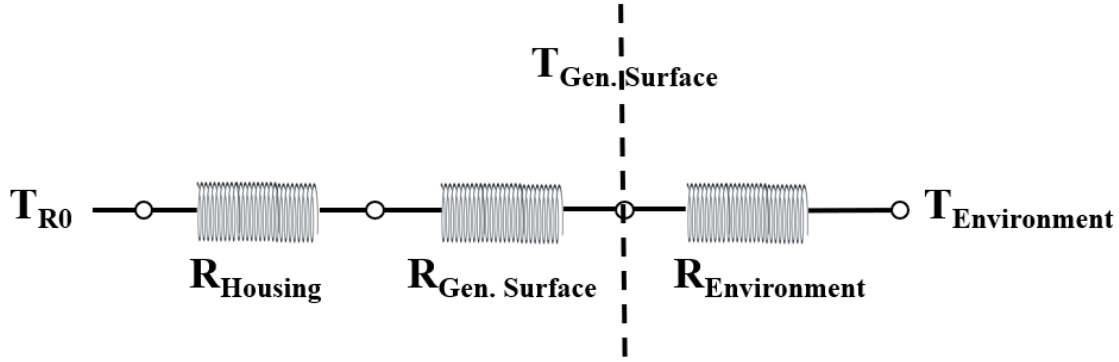


Figure 63: Temperature Circuit Analog.

If one continues with this analogy and find the resistance of the environment, one gets:

$$R_{env} = \frac{1}{\varepsilon A \sigma (T_{surf}^2 + T_{env}^2)(T_{surf} + T_{env})} \quad (38)$$

The equation for analogous resistance of the planetary environment is as follows:

$$R_{env} = \frac{1}{hA} \quad (39)$$

Where h is the thermal convection coefficient. In this case, there are two separate options: either (a) we use a convection coefficient for free air, or (b) we use a convection coefficient for liquid. In all likelihood, it would be a combination of the two, if boom-mounted RTG design is indeed utilized. To simplify the problem and determine if there is indeed a significant difference in power generation efficiency, the internal heat flow of SRTG structure will be assumed the same as previously established models indicate. We will also assume that the SRTG has a thermal convection coefficient that would be expected for a 50-50 mixture of air and liquid water. Free air's convection coefficient ranges between 10 and 100, whereas free liquid water ranges between 50 and 3,000 [73].

The confounding factors are the change in pressure and the significantly higher surface temperatures. For such a 50-50 mixture, a convection coefficient expected would be roughly 790.

$$h_{eff} = \frac{h_{avg,air} + h_{avg,water}}{2} = \frac{\frac{10 + 100}{2} + \frac{50 + 3,000}{2}}{2} = 790$$

There is evidence to suggest that the convection coefficient of various compounds increases as pressure increases, as well as temperature increases, as shown in the following table:

Table 11: Change in Convection Coefficient Versus Pressure/Temperature [74].

Temp (C) ↓	Pressure (Pa) →	18	1000	10000	43000	88500	110000	150000	185000	220000
		40	h_{conv}	0.86	1.78	4.35	7.02	9.01	9.73	10.06
	h_f	6.27	6.27	6.27	6.27	6.27	6.27	6.27	6.27	6.27
50	h_{conv}	1.70	3.12	6.16	9.27	11.90	12.84	13.72	14.87	16.36
	h_f	6.59	6.59	6.59	6.59	6.59	6.59	6.59	6.59	6.59
60	h_{conv}	2.56	4.14	7.40	10.54	13.36	14.47	15.61	16.72	17.98
	h_f	6.92	6.92	6.92	6.92	6.92	6.92	6.92	6.92	6.92
70	h_{conv}	3.16	4.74	7.99	11.44	14.17	15.62	16.37	17.80	18.85
	h_f	7.27	7.27	7.27	7.27	7.27	7.27	7.27	7.27	7.27
80	h_{conv}	3.47	5.11	8.44	11.70	14.67	15.83	16.59	18.32	19.35
	h_f	7.63	7.63	7.63	7.63	7.63	7.63	7.63	7.63	7.63
90	h_{conv}	3.60	5.30	8.56	12.01	14.95	16.14	16.92	18.47	19.64
	h_f	8.00	8.00	8.00	8.00	8.00	8.00	8.00	8.00	8.00
100	h_{conv}	3.51	5.24	8.52	11.99	15.06	16.16	17.02	18.48	19.80
	h_f	8.39	8.39	8.39	8.39	8.39	8.39	8.39	8.39	8.39

It appears that the general trend for convection coefficient scales as follows:

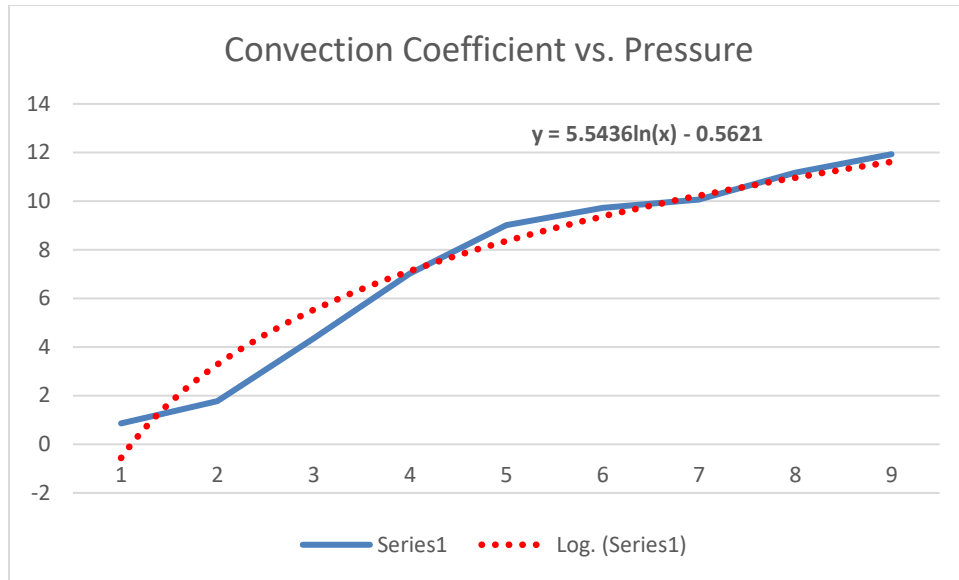


Figure 64: Convection Coefficient with Trendline.

Plugging in the pressure at the tropospheric base of Uranus into the trendline Equation derived from the data yields a convection coefficient as follows:

$$h_{\Delta px} = 5.5436 * \ln(100 * 101,000 Pa) - 0.5621 = 88.845$$

That is, varying from the baseline of 101,000 Pascals, there is a difference of 79.12. That is, the convection coefficient increases by approximately 8 times based purely on the change in pressure. Take 79.12 and divide by 9.73, and a number of 8.13 comes about. Analyzing the change in convection coefficient with temperature is as follows:

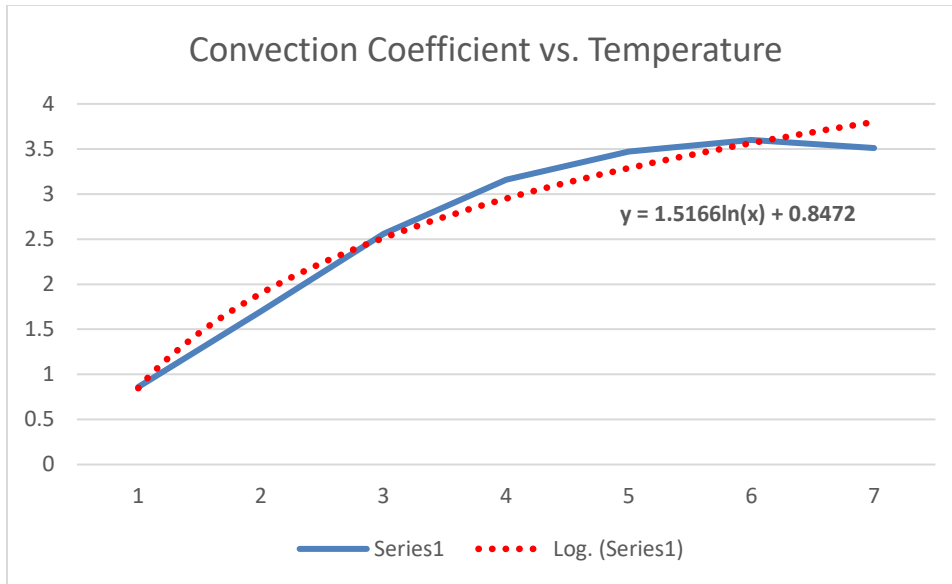


Figure 65: Convection Coefficient Versus Temperature Change.

While it isn't a consistent trend upward for convection coefficient as temperature increases, if we assume the logarithmic equation for the trendline holds until 100 bar of pressure, it would yield a convection coefficient as follows:

$$h_{\Delta T} = 1.5166 * \ln(100 * 101,000 Pa) + 0.8472 = 25.307$$

This is a difference of 2.5 times from the baseline of 10. If we combine these two convection coefficient alterations with the assumed average convection coefficient of a 50-50 mixture of free air and liquid water, we get the following:

$$h_{comp} = h_{\Delta T} * h_{\Delta px} * h_{eff} = 8.13 * 2.5 * 790 = 16,057$$

This is a very simple, generalized methodology for determining the expected convection coefficient of the Uranian hydrospheric surface, also assuming that the media would be half water and half air. It also relies upon large amounts of data extrapolation. Assuming 100% air (SRTGs atop the probe, rather than on booms surrounding it)

changes the convection coefficient expected to approximately 1,118. This is assuming the convection coefficient of the air is 55.

Delving into a much more mathematically robust methodology, we can use the following equations [75]:

$$h = \left(\frac{k}{L}\right) \left(\frac{4}{3}\right) \left(\frac{Gr_L}{4}\right)^{\frac{1}{4}} \left[\frac{0.75Pr^{\frac{1}{2}}}{\left(0.69+1.221Pr^{\frac{1}{2}}+1.238\right)^{\frac{1}{4}}} \right] \quad (40)$$

Where Gr is the Grashof number, analogous to the Reynolds number, but for buoyancy-driven flows. k is the thermal conductivity, L is characteristic length, and Pr is the Prandtl number. The Grashof number is defined as follows:

$$Gr_L = \frac{g\rho^3(T_s-T_\infty)L^3}{T\mu^3} \quad (41)$$

g is the gravitational pull, ρ is the coefficient of thermal expansion, T_s is the surface temperature of the system, T_∞ is the environmental temperature, L is again the characteristic length, and μ is the viscosity. In consistent units, the Grashof number will be dimensionless. Pr is the Prandtl number, which is as follows:

$$Pr = \frac{\mu c_p}{k} \quad (42)$$

Where μ again is viscosity, k is the thermal conductivity, and c_p is specific heat. Broadly speaking, Pr tends to be between 0.7 and 1 for most gases, and for water at 320 K, it is 3.77. Calculating through all the previous equations and assuming a 5-Kelvin differential between the surface temperature and the environmental temperature yielded a convection coefficient of 1,811. It is important to note that this is a highly variable, and

highly iterative process. Using the more conservative estimate for convection coefficient of 1,811, a more robust design for the SRTG system can be created.

4.7 Summary

The final spacecraft design for the Chronos-Chiron Design Reference Mission to be sent to Uranus has seen some massive technological improvements since the previous iteration. Data storage, transmission, and data handling technologies have expanded capabilities by leaps and bounds, and at far lighter weights and generally far depreciated expense. This combined with the equally massive increase in payload capacity and reduction in costs derived from SpaceX's launch vehicle designs yields yet more potential capability. A truly new "triple-point" in spacecraft design has been attained. It is merely a matter of putting the pieces together at this point.

However, to make these astounding improvements useful for the scientific community, inquiry must go deeper, farther, and attain higher fidelity. Mathematical models built through portable personal computer technological suites, like the one built for Doppler and collision broadening simulation in this thesis, create a synergistic, and exponential explosion in understanding, as humanity continues to pierce the veil of the unknown. Even with the presented design, however, the absolute optimized maximum potential of a mission has yet to be attained. This will come with trade studies, mass production, and perhaps even commercialization. It is the first replication of an entirely new regime.

V. Conclusions and Recommendations

5.1 Conclusions of Research

The overall purpose of this thesis was to demonstrate what modern technological capabilities can achieve in terms of total scientific and cultural impact. On the outset, the author had the perspective that the importance of management of the cultural zeitgeist through production of meaningful media that the general public could understand and appreciate has been woefully underestimated. Therefore, the goal was to create a mission set that would yield not only still photos, or even 1 frame-per-second video, of a far-flung world well beyond the purview of most laymen, but to produce full, high-definition, streaming video upon the surface of a planet with characteristics that fly in the face of conventional wisdom of what is possible. That is, to send a probe through a 5,000 km-thick veil of an atmosphere upon a giant planet 3×10^9 km away from the Sun, and to land upon liquid water in an environment that by traditional scientific understanding should be solid ice. To stream it in a near-live manner—only possible with groundbreaking technological feats in data transmission that yield tens of megabits to even gigabits per second data rates—has the potential to reshape the way the general public thinks about space. Namely, it would get them *to think* about space. Suffice to say, it would be dumbfounding if this goal was not accomplished for any person that would read this paper.

5.2 General Algorithmic Development and Doppler and Collision Broadening

While conclusive work is an elusive item in developing design reference missions and initial theoretical models for planetary atmospheric evolution, methodological

constructions can be gleaned; the feasibility of such a scheme was shown in this thesis. MATLAB code used for determining iteratively calculated parameters of the mission, such as launch payload mass, antenna dish size, signal propagation frequency, and more, can and will be re-applied to various other platforms and technological developments. To that point, every aspect of this thesis can be further algorithmically developed to allow for the program to come to conclusions on its own with very few inputs from the user. Of the most critical aspects, however, is the projected cost of a mission, as this above all else, limits what can and cannot be sent into space. This, perhaps, would be the first prompt. An example MATLAB line of code that may prompt such a question is as follows:

```
prompt1 = 'What is the upper limit of acceptable cost for a  
launch vehicle for your mission?';  
DataTableSelect = max(input(prompt1));
```

Continuing, the methodology developed in this thesis on accounting for Doppler and collision broadening effects in the overall attenuation of signal frequencies transmitting through theoretical and real atmospheres is one that can be applied to future work, and constantly refined to improve accuracy and precision. For example, selected filters can have their parameters changed, from attenuation of stop bands, to the steepness of attenuation slopes, and altering filter types to make for a scientifically-supported more accurate filtering regime. If the models developed prove to be an effective means of atmospheric observation, then further algorithmic development can be accomplished to allow for automatically detecting attenuation bands of atmospheres depending upon their compositions. The general purpose of the Doppler and collision broadening calculations

in this thesis was to act as a starting point, using future empirical observations to further discern their construction.

Parameters that do change depending upon the atmosphere in question are its pressure, average temperature, composition of compounds, density, gravitational pull, mass, and the number of compounds within the atmosphere that have any bulk significance. Prompts can be provided for the user to input said parameters. Factors that do not change are molecular weights of compounds in question, and the spectra of said compounds. With a method developed for determining the broadening coefficients of the compounds of interest depending upon the specific atmospheric composition, that method can be applied to any number of atmospheres in the same way.

The crucial component was building the algorithm for determining the broadening coefficient. Once data for the full spectrum of various compounds—what will be commented in the code, and explained as the limits of any algorithm refined in the future—are placed into the data tables for the code, it is as simple as inputting a few easily researched or known figures. Beyond this, more specific calculations on the line shape function (Lorentzian) can be implemented.

5.3 Design Reference Mission Algorithmic Development

As for the design reference mission construction itself, inputs can be discerned from the user as well. Whether it be utilizing data sets for entire launch vehicles, to include said launch vehicle's number of stages, total ΔV , launch mass capacity, and more, or those variables are input directly in the data table for, say, a Delta-IV rocket, it is entirely dependent upon the level of abstraction desired for or from the end user. This

is shown through graphs such as the antenna dish diameter variable (Figure 15). This graph is meant to show how the wavelength and beam width of an outgoing signal change depending upon the antenna diameter in order to meet specifications on signal amplification. If an antenna diameter is, for instance, user-selected by a prompt—and due to the nature of this calculation, no range of values need apply *theoretically*, only practically—then one can determine the beam width to be expected for the mission, which is a critical factor for selecting pointing accuracy equipment. The pointing accuracy equipment itself can again be placed in its own data table, and depending upon the pointing accuracy required, a list of acceptable solutions can be provided. This list of acceptable solutions can itself be filtered with a desired mission mass. As is explained later in this section, this leads to potential utilization of Pareto optimization fronts in the future.

5.4 Significance of Research

Beyond improving the understanding of how signals may propagate through varying atmospheres, data gleaned may determine how atmospheric absorption allows for life-sustaining temperatures and how they may affect planets several billions of kilometers away from their host stars. This thesis has improved the robustness of the *theoretical* body of work explicating that current understandings of would-be Goldilocks zones of planets and stars, a body of work which at present is woefully underdeveloped. Or, rather, stars have Goldilocks zones, but so too do individual planets themselves. Actually developing the design reference mission and accomplishing it will *empirically* do the same.

The Chiron probe, when sent to the base of the troposphere of Uranus, will visually (through pictures and video) and physically confirm that indeed the mass in question is liquid water mixed with ammonia, not solid ice or gaseous, “empty,” space. While this is already well-understood in the scientific community, the scientific community has a habit of underestimating the importance of public relations, as stated in the introduction to this section. The wonder that good pictures and video evidence can develop in the minds of the general population, which itself could lead to further funding and therefore further exploration and space systems development, is hugely important. When video comes back to Earth of the true stillness of the environment the Chiron probe will be visiting, due to the low degree of tidal effects experienced upon the vast oceans of Uranus from other celestial bodies, a new mental framework for the zeitgeist of humanity will be realized. It is essentially a global mental readjustment, or “tune-up.”

5.5 Recommendations for Action

With the work accomplished in this thesis, much action can be taken on the outset. That is, funding for advancements on builds can be accomplished immediately, with minimal bureaucratic friction. There are many low-cost scale models and mathematical simulations and models that can be built through grants to graduate students and others, that by no means need to exceed six figures in yearly value.

5.5.1 Chiron Probe Sub-scale Models

Likely the first, and most easily accessible advancements upon this thesis, and a way to progress its work forward most rapidly, would be to develop sub-scale models of its components, initially of the Chiron probe itself. These can be easily developed

through the available 3-D printers at the Air Force Institute of Technology, and even accomplished with the materials desired for the final construction. As this is done, new lattice configurations can be attempted in order to maximize strength and minimize weight of the model.

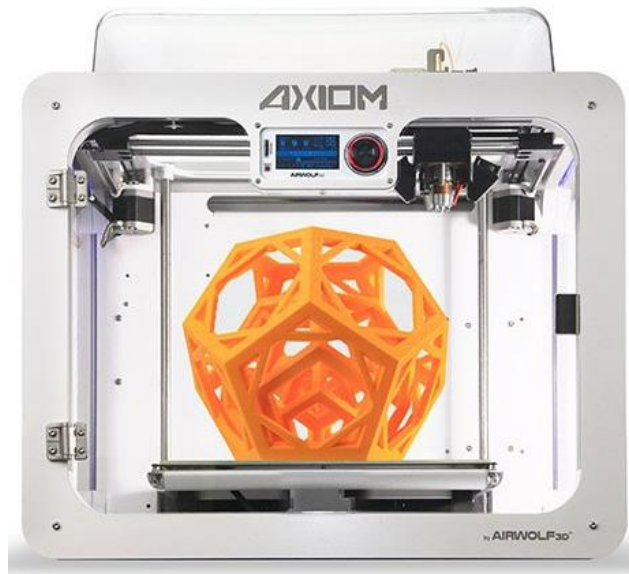


Figure 66: 3D Printer with Sample Lattice.

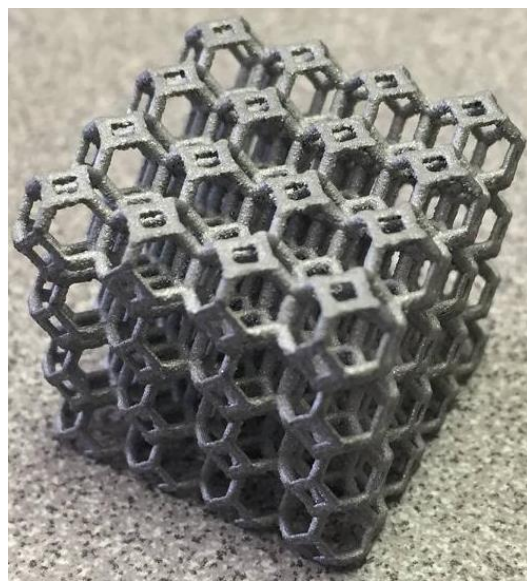


Figure 67: 3D-Printed Aluminum Lattice.

Over time, this model can steadily be scaled up to a full-scale one. To this point, providing adequate funding for a small team of researchers, whether they be thesis students or post-graduates, to further refine such a model would be prudent. Lattice structures like the one shown prior have been created at the Air Force Institute of Technology with strengths several times greater than current structural designs.

5.5.2 Doppler and Collision Broadening Extrapolation Models

For work done in this thesis, the Doppler and collision broadening model should be adapted to other exploratory works in the field of atmospheric science. This model can, in fact, easily be tested and refined without the need to travel to other planets. Vessels with varying pressures, temperatures, atmospheric compositions, and more can be developed and signals passed through them to accomplish this end. This is in fact what is done in order to get the spectra of specific compounds at an Earth standard atmosphere anyway.⁵⁶ There are infinite combinations and permutations that can be tested. Gathering a big enough data set and running it through the Doppler and collision broadening model for refinement could render much interpolation unneeded, and instead outlying factors can be explored with more resources.

Table 12: Sample Variable Ranges for Doppler and Collision Broadening.

Frequency	Compounds	Pressures	Temperatures
Band	Explored	Explored	Explored
1 Hz to 1,000	H ₂ , O ₂ , H ₂ O,	0.1 mbar to	1 Kelvin to
THz	NH ₄ , He, N ₂	100 bar	600 Kelvin

⁵⁶ How the data was gathered for the NIST data sets used in this thesis.

Manipulating one variable at a time, and with logarithmic step sizes, computing a system with four variables in these ranges yields 10^{18} values, and this is only a small sliver of all variable values that can be explored. It is a nearly infinite body of work, and with extrapolation from an initial basis, a Doppler and collision broadening model can be generalized.

5.6 Recommendations for Future Research

Depending upon funding of the many concepts developed in this thesis, this section details the initial steps with respect to each innovation that future prospective engineers and acquisitions programs can take. Advanced mission system building notwithstanding, in addition, there are many models that need to be further refined. A menu of different refinement techniques is provided in the following sections.

5.6.1 Pareto Front Optimizations

Inclination changes for the proposed mission profile upon reaching Uranus were discussed in the previous section. While traditional methodologies by which inclination changes may be employed would indicate that such a maneuver would require a minimum of 2.2 km/s of ΔV , if the methodology discussed by Bettinger et. al. is implemented, such a requirement can be reduced by as much as 85%, or to 330 m/s [76]. This is a ΔV within a feasible region for transport to Uranus, beyond ΔV necessary for orbital maintenance maneuvers. This is particularly important with Uranus due to its high axial inclination of 97 degrees compared to any other planet in the Solar System. For future work, calculations on this matter can be conducted using Bettinger's technique.

After which, the same Pareto Front analysis discussed earlier can be accomplished. This would require very precise measurements of C_L and C_D , which itself requires a completed model of the overall spacecraft design, whether including the probe or not—which may be jettisoned into the Uranian atmosphere before any such maneuvers are attempted.

Such a skip entry technique is shown in the following diagram.

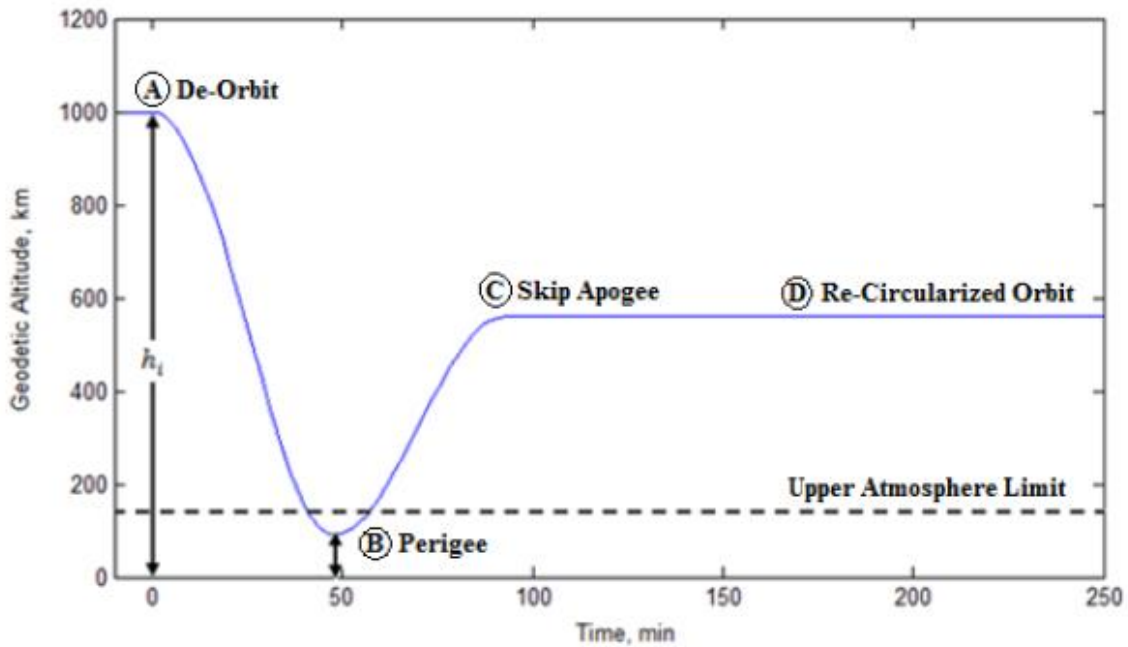


Figure 68: Example Skip Entry Maneuver Diagram.

Continuing with Pareto Front analysis, in future work, Pareto Fronts for greater optimization of this mission design should be considered for optimizing the following fronts in concert:

1. Mission mass to third-stage propellant mass.
2. Maximum ΔV capability possible with Jupiter gravity assist maneuver.
3. Minimizing overall travel time to Uranus.

4. Optimizing mass versus volume within the payload fairing utilized for the launch vehicle.
5. Mass versus heat load.
6. Mass versus fuel type used in the third stage booster.

5.6.2 New/Different Launch Vehicles

Harkening back to the discussion earlier on allowing for user prompting of various aspects of a design reference mission going forward, since the writing of this thesis, new technologies have been developed that yet further advance the frontier of possible mission sets to Uranus and beyond. At the top of the list of innovations is the development of the Starship launch vehicle by SpaceX [77]. This launch vehicle promises to provide greater payload capacity than the Saturn V, will be fully reusable, and will cost a fraction of what any other super-heavy launch system has cost before. The methodologies implemented in this thesis could be re-worked utilizing the Starship launch vehicle instead of the Falcon 9 Heavy launch vehicle going forward. This would easily increase the maximum payload that can be sent to Uranus by a factor of 10.

5.7 Final Remarks

Space exploration, while a rarefied field of commercial endeavor, proves to be a yet further rarefied field when discussing the outer Solar System as opposed to more near-Earth objects such as the Moon, various asteroids, or even Mars. As such, the fidelity on scientific inquiries in this field is rather low, as iterative processes that would lead to further refinement and optimization have not reached their climax, nor even the beginning of the exponential upward slope of a development S-curve. That being said,

any and all inquiries and developments in the field, with robust scientific and engineering merit, must be considered. Society simply does not have the intellectual capital to waste. This, in and of itself, is probably principal amongst all the possible reasons as to why it is so devastating the degree to which it is unknown by the public that Uranus actually has a liquid hydrosphere below its thick atmosphere. The purview of the human collective understanding of the universe is stretched, expanded by pushing this scientific frontier therefore. To put it another way, this thesis served as an articulation of two new space science concepts:

1. *Artificial habitability (Goldilocks) zones.* That is, habitability zones that could be artificially created by man, or by other mechanisms not naturally galvanized by planetary evolution. This ties in closely to many terraforming concepts for the planet Mars.
2. *Internal planetary habitability zones.* As stated in section 2.4, outside a certain threshold of distance from the host star, primary sources of sufficient surface heat for habitability come from the planet itself, rather than the host star.

In the most global, or broadest of terms, what keeps humanity in its near-constant state of living barely above subsistence, constant state of conflict, constant state of being focused upon trivialities? It is the absence of wonder, which comes from a lack of *freedom* to wonder. This thesis, above all else, is strategically important for that very reason. The goal of any military member worth their salt, is to render their profession obsolete. The means by which one does this is to get the common man to think of greater things, to point their minds, hearts, and eyes towards the skies. Society will see, in crystal-clear, streaming high-definition view, what the surface of a planet billions of

kilometers away looks like, one that has no business being warm enough to sustain life, but somehow is. This is more important than we know.

Bibliography

- [1] Coinnews Media Group LLC, "US Inflation Calculator," Coinnews Media Group LLC, 15 July 2020. [Online]. Available: <https://www.usinflationcalculator.com/inflation/historical-inflation-rates/>. [Accessed 6 December 2019].
- [2] J. D. Anderson, J. K. Campbell, R. A. Jacobson and D. N. Sweetnam, "Radio Science With Voyager 2 at Uranus: Results on Masses and Densities of the Planet and Five Principal Satellites," *Journal of Geophysical Research*, vol. 92, no. A13, pp. 14,877-14,883, 1987.
- [3] M. Mozaffari, W. Saad, M. Bennis and M. Debbah, "Communications and Control for Wireless Drone-Based Antenna Array," *arXiv*, 2018.
- [4] United States Navy, "U.S. Navy Diving Manual," Naval Sea Systems Command, Washington D.C., 2016.
- [5] B. A. Smith, L. A. Soderblom, D. Bliss and J. M. Boyce, "Voyager 2 in the Uranian System: Imaging Science Results," *Science Magazine*, vol. 233, pp. 43-64, 1986.
- [6] F. Pohl, *Man Plus*, New York: Random House, 1976.
- [7] A. K. Lal, "Searching for Life on Habitable Planets and Moons," *Ministry of Statistics & Programme Implementation*, 2013.
- [8] P. Pearson, "Artificial Habitability Zones of Stars Shown Through a Hypothetical Planet," *Mars Society Papers*, 2015.
- [9] B. R. Davis, "Gravitational Lens: Deep Space Probe Design," *Air Force Institute of Technology*, p. 3, 2012.
- [10] National Security Agency, "National Security Space Strategy Unclassified Summary," National Security Agency, Washington D.C., 2011.
- [11] U. S. Government, "United States Space Force," 26 July 2020. [Online]. Available: spaceforce.mil. [Accessed 26 July 2020].

- [12] NASA, "Mariner 3 & 4," *Mars Exploration Program*, 2020.
- [13] M. Wade, "Mariner 3 & 4," Astronautix, 2019. [Online]. Available: <http://www.astronautix.com/m/mariner3-4.html>. [Accessed 26 July 2020].
- [14] J. P. Laboratory, "Spaceborne Antennas for Planetary Exploration," *Deep Space Communications and Navigation Systems Center of Excellence*, 2006.
- [15] NASA, "National Aeronautics and Space Administration," 14 May 2020. [Online]. Available: <https://nssdc.gsfc.nasa.gov/nmc/spacecraft/displayTelemetry.action?id=1969-014A>. [Accessed 26 July 2020].
- [16] NASA, "Mariner-Mars 1969: A Preliminary Report," *Scientific and Technical Information Division*, vol. SP, no. 225, p. 17, 1969.
- [17] NASA, "A Study of Mariner 10 Flight Experiences and Some Flight Piece Part Failure Rate Computations," *JPL Technical Memorandum*, vol. 33, no. 759, 1976.
- [18] NASA, "The Viking Mission to Mars," *Scientific and Technical Information Office*, vol. SP, no. 334, 1974.
- [19] NASA, "National Aeronautics and Space Administration," 14 May 2020. [Online]. Available: <https://nssdc.gsfc.nasa.gov/nmc/spacecraft/display.action?id=1975-075C>. [Accessed 26 July 2020].
- [20] NASA, "Viking Orbiter," 14 May 2020. [Online]. Available: <https://nssdc.gsfc.nasa.gov/nmc/spacecraft/display.action?id=1975-075A>. [Accessed 26 July 2020].
- [21] R. Ludwig and J. Tayloer, "Voyager Telecommunications," in *Voyager I and II*, Washington D.C., NASA, 2014, p. 38.
- [22] NASA Jet Propulsion Laboratory, "Voyager Mission Status," 26 July 2020. [Online]. Available: <https://voyager.jpl.nasa.gov/mission/status/>. [Accessed 26 July 2020].

- [23] Space.com, "Challenger: The Shuttle Disaster That Changed NASA," Future US, Inc, 1 May 2019. [Online]. Available: <https://www.space.com/18084-space-shuttle-challenger.html>. [Accessed 26 July 2020].
- [24] A. P. Ingersoll, T. E. Dowling, P. J. Gierasch, G. S. Orton, P. L. Read, A. Sanchez-Lavega, A. P. Showman, A. A. Simon-Miller and A. R. Vasavada, "Dynamics of Jupiter's Atmosphere," *Atmospheric Dynamics*, vol. 6, 2000.
- [25] J. V. Gardner, A. A. Armstrong, B. R. Calder and J. Beaudoin, "So, How Deep Is the Mariana Trench?," *Marine Geodesy*, vol. 37, pp. 1-13, 2014.
- [26] International Telecommunication Union, Attenuation by Atmospheric Gases: P-Series Radiowave Propagation, Geneva: ITU, 2016.
- [27] A. Fowler, "Observations of the Principal and Other Series of Lines in the Spectrum of Hydrogen," *Royal Academy of Sciences*, vol. 73, pp. 62-63, 1912.
- [28] Department of Defense, Military Handbook: Reliability Prediction of Electronic Equipment, Washington D.C.: Department of Defense, 1991.
- [29] J. R. Wertz, D. F. Everett and J. J. Puschell, Space Mission Engineering: The New SMAD, Hawthorne: Microcosm Astronautics Books, 2015.
- [30] T. Stryk, "Mars Pathfinder," 2007. [Online]. Available: <https://web.archive.org/web/20071005010821/http://www.strykfoto.org/pathfinder.html>. [Accessed 26 July 2020].
- [31] H. J. Eisen, C. W. Buck, G. R. Gillis-Smith and J. W. Umland, "Mechanical Design of the Mars Pathfinder Mission," *Jet Propulsion Laboratory*.
- [32] NASA, "Mars Pathfinder Rover," 14 May 2020. [Online]. Available: <https://nssdc.gsfc.nasa.gov/nmc/spacecraft/display.action?id=MESURPR>. [Accessed 26 July 2020].
- [33] L. D. Jaffe and L. M. Herrell, "Cassini/Huygens Science Instruments, Spacecraft, and Mission," *Journal of Spacecraft and Rockets*, vol. 34, no. 4, pp. 509-521, 1997.

- [34] NASA, "A Chronology of Defining Events in NASA History, 1958-1998," NASA History Division, 3 January 2012. [Online]. Available: <https://history.nasa.gov/40thann/define.htm>. [Accessed 26 July 2020].
- [35] NASA, "Cassini," 14 May 2020. [Online]. Available: <https://nssdc.gsfc.nasa.gov/nmc/spacecraft/displayTelemetry.action?id=1997-061A>. [Accessed 26 July 2020].
- [36] R. E. Young, "The Galileo Probe Mission to Jupiter: Science Overview," *NASA Ames Research Center*, vol. 103, no. E10, pp. 775-790, 1998.
- [37] NASA Jet Propulsion Laboratory, "Cassini-Huygens Photojournal," 2005. [Online]. Available: <https://photojournal.jpl.nasa.gov/catalog/PIA07232>. [Accessed 26 July 2020].
- [38] XGC Technology, MIL-STD-1750A: Military Standard 16-Bit Computer Instruction Set Architecture, London: XGC Technology, 2003.
- [39] Russian Space Agency, "Pockocmoc," 15 September 2014. [Online]. Available: https://en.samspace.ru/products/launch_vehicles/rn_soyuz_fg/. [Accessed 26 July 2020].
- [40] E. I. Butikov, "Regular Keplerian Motions in Classical Many-Body Systems," *European Journal of Physics*, vol. 21, pp. 1-18, 2000.
- [41] W. S. Koon, M. W. Lo, J. E. Marsden and S. D. Ross, *Dynamical Systems, the Three-Body Problem and Space Mission Design*, Pasadena: Cal Tech, 2011.
- [42] L. A. Sromovsky and P. M. Fry, "Dynamics of Cloud Features on Uranus," *Icarus*, vol. 179, pp. 459-484, 2005.
- [43] Oxford Reference, "Black Body Temperature," Oxford University Press, 2020. [Online]. Available: <https://www.oxfordreference.com/>. [Accessed 26 July 2020].
- [44] J. Chan, G. J. Wood and J. G. Schreiber, "Development of Advanced Stirling Radioisotope Generator for Space Exploration," *Glenn Research Center*, pp. 11-15, 2007.

- [45] M. Sakovsky, S. Pellegrino and J. Constantine, "Rapid Deployable Antenna Concept Selection for Cubesats," *Cal Tech*, 2016.
- [46] G. Maral and M. Bousquet, *Satellite Communications Systems: Systems, Techniques, and Technology* 5th Ed., Bhushan: Wiley, 2016.
- [47] R. B. Kershner and R. E. Fischell, "Gravity-Gradient Stabilization of Earth Satellites," *Johns Hopkins University Applied Physics Laboratory*, pp. 249-266, 1963.
- [48] D. P. Collins, Interviewee, *Professor of Electrical Engineering, Air Force Institute of Technology*. [Interview]. 5 August 2020.
- [49] R. O. Jenkins, "High Linearity Broad-Band Helix TWTs," Lancaster University, Lancaster, 2003.
- [50] R. Dionisio and C. Paoloni, "The Basics of Travelling Wave Tube Amplifiers," in *46th European Microwave Conference*, Lancaster, 2016.
- [51] A. S. Gilmour, *Klystrons, Traveling Wave Tubes, Magnetrons, Crossed-Field Amplifiers, and Gyrotrons*, Boston: Artech House, 2011.
- [52] B. Khayatian, Y. Rahmat-Samii and R. Pogorzelski, "An Antenna Concept Integrated with Future Solar Sails," *Jet Propulsion Laboratory*, 2010.
- [53] B. D. Gladman, D. Quinn, P. Nicholson and R. Rand, "Synchronous Locking of Tidally Evolving Satellites," *Academic Press*, vol. 117, pp. 169-170, 1995.
- [54] L. A. Panek, E. E. Hornsey and L. R. Lappi, "Determination of the Modulus of Rigidity of Rock by Expanding a Cylindrical Pressure Cell in a Drillhole," *American Rock Mechanics Association*, pp. 28-30, 1964.
- [55] C. Grima, M. Mastrogiuseppe, A. G. Hayes and S. D. Wall, "Surface Roughness of Titan's Hydrocarbon Seas," *Earth and Planetary Science Letters*, vol. 474, pp. 20-24, 2017.
- [56] Space.com, "Calm Seas on Titan: Saturn Moon's Waves Less Than 1 Inch High," Future US, Inc, 7 July 2017. [Online]. Available: <https://www.space.com/37417-saturn-moon-titan-calm-seas-cassini.html>. [Accessed November 2019].

- [57] C. S. Arridge, C. B. Agnor, N. Andre and K. H. Baines, "Uranus Pathfinder: Exploring the Origins and Evolution of Ice Giant Planets," *Springer Science*, 2011.
- [58] G. Kizer, *Digital Microwave Communication: Engineering Point-to-Point Microwave Systems*, Hoboken: Wiley, 2013.
- [59] D. R. Mills, Interviewee, *Professor of Electrical Engineering, Air Force Institute of Technology*. [Interview]. 5 August 2020.
- [60] R. D. Legler and F. V. Bennett, "Space Shuttle Missions Summary," *NASA Center for Aerospace Information*, 2011.
- [61] Space Exploration Technologies, "Falcon 9 Launch Vehicle User's Guide: Rev 1," SpaceX, 2009.
- [62] United Launch Alliance, "Delta IV Launch Services User's Guide," United Launch Services LLC, Centennial, 2013.
- [63] J.-P. Lebreton, O. Witasse, C. Sollazzo and T. Blancquaert, "An Overview of the Descent and Landing of the Huygens Probe on Titan," *Nature*, vol. 438, pp. 758-764, 2005.
- [64] W. E. Wiesel, *Spaceflight Dynamics*, New York: McGraw-Hill, 2010.
- [65] J. M. Wallace and P. W. Hobbs, *Atmospheric Science: An Introductory Survey*, Boston: Elsevier, 2006.
- [66] M. Tauber, P. Wercinski, W. Henline and J. Paterson, "Uranus and Neptune Atmospheric-Entry Probe Study," *Journal of Spacecraft and Rockets*, vol. 31, no. 5, pp. 799-805, 1994.
- [67] S. F. Hoerner, *Fluid Dynamic Drag: Practical Information on Aerodynamic Drage and Hydrodynamic Resistance*, 2nd Edition, Paris: Gauthier-Villars, 1965.
- [68] HITRAN, *The HITRAN Database*, 2020.
- [69] L. Xuqiang, L. Luhua and T. Guojian, "Research on Solar Sail Halo Orbits Around Artificial Lagrange Point," *IEEE*, 2010.

- [70] NASA, "STMD: Tech Demo Missions," 3 August 2017. [Online]. Available: https://www.nasa.gov/mission_pages/tdm/solarsail/index.html. [Accessed 27 July 2020].
- [71] NASA, "NASA's Management of the Mars Science Laboratory Project," NASA Office of Audits, 2011.
- [72] A. K. Hyder, R. L. Wiley, G. Halpert and D. J. Flood, *Spacecraft Power Technologies*, Singapore: Imperial College Press, 2003.
- [73] M. Mirsadeghi, D. Costola, B. Blocken and J. L. Hensen, "Review of External Convective Heat Transfer Coefficient Models in Building Energy Simulation Programs: Implementation and Uncertainty," *Applied Thermal Engineering*, vol. 56, no. 1-2, pp. 134-151, 2013.
- [74] M. Saidi and R. Hosseini, "Air Pressure Dependence of Natural-Convection Heat Transfer," *Lecture Notes in Engineering and Computer Science*, vol. 2, 2010.
- [75] F. P. Incropera, D. P. Dewitt, T. L. Bergman and A. S. Lavine, *Fundamentals of Heat and Mass Transfer*, 6th Edition, New Jersey: John Wiley & Sons, 2007.
- [76] R. A. Bettinger, "The Prospect of Responsive Spacecraft Using Aeroassisted, Trans-Atmospheric Maneuvers," Air Force Institute of Technology, Dayton, 2014.
- [77] SpaceX, "Starship: Service to Earth Orbit, Moon, Mars, and Beyond," SpaceX, 2020. [Online]. Available: <https://www.spacex.com/vehicles/starship/>. [Accessed 5 August 2020].
- [78] Space.com, "Mars' Atmosphere: Composition, Climate & Weather," Future US, Inc, 12 September 2017. [Online]. Available: <https://www.space.com/16903-mars-atmosphere-climate-weather.html>. [Accessed 26 July 2020].
- [79] National Ocean Service, "Tides and Water Levels," U.S. Department of Commerce, [Online]. Available: https://oceanservice.noaa.gov/education/tutorial_tides/tides02_cause.html. [Accessed 27 July 2020].

- [80] Advisory Group for Aerospace Research & Development, *The Aerodynamics of Parachutes*, Leicester: The University of Leicester, 1987.
- [81] SpaceX, "Falcon Heavy: The World's Most Powerful Rocket," SpaceX, 2020. [Online]. Available: <https://www.spacex.com/vehicles/falcon-heavy/>. [Accessed 5 August 2020].

Appendix 1: MATLAB Code

RESCINDED.

REPORT DOCUMENTATION PAGE

Form Approved
OMB No. 0704-0188

The public reporting burden for this collection of information is estimated to average 1 hour per response, including the time for reviewing instructions; searching existing data sources, gathering and maintaining the data needed, and completing and reviewing the collection of information. Send comments regarding this burden estimate or any other aspect of this collection of information, including suggestions for reducing the burden, to Department of Defense, Washington Headquarters Services, Directorate for Information Operations and Reports (0704-0188), 1215 Jefferson Davis Highway, Suite 1204, Arlington, VA 22202-4302. Respondents should be aware that notwithstanding any other provision of law, no person shall be subject to any penalty for failing to comply with a collection of information if it does not display a currently valid OMB control number.
PLEASE DO NOT RETURN YOUR FORM TO THE ABOVE ADDRESS.

1. REPORT DATE (DD-MM-YYYY) 20-09-2020		2. REPORT TYPE Master's Thesis		3. DATES COVERED (From - To) 01-01-2018 - 20-09-2020	
4. TITLE AND SUBTITLE Chronos Spacecraft with Chiron Probe: Exploration of the Hydrosphere, Principle Satellites, Atmosphere, and Rings of Uranus				5a. CONTRACT NUMBER	
				5b. GRANT NUMBER	
				5c. PROGRAM ELEMENT NUMBER	
6. AUTHOR(S) Pearson, Payton E, Capt				5d. PROJECT NUMBER	
				5e. TASK NUMBER	
				5f. WORK UNIT NUMBER	
7. PERFORMING ORGANIZATION NAME(S) AND ADDRESS(ES) Air Force Institute of Technology Graduate School of Engineering and Management (AFIT/EN) 2950 Hobson Way Wright-Patterson AFB OH 45433-7765				8. PERFORMING ORGANIZATION REPORT NUMBER AFIT-ENP-13-M-07	
9. SPONSORING/MONITORING AGENCY NAME(S) AND ADDRESS(ES) Intentionally Left Blank.				10. SPONSOR/MONITOR'S ACRONYM(S)	
				11. SPONSOR/MONITOR'S REPORT NUMBER(S)	
12. DISTRIBUTION/AVAILABILITY STATEMENT Distribution Statement A. Approved for Public Release.					
13. SUPPLEMENTARY NOTES					
14. ABSTRACT A design reference mission using more modern technological innovations has been developed for exploration of the outer reaches of our Solar System, specifically Uranus and its system of satellites. This mission will utilize theoretical technologies mostly without regard to their current technological readiness level (TRL), though most systems have a TRL of at least 5. The primary innovations explored in this thesis are the new launch systems that provide far greater payload capacity potentially sent to anywhere in the Solar System, new Stirling-engine radioisotope thermoelectric generators (SRTGs), vastly improved data storage technologies, optimized satellite antenna relay of data using much higher transfer fr					
15. SUBJECT TERMS Space, Uranus, Probe, Falcon Heavy					
16. SECURITY CLASSIFICATION OF:			17. LIMITATION OF ABSTRACT	18. NUMBER OF PAGES	19a. NAME OF RESPONSIBLE PERSON
a. REPORT	b. ABSTRACT	c. THIS PAGE			Captain Payton E Pearson, AFIT/ENY
U	U	U	UU	179	19b. TELEPHONE NUMBER (Include area code) (916) 792-2582 payton.pearson.1@us.af.mil

INSTRUCTIONS FOR COMPLETING SF 298

1. REPORT DATE. Full publication date, including day, month, if available. Must cite at least the year and be Year 2000 compliant, e.g. 30-06-1998; xx-06-1998; xx-xx-1998.

2. REPORT TYPE. State the type of report, such as final, technical, interim, memorandum, master's thesis, progress, quarterly, research, special, group study, etc.

3. DATE COVERED. Indicate the time during which the work was performed and the report was written, e.g., Jun 1997 - Jun 1998; 1-10 Jun 1996; May - Nov 1998; Nov 1998.

4. TITLE. Enter title and subtitle with volume number and part number, if applicable. On classified documents, enter the title classification in parentheses.

5a. CONTRACT NUMBER. Enter all contract numbers as they appear in the report, e.g. F33315-86-C-5169.

5b. GRANT NUMBER. Enter all grant numbers as they appear in the report. e.g. AFOSR-82-1234.

5c. PROGRAM ELEMENT NUMBER. Enter all program element numbers as they appear in the report, e.g. 61101A.

5e. TASK NUMBER. Enter all task numbers as they appear in the report, e.g. 05; RF0330201; T4112.

5f. WORK UNIT NUMBER. Enter all work unit numbers as they appear in the report, e.g. 001; AFAPL30480105.

6. AUTHOR(S). Enter name(s) of person(s) responsible for writing the report, performing the research, or credited with the content of the report. The form of entry is the last name, first name, middle initial, and additional qualifiers separated by commas, e.g. Smith, Richard, J, Jr.

7. PERFORMING ORGANIZATION NAME(S) AND ADDRESS(ES). Self-explanatory.

8. PERFORMING ORGANIZATION REPORT NUMBER. Enter all unique alphanumeric report numbers assigned by the performing organization, e.g. BRL-1234; AFWL-TR-85-4017-Vol-21-PT-2.

9. SPONSORING/MONITORING AGENCY NAME(S) AND ADDRESS(ES). Enter the name and address of the organization(s) financially responsible for and monitoring the work.

10. SPONSOR/MONITOR'S ACRONYM(S). Enter, if available, e.g. BRL, ARDEC, NADC.

11. SPONSOR/MONITOR'S REPORT NUMBER(S). Enter report number as assigned by the sponsoring/monitoring agency, if available, e.g. BRL-TR-829; -215.

12. DISTRIBUTION/AVAILABILITY STATEMENT. Use agency-mandated availability statements to indicate the public availability or distribution limitations of the report. If additional limitations/restrictions or special markings are indicated, follow agency authorization procedures, e.g. RD/FRD, PROPIN, ITAR, etc. Include copyright information.

13. SUPPLEMENTARY NOTES. Enter information not included elsewhere such as: prepared in cooperation with; translation of; report supersedes; old edition number, etc.

14. ABSTRACT. A brief (approximately 200 words) factual summary of the most significant information.

15. SUBJECT TERMS. Key words or phrases identifying major concepts in the report.

16. SECURITY CLASSIFICATION. Enter security classification in accordance with security classification regulations; e.g. U, C, S, etc. If this form contains classified information, stamp classification level on the top and bottom of this page.

17. LIMITATION OF ABSTRACT. This block must be completed to assign a distribution limitation to the abstract. Enter UU (Unclassified Unlimited) or SAR (Same as Report). An entry in this block is necessary if the abstract is to be limited.